CIRP Annals - Manufacturing Technology 72 (2023) 753–779

Contents lists available at ScienceDirect

CIRP Annals - Manufacturing Technology

journal homepage: https://www.editorialmanager.com/CIRP/default.aspx

Modeling and simulation of surface generation in manufacturing

Guido Tosello (2)[a,*], Giuliano Bissacco (1)[a], Jian Cao (1)[b], Dragos Axinte (1)[c]

[a] Department of Mechanical Engineering, Technical University of Denmark (DTU), Building 427S, Produktionstorvet, DK-2800 Kgs. Lyngby, Denmark
[b] Department of Mechanical Engineering, Northwestern University, 2145 Sheridan Road, Evanston, IL 60208, USA
[c] Faculty of Engineering, University of Nottingham, Department of M3, Coates Building, University Park, Nottingham NG2 2RD, United Kingdom

ARTICLE INFO

Article history:
Available online 29 May 2023

Keywords:
Surface
Manufacturing
Modelling
Simulation

ABSTRACT

The paper describes the state-of-the-art in modeling and simulation of surface texture and topography generation at micro and nano dimensional scales. Three main classes of manufacturing processes used for the generation of engineering surfaces are considered: material removal processes, material conservative processes, and material additive processes. Types of modeling techniques for the simulation of surface generation are reviewed and discussed including analytical models, numerical multi-physics models, and data-driven methods. After presenting the application of those modeling techniques for the prediction of characteristics and geometry of surfaces generated by different manufacturing processes, their performance, implementation, and accuracy are discussed. Finally, a roadmap for the realization of a complete surface generation digital twin in manufacturing is outlined.

1. Introduction

Surfaces represent the interface between a body and its surrounding environment. In the context of product development and manufacturing engineering, the surface of a component is in fact that entity that separates the part being considered and the external environment. The environment is either represented by another component in contact with the part or by a medium (e.g., air, oil, water, etc.) surrounding the considered product. Depending on the intended functionality of a component, once the relevant material is defined, the surface geometry can be specified, designed and eventually generated having specific properties. Examples can be, depending on both the surface geometry and the material, optical properties (refractive, reflective, diffractive), wetting properties (hydrophobic, hydrophilic, drag reduction), biocompatibility properties (e.g., for medical applications), wear resistance properties, etc. [26,46,71,169,193,233].

Research and industrial advancements in recent years have focused on the development of production technologies that are able to confer the surface specific properties based on the surface geometry at the micro and nano scales that is directly generated by the manufacturing process [45,96,112]. To predict whether the surface will have the intended functionality prior to manufacturing, modeling techniques and simulation tools have been continuously developed for the past 40 years. This trend started first with analytical models of very established process technologies (e.g., machining) and it has expanded throughout the years to virtually all manufacturing operations. The ability to predict the generated surface properties is instrumental in the design of the manufacturing process and for the verification that the surface component specifications will be met.

Simulation of surface generation in manufacturing has benefitted from the increasing availability of computation power experienced in recent years. The analytical models first developed for one- or two-dimensional systems can be now applied and scaled up to the entire geometrical model of complex three-dimensional components. They can predict the actual surface geometry at different scales (including form, waviness, deterministic features, roughness) based on multi-

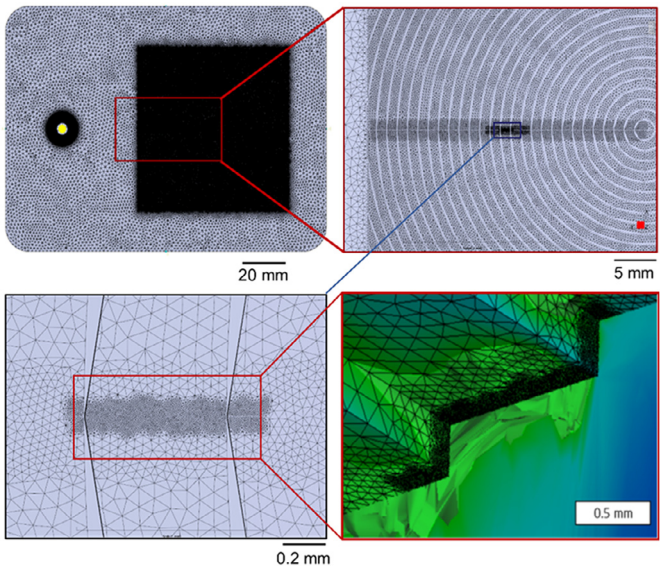

Fig. 1. Top left: three-dimensional discretization of a full component (Fresnel lens); top right: high resolution mesh of the structured area; bottom left: higher mesh density for the analysis of the generation of a single micro feature; bottom right: simulation of generation of a surface micro feature during production by injection molding [162].

* Corresponding author.
E-mail address: guto@dtu.dk (G. Tosello).

https://doi.org/10.1016/j.cirp.2023.05.002

physics and multi-scale simulation models (see example in Fig. 1). The focus of the present keynote paper will be on modeling and simulation of surface generation of features and roughness at the micrometer/nanometer dimensional range. With the spreading of Industry 4.0 and Industrial Internet of Things, sensing has become almost ubiquitous in manufacturing. The result is that the availability of data during production nowadays is becoming extremely large. The availability of large computational power is allowing now to process vast amounts of data that in turn are used to train statistical models for the prediction of surfaces generation and their properties. The acquisition of surface measurements to generate large amounts of geometrical data (i.e., topography) can be a resource intensive and time consuming task that limit the availability of useful data for model training purposes. In this case an emerging trend that can be observed is the use of modeling and simulation tools to predict surface geometrical properties and for the generation of surface data for statistical model training.

The advantage is that statistical models are orders of magnitude faster than high resolution multi-physics simulations.

The constituent components of a surface, i.e., roughness (short wavelength), waviness (mid length wavelength) and form (long wavelength) are, accordingly, simulated at different scales. Longer wavelengths are typical of distortions of the component, while shorter wavelengths are generated by the tool/workpiece interaction at the topographic scale of the surface (i.e., micro scale). The wavelength of interest of the present keynote paper is that of the roughness (short wavelength).

Depending on the development history of different manufacturing processes, several types of modeling and simulation methods have been developed and are currently applied. In this paper the most relevant manufacturing processes are reviewed in the context of the state of the art of modeling and simulation of surface generation.

The paper is structured as follows. After the main concepts of surface generation modeling are introduced in Section 2, processes are classified and the corresponding surface generation modeling approaches discussed in three main groups: material removal processes (Section 3), material conservative processes (Section 4), material additive processes (Section 5). In Section 6 the capabilities of today's modeling techniques to predict surface generation are summarized, along with opportunities for their application, the remaining challenges and the directions for future research.

2. Concepts of surface generation modeling

For surface generation simulation to achieve its full potential and allow for prediction of critical characteristics such as surface topography, features geometry, and corresponding surface properties, modeling accuracy is of paramount importance. This is obtained by extensive and comprehensive experimental validation of the developed models, both for multiphysics models and for statistical models (see Fig. 2).

In case of multiphysics models, experiments provide the necessary model boundary conditions in terms of manufacturing process data, usually produced by on-machine sensors. Process data is then used for model assessment and refinement in order to further increase the prediction accuracy. Areal surface topography measurements obtained with high resolution and high accuracy three-dimensional instrumentation provides then the term of comparison for the determination of the modeling accuracy. It is important to ensure that the lateral resolution of the model and of the measurements are comparable. Depending on the application, sensible surface profile, waviness, roughness cutoffs/filters will need to be selected to achieve an appropriate comparison in the validation stage.

For statistically based simulations, experimental data determines the input to the models for training purposes. The generated surface data are then compared with the prediction of the model. Once the training is completed and the statistical model is established, alternative experimental data (generated by additional experiments) are then fed to the model and the accuracy (in terms of deviation between the predicted and the experimental surface) is assessed. Typically, when the accuracy is not sufficient for the intended application, the training data set is enlarged, and the validation is repeated until the desired accuracy is achieved.

High accuracy of validated multiphysics simulations can allow the use of the modeling to virtually generate experimental data in a more resource efficient and effective way compared with executing physical experiments (see Fig. 2). This approach is also referred as digital twin [182]. Improvements in term of accuracy and resource optimization can then be obtained by performing statistical modeling (which is considerably faster than the corresponding multiphysics modeling) combined with training and validation based on virtual experiments (i.e., the digital twin of the surface generation by multiphysics simulation).

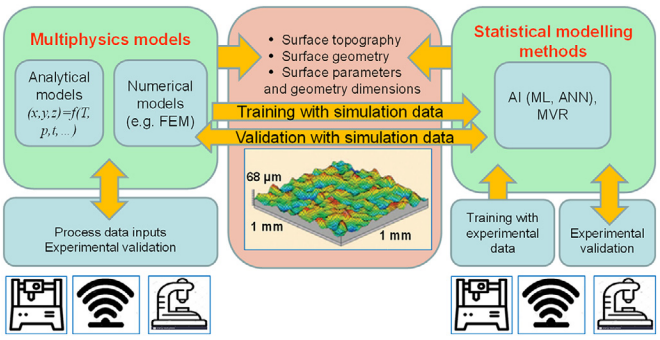

Fig. 2. Concepts of surface generation modeling: multiphysics modeling using experimental data for calibration and validation; statistical modeling using experimental data or multiphysics modeling for training and validation (FEM: finite element method; AI: artificial intelligence; ML: machine learning; ANN: artificial neural network, MVR: Multivariate Regression).

3. Modeling of surface generation by material removal processes

This section presents an overview of the state of the art in modeling surface generation in material removal processes. Different means of removing material in discrete and controlled units are possible. The section thus clusters processes into three groups, based on the material removal mechanism: mechanical material removal (Sections 3.1 and 3.2), material removal by thermal energy (Section 3.3) and material removal by chemical and electrochemical processing (Section 3.4). Within mechanical material removal processes, a further distinction is made between material removal processes with geometrically defined cutting edges (3.1) and abrasive processes (3.2), where the geometry and position of the individual feature or particles generating the removal action are known and not known respectively.

3.1. Mechanical material removal with tools having geometrically defined cutting edges

Modeling the performance of machining operations has been in focus for many years and overviews of the state of the art in the field have been provided periodically by CIRP keynotes at different moments, with the most recent being [5,12,89,221]. Van Luttervelt in 1998 [221] prepared a comprehensive overview table distinguishing between models for specific machining variables (e.g., local stresses, strains and temperatures) and specific machining performance (e.g., forces, tool wear, surface roughness and part accuracy) and clustering available models by the specific modeling technique (analytical, numerical, experimental and AI-based). The resulting picture with respect to modeling of surface generation (surface roughness and part accuracy) was that there were "very limited predictive modeling attempts" and that surface roughness prediction was limited to consideration of purely geometric relationships. Most reported work was based on either analytical, numerical or experimental approaches, with very few attempts at using AI-based techniques. An increasing effort has been placed in the last 25 years in improving our understanding of the complexity of surface generation in machining processes and our ability to accurately predict the resulting surface characteristics at different length scales, from form to roughness.

A generic surface can be represented by surface components in different wavelengths. In the following description we distinguish

between the form component (part geometry) and the topography component (surface roughness). While a quantitative separation must take into account the size and field of application of the component, for the sake of clustering models and distinguish the considered contribution to surface generation, in the following we consider a wavelength of 50 µm a limit between the two. Thus, in the following, a general presentation is initially given with respect to approaches to model (i) part geometry, (ii) surface topography and (iii) local surface artefacts (such as burrs), followed by a discussion of models for individual process configurations, such as milling, drilling, turning, etc.

3.1.1. Modeling of part geometry

The geometry of a part produced by a machining operation is the result of a complex interaction between the tool, the workpiece, the cutting fluid, the machine tool and the environment. Extensive work has been carried out to model such interaction. Comprehensive generalized models, applicable to multiple machining operations (milling, turning, drilling), have been developed [4,84,135,136]. Some models are embedded in commercial software for machining process optimization (e.g., MACHPRO by Manufacturing Automation Laboratories Inc., Vancouver, Canada). Starting from the analytical representation of the nominal cutting edge geometry and describing analytically the kinematics of the cutting edges, the models estimate static and dynamic displacements of the cutting edge segments and predict the surface location errors which, added to the nominal tool path trajectory, provide the estimated workpiece geometry. Accounting for the effects of kinematic error motions deriving from tool clamping (tool run out), machine limitations and system dynamics, such models estimate the instantaneous local cutter-workpiece engagement (CWE) and cutting forces.

The objective of such models is to compensate the surface generation error by either reduction of the cutting forces (feed scheduling) or variation of the position and orientation of the cutting tool. The surface location error is calculated on cutter location points along the tool trajectory and therefore can essentially provide an areal representation of the predicted geometry and surface error distribution.

For the many different machining operations, with specific tool geometries and process kinematics (e.g., turning, milling, drilling, etc.), dedicated mathematical models have been developed for each case. Since the physics of mechanics and dynamics are the same, a unified mathematical model for all metal cutting operations has been proposed in [135] and [136].

The complexity of the models has increased along the years by including tool static deflections [48], dynamic deflections [3], tool rotation errors [11,34], and NC control errors [200]. For thin-walled components, such as turbine or compressor blades, a dominant contribution to the surface generation error is due to workpiece deflection. Errors induced by tool deflection are easier to calculate as tool stiffness does not change with time. For slender parts, workpiece stiffness changes with position and time, as it is affected by the removal of material of previous passes. This requires more complex approaches to update the static stiffness of the in-process workpiece. [6] proposed physics based digital prediction and compensation of deflection errors on the surface of ball-end milled, highly flexible blades (Fig. 3). In this approach, the stiffness of the blade is updated analytically as the material is removed along the tool path and the cutter–workpiece engagement and cutting force are calculated iteratively by considering both the tool and workpiece deflections induced by cutting forces. The deflection errors are thus predicted and then compensated by modifying the tool path. The model has been further improved by [111] by introducing error compensation based on tool orientation modification to drastically reduce computational time. Further improvement would enable to include machine tool positioning errors and thermal errors.

The accuracy of the above models is related to the simplifications introduced in the mathematical representation of the complex tool-workpiece-machining system interaction and to the accuracy of determination of the input quantities. Specifically, the prediction accuracy of such virtual machining systems is most affected by the cutting force coefficients, the mathematical model of the physical

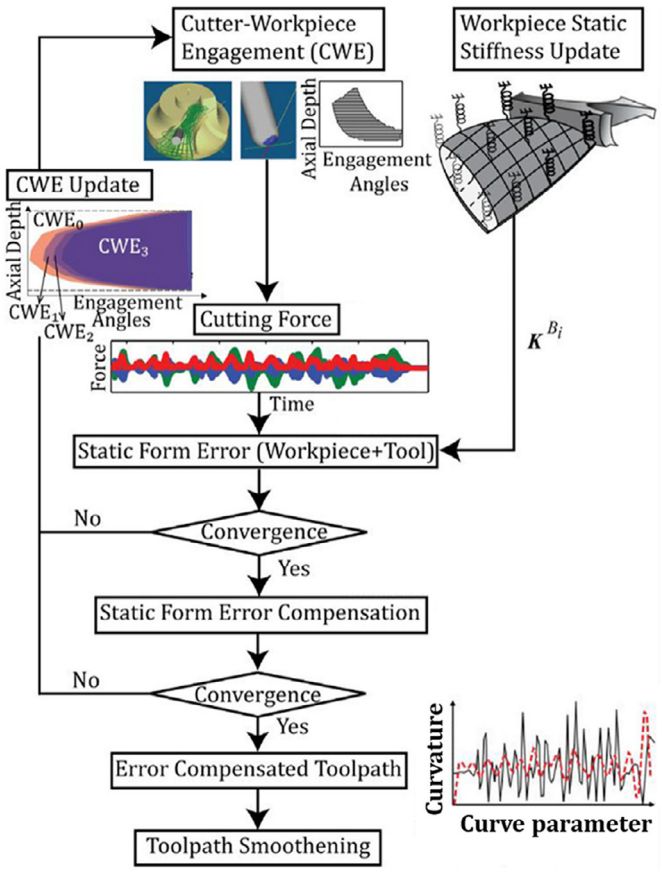

Fig. 3. Flowchart of model for virtual compensation of deflection errors in ball end milling of flexible blades [6].

processes and cutter–workpiece engagement conditions [47]. Surface generation prediction accuracy in the order of a few micrometers has been demonstrated in five axis milling of flexible components (Fig. 4) [111].

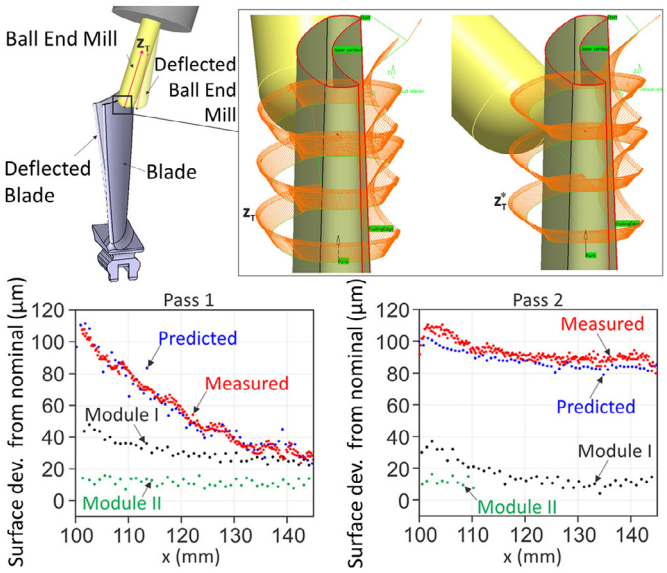

Fig. 4. Top left: representation of the machining process; top right: initial tool path and tool orientation optimized tool path; bottom: comparison of surface errors, blue – predicted for nominal NC code, red – measured for nominal NC code, black – measured for the modified NC code using tool orientation modification (module I), green – predicted for the modified NC code using tool position modification (module II) [111].

Part distortions due to residual stresses (particularly in thin components) and metallurgical transformations can also play an important role in determining the part geometry. However, these

contributions are not dealt with in this keynote and will be the focus of future keynote papers.

3.1.2. Modeling of surface topography

The purpose of modeling the generation of surface topography in machining processes is generally to enable selection, tuning and optimization of processes with respect to the ability to deliver surfaces within defined functional specifications. Although surface requirements in engineering drawings are often specified using a single surface roughness indicator (most often *Ra*) [82,216], this is not sufficient to completely characterize the performance of the generated surface [132]. Indeed, it is necessary to consider the three-dimensional characteristics of the surface to verify its compliance with multiple functional requirements. Therefore, models providing a complete three-dimensional digital representation of the surface are inherently more useful than those providing outputs in terms of individual roughness indicators (e.g., *Sa*). As will be discussed in the following, higher resolution in the digital representation of the predicted surface enables representation of contributions to the surface topography on a lower wavelength and therefore suitable for fine finishing operations.

For machining with tools with geometrically defined cutting edges, the kinematic surface roughness is the surface topography generated by the nominal kinematic motion of the cutting edges with respect to the machined surface. Deviations of the nominal cutting edge trajectories due to error motions, such as tool and spindle run out, lead to an increased surface roughness, with recognizable surface patterns (see Fig. 5) [33].

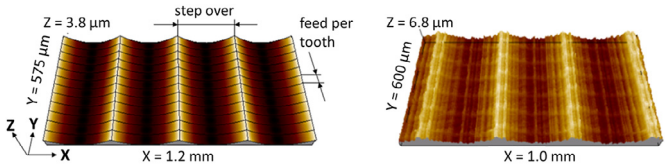

Fig. 5. Ball end milled surface generated with tool diameter 6 mm, step over 300 µm, feed per tooth 48 µm. Left: simulated kinematic surface topography. Right: measured surface [32].

Models briefly introduced in the previous section can also provide information on the surface topography generated by considering the complex cutting edge trajectories resulting from the combination of nominal cutter motion, tool trajectory errors [10], tool and workpiece deflections [111], as well as tool vibrations [11].

While this information is sufficient when simulating operations with relatively large values of the cutting edge curvature radius and engagement parameters defining the kinematic surface topography (e.g., step over and feed per tooth in milling, feed per revolution in turning), such as in roughing operations, the anticipated assessment of surfaces from fine finishing operations requires consideration of phenomena occurring at a smaller length scale. Such contributions include cutting edge micro topography, local edge defects, smearing, plastic side flow and spring back phenomena related to the minimum uncut chip thickness and the transition from cutting to ploughing, tool wear and built-up edge formation, workpiece material small-scale inhomogeneity, differential springback at grain boundaries, inclusions, as well as thermal phenomena. Therefore, the increased resolution and prediction accuracy requirements of ultraprecision machining induce an increased complexity of suitable surface generation models.

In fine finishing operations, ultraprecision machining and micro machining, characterized by small values of the cutting parameters defining the cutting edge engagement, contributions such as plastic side flow and material spring back become quantitatively comparable to the kinematic roughness. In [118] He et al. classify contributions to surface topography generation in turning in “easy modeling factors” and “difficult modeling factors”, indicating that a great effort has been placed in modeling the easy ones, essentially representing the kinematic surface topography. A further distinction is made between “certain factors” and “uncertain factors”, according to their influencing modes. Uncertain factors include grain boundaries and orientation of workpiece material, hard inclusions as well as the coolant, which jointly affect the surface roughness randomly.

While empirical modeling methods relate process parameters to corresponding surface roughness values using data mining of process signals outputs to develop statistical predictors of specific roughness parameters (such as *Ra* and *Rt*), theoretical modeling methods focus on identifying the sources of surface topography features and try to understand and interpret the underlying mechanisms for their formation. Each topography feature formation mechanism can thus be individually modelled and then combined into more comprehensive models taking into account multiple mechanisms. In the next section, the most relevant individual sources of surface generation artifacts, adding to the kinematic surface topography, are briefly presented.

3.1.3. Local surface artifacts

Local surface artifacts (or surface features) are generated during machining processes because of the complex interaction between the tool, the workpiece material, the machining system and the environment. Such artifacts add to the kinematic surface topography to define the resulting generated surface. The main sources generating such artifacts, the mechanisms they activate, and the modeling approaches used to predict the related surface features are discussed in the following sections.

Cutting edge related artifacts. While the contribution related to the overall tool geometry is well accounted for in the kinematic surface modeling (e.g., tool nose radius in turning), cutting tool dependent small scale surface features are mostly related to the characteristics of the cutting edge such as the cutting edge radius and the cutting edge topography (indicated as waviness by some authors).

At micrometric scale, the tool cutting edge (CE) cannot be considered perfectly sharp. When the instantaneous uncut chip thickness is comparable to or smaller than the minimum uncut chip thickness (MUCT), the material is not removed but is deformed, remaining on the surface to form local material features affecting the surface topography. Springback features are generated by elastic deformations, while side flow and smearing are generated by plastic deformations. Specifically, plastic side flow is generated when, due to the stress concentration ahead of the cutting edge, deformed material flows to the side of the active cutting edge to release the stress [118]. Smearing instead is obtained when the material accumulating ahead of the cutting edge is displaced in the direction of the cutting velocity and accumulating in specific locations on the surface, giving rise to characteristic smearing structures shown in Fig. 6.

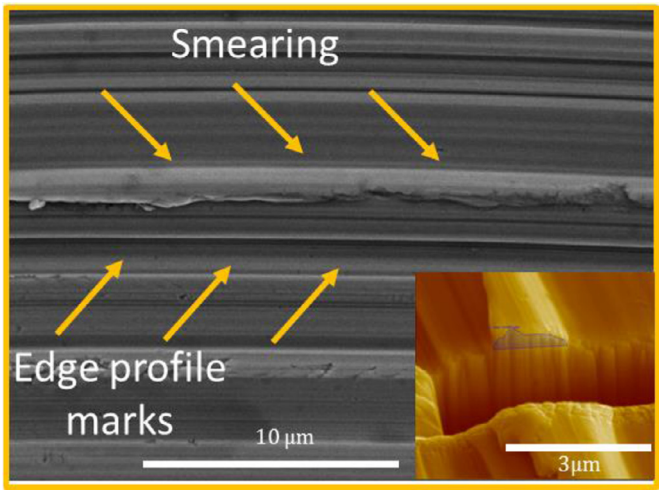

Fig. 6. Smearing and cutting edge profile marks on ball nose milled surface. Bottom right: focused ion beam cross section of smearing feature [30].

Several authors have investigated the determination of the MUCT using experimental [29,79,137,180,253], analytic [160,168,205] and simulative [128,153,234] approaches and there is extensive evidence

that for a given material, the ratio between the MUCT and the edge radius r_e is constant.

Modeling of springback and plastic side flow have been investigated mainly in connection with turning operations often using diamond tools. Arcona et al. [9] proposed an empirical model for calculation of the height of springback in turning based on tool cutting edge radius, hardness and elastic modulus of the workpiece material. Starting from this formulation and assuming the sum of elastic and plastic strain under the cutting edge to equal the MUCT, [117] developed a relationship between height of springback and cutting edge radius. In [65] Chen at al defined a swelling proportion SP to quantify the swelling effect, which includes both springback and plastic side flow, based on measured roughness profiles. In [66] the Hertz elastic contact theory is used to calculate the height of the elastic deformation recovery after squeezed by tool (i.e., springback).

Plastic side flow was experimentally investigated by Kirshawy et al. [139] as a function of process parameters in turning. The same author later presented a three-dimensional thermo-elasto-viscoplastic finite element model to investigate the effect of different process parameters on the extent of plastic side flow [140]. Material side flow in micro turning is modeled in [161] using theory derived from scratch test. Theoretical modeling of plastic side flow height in turning was proposed in [66] as a function of tool nose radius and using a Johnson-Cook workpiece material model. In [117] an empirical model is used to calculate the height of plastic side flow in diamond turning with coefficients related to feed rate, tool corner nose radius, MUCT and cutting width. In [119] a quadratic function is used to formulate the general distribution of material spring back and plastic side flow in one period along the feed direction in diamond turning.

Smearing of plastically deformed material occurs in operations with interrupted cutting where the uncut chip thickness varies during a cycle of engagement as in milling operations. A description of smearing structures in micro milling was provided in [33] and experimental quantification using a combination of observations of focus ion beam cross sections of the smeared material and electron microscopy was shown in [29]. The complexity of modeling this phenomenon in milling operations is related to the many different smearing patterns that can be generated due to different tool path planning options. In [30] the smearing volume is computed as the fraction of the uncut chip volume with local thickness below MUCT and added as an element with triangular cross section at specific locations which are dependent on the relative orientation of feed and speed vectors as previously identified in [28] and [31].

Cutting edge topography, often addressed by authors as cutting edge waviness, is a further contributor to the generated topography during machining operations. The cutting edge profile, including the short wavelength components, is duplicated onto the machined surface during cutting edge engagement. While this can be a dominating factor, modeling of this contribution requires the a priori knowledge of the cutting edge topography, which can be obtained by direct measurement of the cutting edge. So far only a few studies reported the influence of tool edge waviness due to the limitation of measuring instruments and methods. The resolution of the cutting edge measurements act as a low-pass filter with respect to the spatial frequency spectrum of the generated topography that can be simulated by the models. Thus, high resolution measurements are necessary in order to model shorter wavelength components. [30] used point clouds obtained from confocal microscope images of the cutting edges of ball nose end mills and generated the cut surfaces by rotating the digital edge profile along the virtual tool axis of an angle corresponding to the radial engagement angle. In [155] the measured geometry of the cutting edges from a focus variation profilometer used to represent the geometrical envelope of the surface generated in 5 axis milling operation using a Z-buffer technique. In [117] the cutting edge waviness of diamond tools was acquired by using a dedicated microscope system. An alternative approach is to measure the cutter marks imprinted on a test surface and use this as a representation of the cutting edge profile. This approach was used in [144] to model surface generation in hard turning and in [95] to characterize tool wear in diamond turning.

Tool wear has the effect of changing the geometry and topography of the active part of the cutting edge, thus influencing all the cutting edge related contributions described above as well as the kinematic surface topography. However, the complexity of wear phenomena in machining makes it difficult to incorporate time efficient thermo-chemical-mechanical models describing tool wear along the active cutting edge. Therefore, empirical-statistical models are better suited for incorporation of the effects of the time dependency of cutting edge geometry and topography on surface generation in machining.

Workpiece material dependent artifacts. Material small scale inhomogeneity affects the response of the material to the cutting process. Grain boundaries, crystal orientation, segregations and inclusions influence the topography of the generated surfaces in machining due to the formation of local surface features. These contributions are difficult to model in a quantitative way due to the unknown dimensions, locations and orientations of individual grains and inclusions. However, it can be accounted for by assuming a random probability distribution and analyzed statistically.

The variation of the elastic modulus *E* between the grains and the grain boundary in a polycrystalline material is responsible for differential springback. This generates protrusions, after the passage of the cutting tool, in the areas with higher elastic modulus (typically at the grain boundaries). In [119] an expression for the height of springback as a function of *E* and the MUCT is presented. The effect of differential springback due to the tool cutting path from one grain to the next is schematically shown in Fig. 7, where the elastic modulus of the grain boundary is *Eg* and the elastic modulus of the material matrix is E_1.

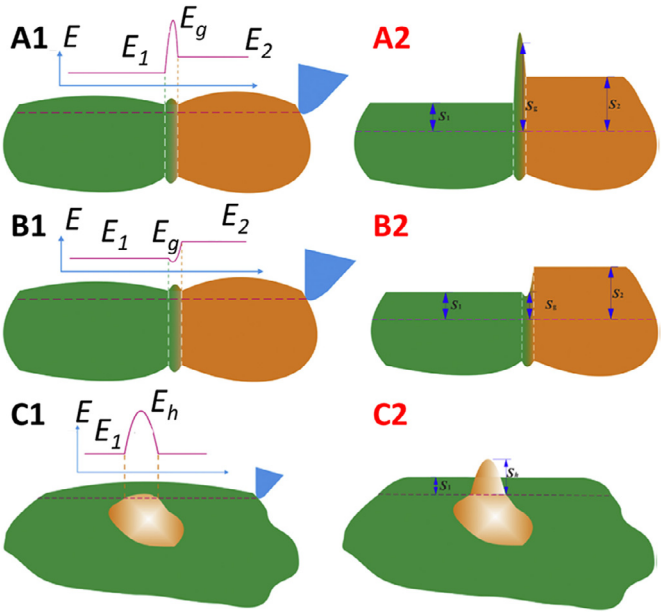

Fig. 7. Surface artifacts generated by differential springback and hard inclusions: (A) material springback related deformation on grain boundary of metal alloys; (B) material springback related deformation on grain boundary of highly pure metals; (C) influence of a hard inclusion. (1) before cutting; (2) after cutting [119].

Differential springback at grain boundaries on diamond turned copper surface has been observed and steps of 30 nm were measured between the grains [44]. Similar to grain boundaries, hard inclusions also generate local steps after the passage of the cutting tool. The elastic modulus of the hard inclusions *Eh* is larger than that of the substrate material E_1 and this generates a protruding feature. Protrusions height due to hard inclusions relative to the substrate material in diamond turning of AL6061 in the range from 10 nm to 25 nm have been observed [119].

3.1.4. Comprehensive models of individual processes

A description of individual contributions to surface generation in machining and related modeling solutions have been presented in the sections above. Such contributions and modeling approaches are

of general applicability and can be combined with the specific process kinematics to model individual machining operations. Thus, physics-based surface generation models for specific machining operations include one or more of those contributions to provide a representation of the surface suitable for evaluation. In the following comprehensive models for surface generation in turning and milling operations are presented.

Turning. Modeling of turning operations have been extensively studied. The continuous engagement of the tool with the workpiece simplifies the description of the kinematics and the inclusion of the small scale contributions in the models. The basic analytic formula $Rt=f^2/8r_\varepsilon$ [105] (where f is the feed rate and r_ε is the corner radius) for calculation of the kinematic peak to valley roughness has been used for many decades for turning with round nosed cutting tools. One approach followed by researchers has been to add correction terms into the kinematic formula for the consideration of the MUCT, material springback, plastic side flow, etc. In most cases, correction terms accounting for springback and plastic side flow contain expressions of the MUCT and nose radius, but not the cutting edge radius, thus missing the relationship edge radius and MUCT. Such correction terms contain experimentally determined coefficients which are dependent on the material and cutting tool characteristics. In [105] an expression of Rt containing MUCT and tool corner radius is developed, where the MUCT was derived from the molecular-mechanical theory of friction through the Kragelskii-Drujanov equation. In [144] a polynomial function of MUCT and nose radius combined with a material partition equation of the fractions of MUCT undergoing plastic and elastic deformations is proposed. In [161] a model for peak to valley roughness prediction in micro-turning is developed consisting of three terms: (i) the kinematic surface roughness, (ii) the roughness due to plastic side flow derived from scratch test theory and experimental calibration, and (iii) roughness of the cutting edge.

Similar approaches based on modified expressions of the peak to valley roughness Rt were proposed in [65], taking into account plastic side flow and material springback, and in [117] taking into account kinematics, MUCT, tool edge waviness, plastic side flow and material spring back and adding material related random effects assuming a Gaussian distribution.

The usefulness of the above solutions is rather limited as they do not provide a true representation of the surface which is required for functional assessment.

He et al. proposed in [119] a comprehensive profile/areal topography model for turning with consideration of kinematic roughness, springback and side flow, as well as additional contributions related to random factors such as grain boundaries and inclusions in the material matrix, cutting edge waviness and tool vibrations. The model consists of a generic three-dimensional surface formulation that adds specific terms to the profile obtained from the kinematics of the cutting tool. Eq. (1) represents the expression of the surface profile in one tool track, where x is the feed direction, $x = 0$ indicates the center of the track, $R_{tew}(x)$ is the kinematic component function including tool edge waviness, s(x) is the springback function, w(x) is the plastic side flow function and ε_t contains the effects of material related random factors such as grain boundaries and inclusions as well as tool tip vibration. The terms s(x) and w(x) are quadratic functions representing the distribution of springback and plastic side flow. When the model is limited to the first three terms and no edge waviness is considered, the surface profile can be simplified as function of the cutting edge radius, corner radius, feed and depth of cut through experimentally determined coefficients as described in [119].

$$F(x) = R_{tew}(x) - s(x) + w(x) + \varepsilon_t(x) \quad (1)$$

For material defect-dependent components contained in the term ε_t such as grain boundaries and hard inclusion, the height of the corresponding protrusions are derived from their higher elastic modulus relative to the work material. A random simulation method is used in the model to imitate the material defects in the material matrix and additional functions for each defect type must be established for every material according to actual measurement results. As an example, a comparison of the of the model simulation with the corresponding diamond turned surface on Al6061 is shown in Fig. 8.

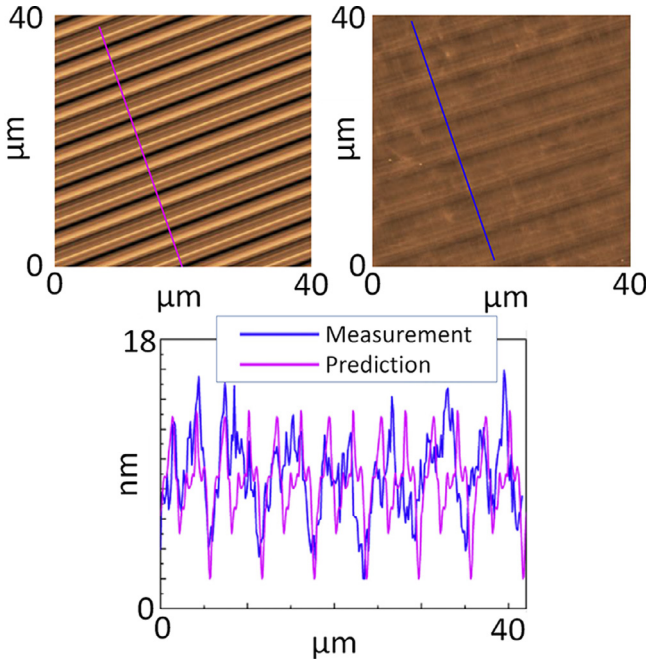

Fig. 8. Example of output of an areal topography model applied to diamond turning of Al6061. Top left: simulation; top right: measured surface; bottom: profiles comparison [119].

In the above model, several material dependent quantities must be characterized through experimental tests for the specific workpiece materials to simulate the contributions of springback, side flow, grain boundaries, inclusions and voids. The characterization effort with respect for any new material is therefore not negligible.

The approach to modeling of material dependent defects can potentially be directly used in modeling different machining processes, such as milling. However, the kinematic model as well as the size and distribution of springback and side flow related surface defects need to be reconsidered when adapting the model to other machining processes. This is because the expressions used to describe springback and plastic deformation contributions are related to the specific description of the tool-workpiece engagement in turning.

Milling. Due to the large freedom in terms of machinable part geometries, milling operations have been extensively studied. In Section 3.1.1, models for milling processes have been introduced providing the means of prediction of surface geometry as well as the kinematic component of surface topography, including kinematic errors such as runout and tool vibrations. However, only more recently models enabling the prediction of the short wavelength components of areal surface topography have been developed. This is mainly due to the difficulty of incorporating the effects described in Section 3.1.3, such as cutting edge related artifacts and workpiece material dependent artifacts, in a machining process with interrupted cutting edge engagement, involving multiple cutting edges, contact on different length segments of the cutting edge (e.g., in ball nose end milling) and complex tool paths. This section focuses on surface generation prediction capability beyond the kinematic component.

Early consideration of material springback in milling operations was introduced in [224] where a surface generation model for flat end milling was developed to predict surface roughness at the bottom of micro milled slots. The model used the definition of the surface profiles generated by two consecutive cutting edges, where the edge profile was offset by a value corresponding to the MUCT. The model was validated by comparing predicted and measured Ra values when micromilling single phase materials.

In [155] a methodology is proposed to improve the areal surface topography prediction in milling by characterizing the actual cutting edge of the tool using an optical profilometer. From the measured

cutting edge surface an STL model of the cutting edge was obtained and introduced in Z-buffer method simulations.

In [30] a comprehensive model for surface generation prediction in ball nose end milling is developed. It takes into account the plastically deformed material along the engagement profile, material spring back, cutting edge radial location errors as well as the effect of edge profile micro geometry. The model requires as input a high-resolution measurement to produce a digital representation of the tool edges, where the points with the largest distance from the axis of rotation are selected as those generating the part surface, thus obtaining the digital cutting edge profiles. The surfaces swept by the cutting edges during each cutting action are generated by rotating the digital edge profile along the virtual tool axis and resampled over a regular grid (Fig. 9). The generation of a generic milled surface consists of multiple intersecting elemental cut surfaces as generated by the individual cutting edges. Tool and spindle run out are accounted for in the surface generation by orienting accordingly the engaged cutting edge segments in the space. For the estimation of smearing and springback, the instantaneous local uncut chip thickness is calculated and compared with the local cutting edge radius. If the chip thickness is larger than MUCT the material is considered removed, otherwise the material is not removed and can be either elastically deformed and left in place (spring back) or plastically deformed and displaced in accumulation areas (smearing). In the case of smearing the fraction of the uncut chip volume with local thickness below MUCT is computed and added as an element with triangular cross section at specific locations which are dependent on the relative orientation of feed and speed vectors as previously identified in [28]. The output of the model simulation consists in a virtual three-dimensional surface that can be imported in a commercially available post-processing software for surface analysis, through which quantitative roughness parameters can be calculated (Fig. 10). The model is experimentally validated in the case of fine finishing ball nose end milling of tool steel and copper, with a final surface roughness *Sa* in the range

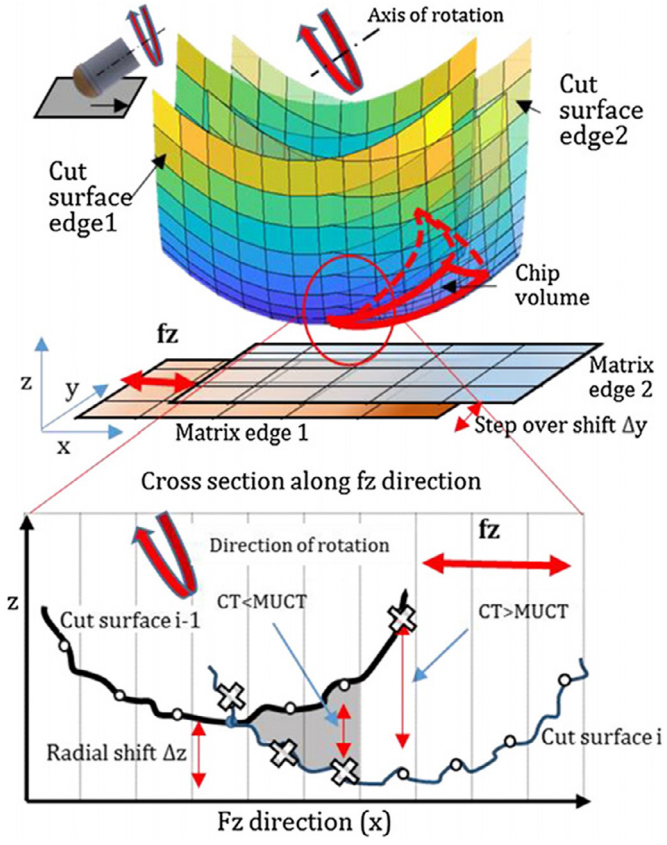

Fig. 9. Surface generation model for ball end milling accounting for material spring back and cutting edge micro topography contributions. Top: 3D representation of the cut surfaces for two cutting edges. Bottom: cross section of the cut surfaces along the feed direction. The Z valued are compared, the points indicated by a cross are disregarded while the dots define the generated surface [30].

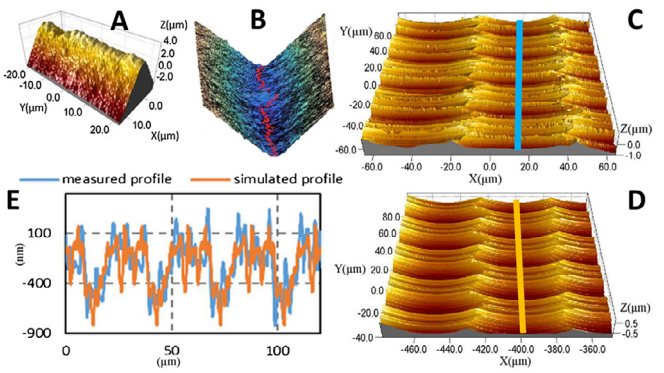

Fig. 10. (A) Confocal microscope scan of a cutting edge; (B) digital cutting edge where the points at highest radial distance marked in red; (C) measured surface patch; (D) simulated surface patch; (E) profile comparison of measured and simulated surfaces [30].

of 100–700 nm and a relative accuracy of the predictions within −8% and 12%.

In [86] a model is developed for the prediction of surface generation in 5-axis ball end milling by applying numerical material removal simulations (MRS) including the contributions of dynamic tool deflection, cutting edge topography and plastically deformed volume where the chip thickness is below the MUCT. In these simulations, a multi dexel model was used to discretize the workpiece, with three redundant dexel grids aligned with the coordinate axes. The geometries of rake and flank faces of the tool were obtained from measurements of the tool geometry using a focus variation optical profilometer. Rake and flank faces were modelled using quadrilaterals with length along the cutting edge of 0.1 mm. The simulation can include the influence of the cutting edge roughness on the surface generation. The model was validated in engagement conditions corresponding to step over and feed per tooth of 500 μm using a 10 mm diameter two fluted ball end mill, yielding a kinematic roughness in the order of *Sz* 20 μm, thereby hiding the quantitative influence of small scale contributions such as cutting edge roughness and material smearing.

In [258] an experimentally calibrated stochastic approach is introduced to model the effect of tool wear on surface generation in flat end micro milling. The model accounts for the process kinematics, including runout errors and material springback in the assumption of a full elastic recovery of the engaged volumes where the uncut chip thickness is smaller than the MUCT. The effect of tool wear was introduced by updating the tool profile and thus the engaged workpiece material volumes. To model tool wear, a probabilistic approach based on the particle filter algorithm is used, linking online measurement data of cutting forces and tool vibrations with the state of tool wear measured offline. The model is eventually validated by visual comparison of measured and predicted surfaces as well as by comparison of profile arithmetic mean roughness *Ra* in the range 0.8–1.8 μm with a relative accuracy of the predictions between −17% and 4%.

In [85] and [87] a method is developed in which the surface topography of milled surfaces is considered as a combination of a kinematic component and a stochastic component. The developed approach isolates the experimentally determined stochastic component from measured surfaces by subtracting the kinematic topography. The stochastic component can then be added to surface generation simulations of general ball nose end milled surfaces by calculating the kinematic topography and adding the stochastic component previously determined. This approach does not recognize the sources of the short wavelength components of surface topography in ball end milling and assumes that surface generation is independent from the characteristics of the cutting edge. Due to the complexity of the phenomena involved in surface generation in milling operations, several authors have investigated the use of artificial neural networks (ANN), Bayesian Networks (BN) and Fuzzy Logic (FL) for predicting specific surface attributes. Such methods have attractive properties for modeling complex problems, including universal function approximation, resistance to noisy or missing data,

accommodation of multiple nonlinear variables with unknown interactions, and good generalization capability [191]. In most cases, e.g., [78] and [149], a number of input process parameters (e.g., rotational speed, tool diameter, number of flutes, feed per tooth, axial and radial depth of cut, etc.) is put in relation to the desired output parameters consisting of one or more selected surface roughness indicators, most commonly *Ra* or *Rz*, through a number of training data sets. While this approach can be effective with respect to a fast implementation of some predictive capability, the models cannot be adapted to different application conditions and generally do not provide in output the three-dimensional surface topography. A useful implementation of ANN is related to the influence of tool wear on surface generation. [242] implemented an improved case-based reasoning (ICBR) to predict the surface roughness and residual stress in face milling operations considering tool wear. The inputs of ICBR are cutting parameters and tool wear status. The corresponding outputs of ICBR are surface roughness *Ra* and residual stress. The method is mainly composed of four parts: case retrieval, case reuse, case revise and case retain. To improve the retrieval performance, the weights of condition attributes are extracted from the trained ANN model. Model validation showed an optimal number of similar cases of 3, yielding a prediction accuracy between −44% and 19%, while excessively similar cases, introducing some irrelevant cases, reduced the estimation performance of the model.

An interesting approach was reported in [92] who developed ANN models for the analysis and prediction of the relationship between the cutting conditions and the corresponding fractal parameters of machined surfaces in face milling operations. The output consists of the profile of the predicted surface. As the validation was limited to relatively coarse surfaces application to the simulation of finer surfaces showing short wavelength surface features would be interesting.

While predictive models can be used for verification, a future improvement would be to generate inverse models that, starting from the desired surface characteristics, define the necessary operating conditions. However, while this is clearly feasible for the geometric component of surface (geometry and kinematic roughness), the influence of local errors is difficult to take into consideration and the actual tool profile provided for the operations is a constraint to the optimization.

3.2. Abrasive processes

3.2.1. Grinding

In contrast to machining with defined cutting edges, modeling of surfaces obtained by grinding operations, with randomized shapes, distribution and edge geometries of the abrasive grits, could be considered challenging, and is subjected to simplifying assumptions. Grinding tools can be categorized based on their compliance to the workpiece as follows: (i) “rigid” tools assumed with negligible deformation during the grinding process (hence the workpiece-tool contact area is constant during the process) [110]; (ii) “compliant” tools, with reduced stiffness, which adapt their shapes to the workpiece (macro) geometry (hence the workpiece-tool contact area is changing during the process) [62]. This is an important distinction in the context of modeling of surface generation in grinding.

In case of “rigid” tools, one approach for surface modeling is, by knowing the wheel’s active surface [148], to simulate the geometries and distribution of the abrasive grits on the active surface of the wheel. Subsequently, the workpiece surface micro/macro geometry can be derived geometrically by convoluting the grits’ scratches [16,98,158] and generate an “instantaneous” geometry of grit footprint [259] and the micro-geometry of the wheel along [166] the tool path (also by considering further, more detailed, aspects of the process such as wear and fracture of the abrasive grits) [13]. This is achieved computationally, and it can be considered relatively time consuming.

The initial models presented in [167] relate the maximum undeformed chip (calculated based on process parameters) with the workpiece topography. These models have been continuously improved by taking into consideration the stochasticity of the abrasive distribution and size, assuming primitive geometries of the abrasive (e.g., spheres, conical, etc.), and varying the overlap depending on the grinding tool design characteristics [120,126]. With so many aspects to consider in the hybrid (analytical coupled with stochastic aspects) models it is computationally expensive to simulate and entire workpiece surface topography; as such, an indication of the workpiece surface roughness is a common output when applying these approaches. With the development of grinding tools on which the abrasive grits (e.g., diamond, CBN) are placed in particular positions/patterns, it is possible to adapt these models and predict workpiece surface quality more accurately (see Fig. 11) [88].

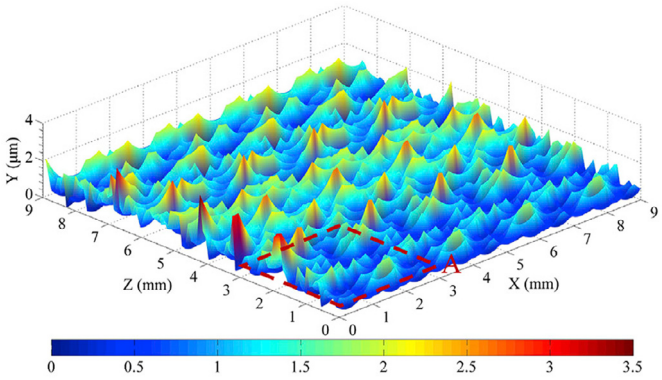

Fig. 11. Simulated workpiece surface generated by a grinding wheel with abrasives placed in specific patterns [88].

Recently, highly engineered grinding tools, with precisely defined micro-geometry and distribution of the abrasives have been obtained from solid ultra-hard materials by means of some material removal process, e.g., pulsed laser ablation [50]. These not only significantly improved the process outcomes (e.g., surface roughness, *G* ratio) but also it opens the possibility to predict the workpiece surface at a high degree of confidence. Basically, the models developed for workpiece surface prediction in machining with defined cutting edges (e.g., milling), see Section 3.1, can be employed on these tools [101]. The stochasticity aspects that are included in the models for surface generation when considering the conventional grinding are taken out of equation when employing these novel grinding wheels (see Fig. 12).

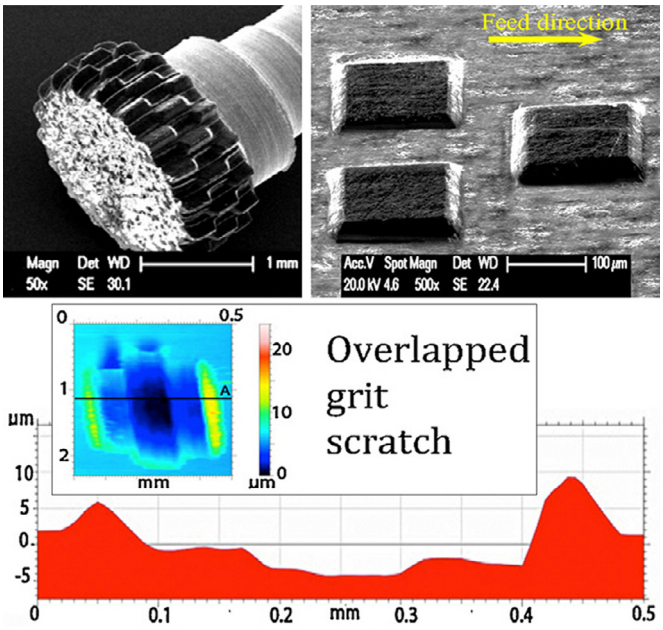

Fig. 12. Engineered grinding tools with defined geometries and arrangement of abrasive grits can allow more precise prediction of the workpiece surface [51].

As far as the “compliant” grinding tools are concerned, the prediction of workpiece surface gets to a much higher order of complexity. This stems from the fact that the tool adapts its shape to

that of the workpiece, leading to a continuous variation of tool-workpiece contact area and the contact pressure distribution. No matter the compliant tool has geometrically undefined or partially-defined cutting edges, the rubbing, ploughing and cutting stages of each grit changes all the time along the tool path because of the varying workpiece-tool contact pressure and contact area [261]. This refers to the case when grinding complex geometric surfaces where the compliant grinding tools find their unique use. In such case, there is a need to firstly model the stiffness of the compliant tool and considering a particular tool offset, the instantaneous area and pressure of workpiece-tool contact needs to be calculated. Then, it is necessary to consider the trajectories of each grit from which, depending on the instantaneous chip thickness, the rubbing/ploughing/cutting zones are defined. This will ultimately enable the prediction of the micro-geometry of the workpiece surface in a particular moment (i.e., contact area/pressure). Of course, this tedious procedure needs to be repeated every time the geometry of the part is changing. This approach is computationally expensive and is used more for providing an indication of the surface quality rather than a daily operational tool for predicting surface of every single area of the (freeform) workpiece. To address this challenge, recently a fast simulation method for surface roughness prediction has been developed and implemented on three machine platforms to prove its efficiency (see Fig. 13) [263,264].

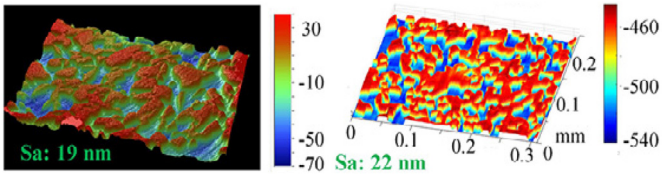

Fig. 13. Example of experimental (a) and modelled (b) surface roughness processed with a compliant grinding tool [160].

When using these compliant tools against a theoretically infinitely stiff workpiece (that related to most applications, for example in the case of grinding and polishing of lenses or molds), and knowing the stock of material to be removed from the surface, there is a possibility to calculate a priori, with some errors, the contact area and pressure between workpiece and tool to predict the workpiece surface. However, a much more complex problem to solve is that when the compliant tool is in contact with a compliant workpiece (e.g., thin walls, membranes). In this case there is a huge challenge to calculate the instantaneous area and pressure of the contact. But, even for a constant stock of material that needs to be removed, there is an analytically proven need to continuously change the tool offset. This fact lies on the assumption that there is a model to calculate both the deformation of compliant tool and compliant workpiece, a situation which is not always (easily) available. If there is a further need to change the orientation of the compliant tool, the complexity of the problem increases even further (see Fig. 14). As such, it could be commented that the modeling and computational challenges in predicting the surface quality on compliant grinding is of some order of complexity higher than when compared with that when conventional (i.e., rigid) grinding tools are employed.

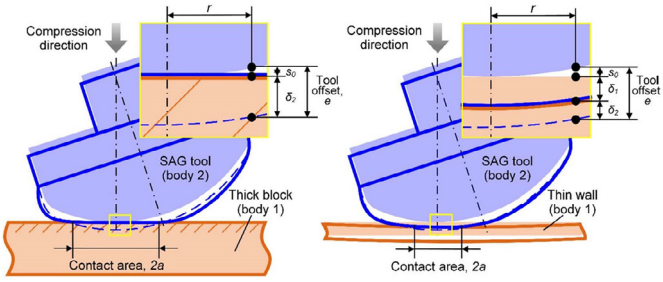

Fig. 14. Grinding with the compliant tool of a high (left) and low (right) stiffness part; in this case the deflection of the part (unlikely linear) needs to be taken into consideration [247].

3.2.2. Polishing

Polishing operation relies on a flux of loose abrasives (i.e., not rigidly bound on a solid/tool body) that in their relative movement to the workpiece surface ensure material removal. As such, the polishing processes could be generically grouped as: (i) three bodies contact: two solids (workpiece – counterpart/tool) without contact and the abrasive media between them entrained by the relative movement of the solids; (ii) two media: solid (workpiece) and abrasive media under external pressure or entrained by the movement of the part itself.

In respect to the three-body polishing, a typical example is lapping where semi-empirical models, dependent on applied pressure, workpiece material properties (e.g., Young modulus, hardness) and size and distribution of abrasive particles, have been reported to predict the resultant surface roughness [49,64] as a function of the normal load on particle (that can be derived from total load and knowing the density and size of abrasives), the Young's modulus and hardness of the workpiece, and of the particle shape.

Another variable included in the setup is the relative (e.g., planetary) motion between the two solid bodies (platan and carrier). Although these motions can be analytically described, what resultant trajectories the loose abrasives will follow, necessary to develop models for the resultant surface roughness, is difficult to predict. Recently, for the lapping setup, where a dimensional clearance between the part and carrier exists, a parasitic motion of the sample has been predicted and experimental observed [246]. This proves that the conventional considering the part follow cycloidal movements [218] is not applicable. Hence, models based on the force balance in time domains need to the developed for each polishing (e.g., lapping) setup. As such, it could be commented that, considering the assumptions of distribution, sizes and, especially the trajectories (that should be also experimentally proven) of the loose abrasives entrained by solid counterparts in complex relative movements to each other, modeling of workpiece surface roughness is very challenging.

For magnetorheological polishing, starting from material removal models, methods to predict the change (from an initial value) in surface roughness have been reported for cases in which such abrasive media works within part boundary, e.g., pipes, gear teeth, etc. [133,151]. This is a sensible approach since balance of forces could be defined for these variable stiffness abrasive media when they are within constrained boundaries.

For polishing processes that rely on non-Newtonian fluids, the relative position and movement of the two solid bodies is changed so that the unique property of the abrasive media can be controlled, i.e., with the increase of shear rate the behavior changes from fluid to viscous [157] (Fig. 15). Such behavior of the abrasive media has been addressed via fluid dynamics multiphysics modeling approaches which enabled the determination of abraded footprint and the prediction of the workpiece macro/micro geometry (Fig. 16) [264]. Similar approaches are followed when dealing with electrorheological polishing [254] for predicting the abraded footprint [99].

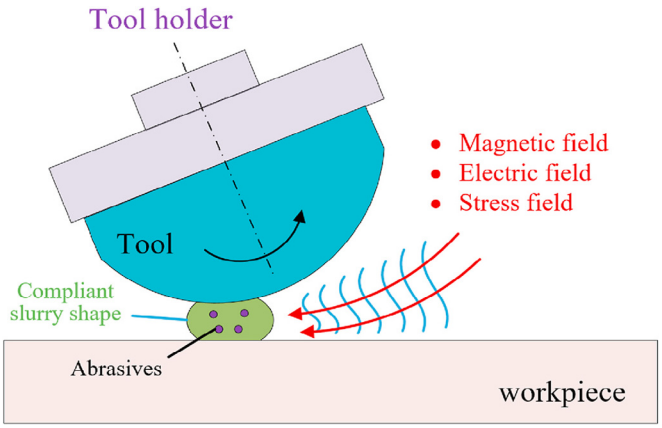

Fig. 15. The concept of slurry compliance that can be reversibly varied by the application of an external field [262].

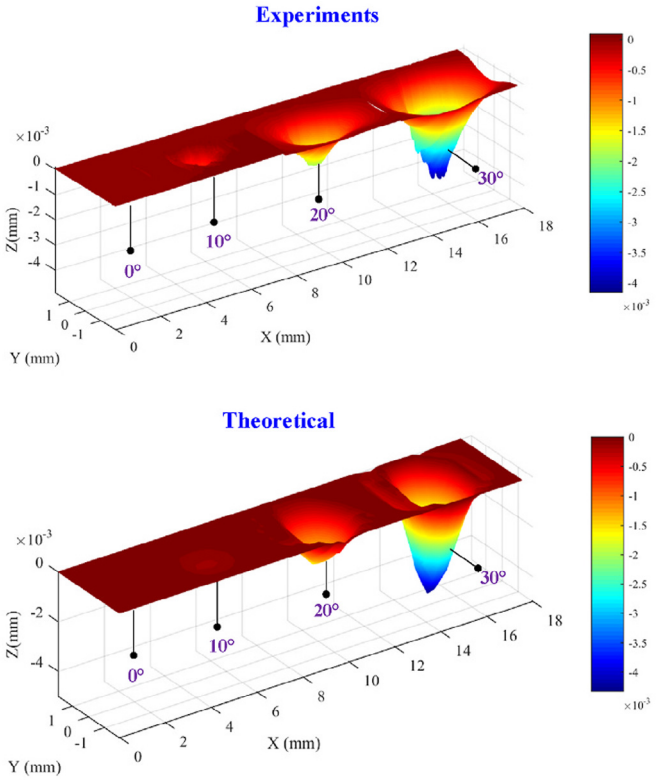

Fig. 16. Experimental vs. modelled abraded footprint when using bonnet tools to entrain shear sensitive polishing (non-Newtonian) fluid [264].

When it comes to two body polishing processes, a typical example is fluid jet polishing. Here recent approaches for modeling the workpiece surface geometry/morphology (roughness) resides on a methodology that consists of formulating an analytical/numerical model for the time dependent abraded footprint and then convoluting it along a predefined path. Such methodology has been applied for both liquid in [55,56] and [114] (Fig. 17), as well as air abrasive jets [229].

Abrasive flow machining, in which the abrasive media is constrained within the rigid boundaries of the workpiece (e.g., hole, channels) and it is pushed alternatively in different directions, also belongs to the group of two body polishing methods. While there is a number of researches that report on empirical modeling (with well-known limitations in capturing the physics of the process) approaches to predict the workpiece surface roughness, few attempts have been done to address this topic by analytical methods. Here, it can be noted the modeling approach of Jain et al. [129,130] that predicts the progression of surface roughness based on time domain (i.e., number of polishing stokes/cycles) while considering the micro-material removal mechanism performed by individual abrasives. Other two body polishing methods such as vibratory finishing and drag finishing, although some material removal mechanisms are in place [115], analytical models for surface roughness prediction are yet to be reported.

3.2.3. Fluid jet machining

For this group of processes, the abrasive particles are fed into a high velocity fluid media (e.g., water, air) stream/jet and, thus, provided with enough kinetic energy that, when impacting the workpiece surface, material removal occurs in a form of a abraded footprint [14]. To enable high velocity of the fluids, and consequently of the abrasive particles, apart from using high pump pressures, it is common that the nozzle jets have relatively small diameters (usually <1 mm).

The velocity of the fluid and, consequently, of the abrasives not only varies across the jet diameter but also with the distance from the nozzle. Because of this, the abraded jet footprint on the target surface varies in shape and amplitude not only on the jet defocus and density of the abrasives but, more challenging, on the jet exposure time upon the surface. As such, here, we deal not only with the process having high stochasticity (e.g., various shapes of abrasives as well as changing distributions of their

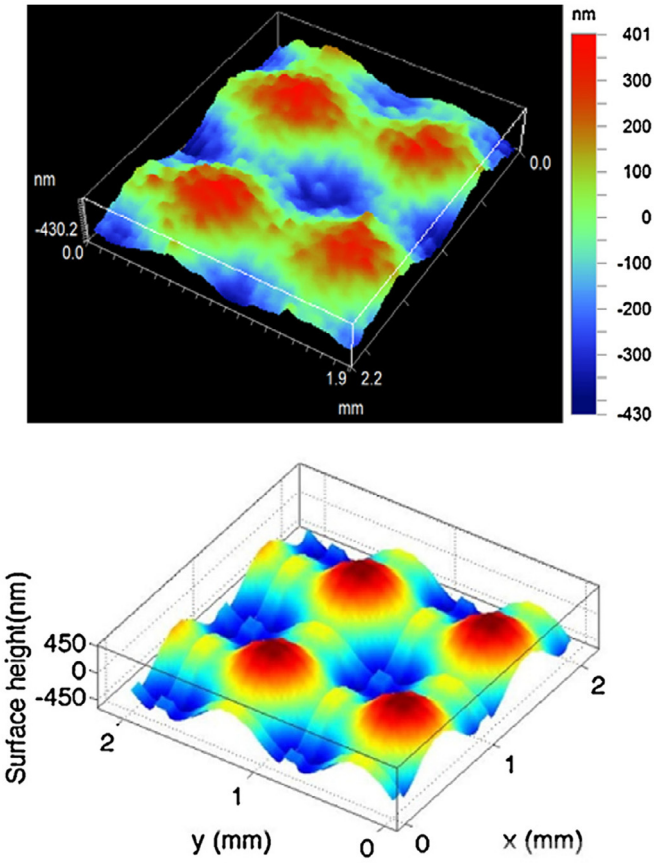

Fig. 17. Fluid jet polishing of steel: measured (top) and simulated surface (bottom) [56].

density distribution and velocities across the jet) but also with one that is time-dependent. Consequently, the modeling of the resultant eroded surface (that is resultant of the jet footprint convolution along a given path) is a highly complex problem. The whole modeling of the resultant abraded surface revolves around how to predict the shape of the abraded footprint when changing the operating parameters, and especially the dwell-time. And here there could be two main approaches.

A first method would be to try to predict the footprint based on analytical/numerical models on the impact of all the abrasives upon the time-evolving footprint [7,217,230]. Of course, this will rely on a significant number of assumptions, e.g., shapes of abrasives, their orientation and speeds when impacting the surface as well as the cutting mechanism (ploughing, cutting) with, sometime unrealistic, simplifications (e.g., non-fractured particles, no side-abrasions). These are very complex problems, and they realistically need to be solved numerically. The computational times for the simulation of a single footprint, i.e., for a particular set of parameters (e.g., pump pressure, nozzle stand-off distance, flow and shapes of abrasive, jet feed speed) is currently still measured in hours to date. Added complexity here comes when surfaces need to be "milled", i.e., machined by controlled jet penetration (see Fig. 18), as there is a need for overlapping the jet abraded footprints. As such, realistically, the numerical modeling could be considered more of an academic exercise that could give deeper understanding of the material removal process rather than useful tools to predict the abraded footprints/surfaces.

Alternatively, another method would be to try to predict the abraded footprint by ignoring the in-depth physics (e.g., single particle impacts and their cutting mechanisms) of the material removal through the introduction of a geometrical model on which the time-varying eroded footprint is dependent on the kinematic parameters (feed speed, and orientation) (see Fig. 19) of the jet while encapsulating of the physics of the material removal process into an "etching" function that can be easily calibrated for a particular set of process parameters (e.g., pump pressure, abrasive mass flow, nozzle diameters) and then extended to a complete surface [27,146,147].

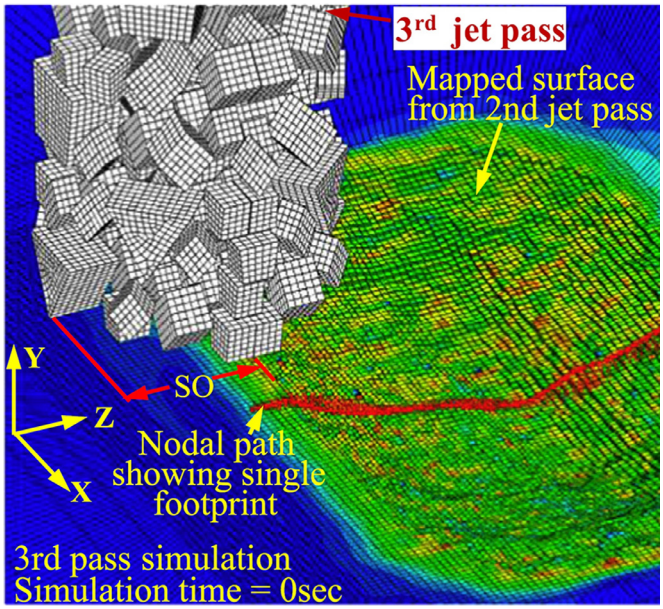

Fig. 18. Example of FE simulation of abrasive water jet milling, i.e., with controlled jet penetration, in which the jet containing various shapes of abrasives impact a flat workpiece (Ti6Al4V) surface [8].

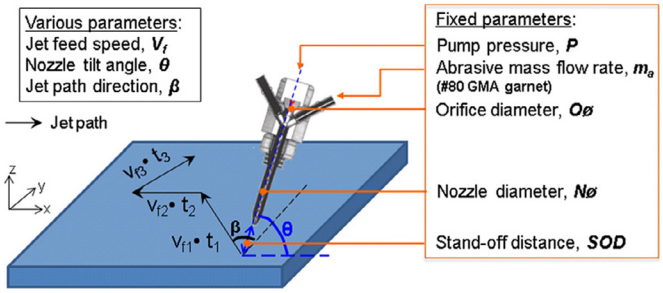

Fig. 19. Generic representation of jet-workpiece relative position and fixed/varying parameters to model the single/overlapped eroded footprints based on adjustment of kinematic parameters (i.e., jet speed feed and orientation) [147].

There is a common practice to keep these parameters constant as their in-process change is much slower than the speed of the material removal. This modeling approach allows for in-process adjustment only of kinematic parameters of the jet. This is a very effective way to online change the abraded footprint since the adjustment of these parameters can be speedily changed via G-code on which these machines run. Such approach has been implemented for generating surfaces (e.g., flat/ramped pockets) on a variety of workpiece materials from metals (e.g., Ti6Al4V, Nitinol) to ultra-hard ceramics (e.g., SiC).

However, for to the generation of complex, i.e., freeforms, by the overlapping the eroded footprints, a very big challenge appears, i.e., how to optimize he jet path considering that the target surface has varying gradients (that influences the shape and amplitude of the footprint). This is in the conditions of added complexity by the dynamics of the machine tool that could affect the dwell time when the jet moves on varying directions [106]. As such, the Direct Problem in fluid jet machining, i.e., given an abraded footprint that is dependent on the jet orientation vector and its feed speed, and a predefined jet path, determine the resultant machined surface, is by far inadequate because the errors between the resultant and desired surfaces significantly increase with their geometrical complexity. This results in an extensive trial and error experimentation with the jet path choice based on operator experience. Similar problem appears on other time-dependent jet polishing processes [38,206].

As such, the correct manner to address this challenge is to solve the “inverse problem” in fluid jet machining, i.e., given the model of the abraded footprint (dependent on the vector and feed speed of the jet) and the desired freefrom surface determine the optimal jet path [106]. For the first time Axinte and Billingham [15] have flagged up to the research community the necessity of this approach and the ways to numerically solve the inverse problem in fluid jet machining both on linear and non-linear conditions [107]. Various freeforms have been generated with a high level of accuracy only by optimizing the jet path and its exposure time (i.e., feed speed) upon the target surface, i.e., the inverse problem (see example in Fig. 20).

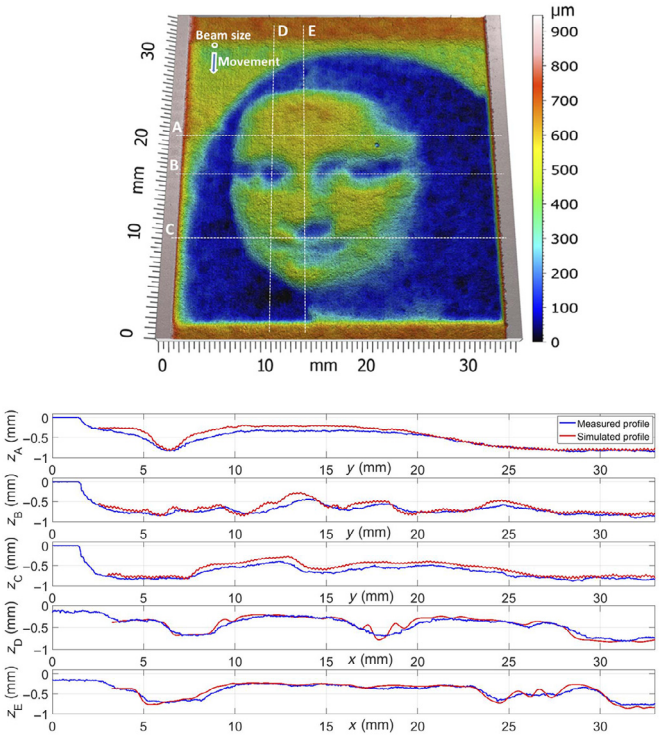

Fig. 20. Example of complex surface generated by abrasive water jet milling (without masking) by optimized jet path and its feed velocity by solving the inverse problem and errors between the programmed values across different directions [15].

3.3. Material removal by thermal energy

3.3.1. Laser machining

While lasers have been widely employed for through cutting, when it comes to the generation of freeform surfaces, the use of pulsed laser ablation (PLA) has been proven as a viable technology for micromachining complex structures within micron-scale tolerances and to cut virtually any material [143]. Being a time-energy dependent process (i.e., the amount of removed material depends on time exposure of the beam over a particular area, as well as the energy of the beam itself), PLA for generation of complex surfaces often requires experimental trial-and-error calibration to generate a desired workpiece geometry. This method is particularly time consuming. It is also not flexible, as any change in the machining requirements (e.g., size of the machined feature) or processing conditions (e.g., beam size) requires a separate trial-and-error calibration. As such, the use of predictive models to facilitate planning of the machining task could represent a significant improvement over current practices, even though this however doesn’t come without its own challenges.

Complete physical modeling of the ablation process to be translated to the prediction of the freeform machined surfaces represents a challenging and computationally expensive task, often infeasible for large structures with hundreds of thousands of pulses. The physical phenomena that occur during PLA span several time scales, ranging from picosecond (photon absorption, thermalization) [74], to nanosecond (phase changes, plasma formation) [40,207], microsecond (ejection [83] and re-solidification [40]), and all states of matters (solid, liquid, vapor and plasma). Often, physical models/simulations must rely on sets of assumption, such as constant material properties [206], a 1- or 2-dimensional domain [53,198], or simplified plasma dynamics [213], to avoid excessive computational time. Additional

issues are related to the presence of non-linear interactions between successive laser pulses, which render most of the current approaches to predict real output geometries inconclusive in industrial applications with thousands of overlapped pulses. This is further complicated when considering a moving laser source. In this case, the effect of the separation distance between pulses (i.e., feed speed) can assume a major role in dictating the degree of interaction, and hence, the material removal rate per pulse. When considering laser micromachining of metals, additional phenomena arise due to the presence of molten material, often present in significant quantity during ablation in the thermal regime. Some of the molten material is ejected [100], while the rest sticks to the surface giving rise to the characteristic redeposition pile-ups features produced on the side of an ablation crater. As such, all the above-mentioned phenomena occurring during material ablation are very difficult to be captured in a single model and further used for the prediction of the machined surfaces.

Approaches that (partially) circumvent the complex modeling physics of the material removal have been developed. One of this is the use of models based on machine learning. Such as neural networks [186,251]. These models are able to assess the influence of process parameters (feed speed, laser power) on the material removal rate, provided a clear relationship is present. This on itself represents a significant challenge, as the phenomenon of PLA is highly non-linear. Hence large datasets are required during the learning/training stage. The major advantage these approaches provide is the ability to obtain excellent prediction within the range of conditions for which the model has been trained, often better than any other simulation technique (e.g., models based on simplifying assumptions) that could be used. However, the requirements of large datasets, and the associated difficulties of producing them, severely limits the flexibility of these methods. These models are not able to produce sensible results outside the range for which they have been trained for, as any physical quantity (e.g., the relation between laser power and beam diameter) loses meaning, unless specifically considered during the model formulation, which adds complexity. As such, the training of a general-purpose model to predict PLA machining of a feature with an arbitrary geometry, i.e., freeform, can be excessively expensive in both time and resources, and often unfeasible in an industrial scenario.

In response to such modeling challenges, predicting tools for PLA complex geometry surfaces have been developed using models based on geometrical analysis. This approach is often the least computationally expensive, and therefore particularly suited to simulate large number of pulses. As such, it has attracted the most interest from an industrial application point-of-view. The majority of these models require calibration from experimental data. In some cases, the calibration is used to overcome gaps in the theoretical knowledge (e.g., material properties) [103], in others it can be used to capture the non-linear interaction between different pulses [52].

The simplest form of these models considers the material removal resultant from a single pulse, measured experimentally at the center of an ablation crater, and simulate the process by superposition of single-pulses footprints [103,146] (Fig. 21). Often this is done by considering the concept of threshold fluence required to remove a particular volume of material. In this scenario, while the physical process occurring during the ablation process is ignored, some physical relationships are conserved (e.g., the relationship between power density, the beam spot size and the stand-off distance are considered using the corresponding propagation law of laser beams).

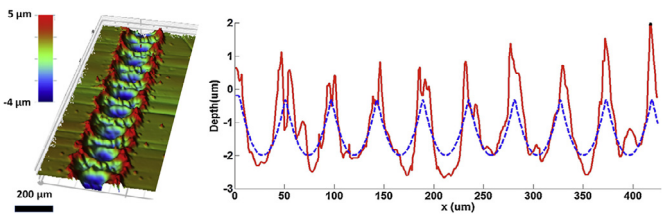

Fig. 21. Example of ablated track differences between experimental (solid red line) trial and simulation (dashed blue line) by convoluting a single pulse (with statistically modelled redeposition ring) along the scan direction of the laser beam (material = Inconel 718, fluence = 31.5 J/cm^2, speed feed = 1150 mm/s) [103].

This approach allows to simulate large (10^4) number of pulses with ease, and has demonstrated acceptable level of prediction accuracy, in particular for the case of low pulse overlapping. This approach can also account for the presence of molten material [146], as the footprint of the laser beam can be used to describe not only the volume of material removed, but also the volume of material redeposited. However, the interaction between successive pulses is not taken into consideration in these models, which introduce significant errors when the overlapping between pulses is high. To overcome this limitation, some models have tried to consider some of the non-linear effect present when overlapping multiple pulses. The model developed by Neuenschwander et al. [177] considers the reduction of threshold fluence by an additional functional equation of the form $F_{th}(N) = F_{th}(1)\cdot N^{s-1}$ which link the resultant fluence threshold F_{th} after the N_{th} pulse with the single-pulse fluence threshold $F_{th}(1)$ by use of an incubating coefficient $s<1$.

More recently, a novel class of models has emerged to allow simulation of any generic energy beam process [52]. Here, the material removal process is modelled by considering the footprint, i.e., trench, that is the result of a close overlapping of individual pulses, while the non-linearity of the process is modelled by use of an additional function which depends on the process parameters (e.g., feed speed). As such, treating the ablated footprint as a continuous trench is applicable since smooth surfaces are the target of pulse lase machining by having significant overlapping of the individual pulses. In this approach both the footprint, and the non-linear function are calibrated simultaneously on the same set of data over a range of process parameters (e.g., feed speed). This effectively allow to exactly define the behavior of the process within the calibration range, without imposing any constrains in the behavior of the process. The ablation rate, E, is calculated from experimental data using the profile of a trench. It was found that the profile of a trench at constant feed speed and power can be expressed as function of the effect of the pulse interaction on the profile depth. By performing few PLA trenches with varying feeds and powers, followed by their scanning to obtain the depth and profiles of the trenches, the model can be calibrated.

The application of this approach has successfully demonstrated to predict and account for the non-linear effects present during ablation of particular classes of materials (graphite and diamond) with excellent results [52]. However, the framework is currently not able to capture the effect and non-linearity intrinsically present in the ablation process due to the presence of material re-deposition that happens in most of PLA applications. Following on this approach, Cha et al. formulated a combined model that captures the change of both shapes and amplitudes of removed and redeposited material dependent on dwell-time [61]. The model takes into account the footprint (i.e., shape) of the crater produced by a single laser pulse which includes both material removal via vaporization and melt displacement/ejection, representing the dominant processes in nanosecond PLA of metals, as well as material redeposition (Fig. 22).

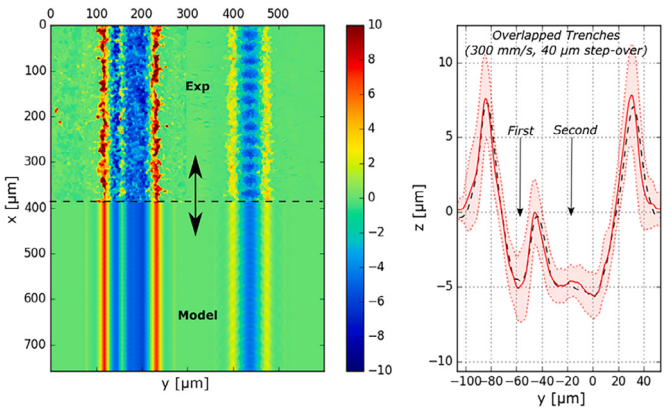

Fig. 22. Example of calibration for overlapped laser ablated trenches (i.e., small pulse overlapping) modeling using 2 trenches at 300 mm/s: (left) experimental and modelled surfaces, (right) comparisons of average section profiles; Ti-superalloy sample at 70% power (12 W) [61].

The behavior of molten/redeposited material during PLA of metals can also be encapsulated in this approach. All the above models treat the "direct problem", which as commented in the paragraph 3.2.3 does not lead to low machining errors and still does not solve the need for trial-and-error approach until the "optimized" beam path and scan velocity is achieved. As such, again, there is the need to solve the actual problem in PLA, i.e., the "inverse" one [107]. By using this comprehensive approach Axinte and Billingham [15] have successfully demonstrated, by numerically solving the inverse problem, that the laser path can be truly optimized to obtain high accuracy freeform by PLA (see Fig. 23). However, these modeling approaches cannot cover laser polishing [187,192] that involves complex liquid surface tensions, mass transfer, etc.

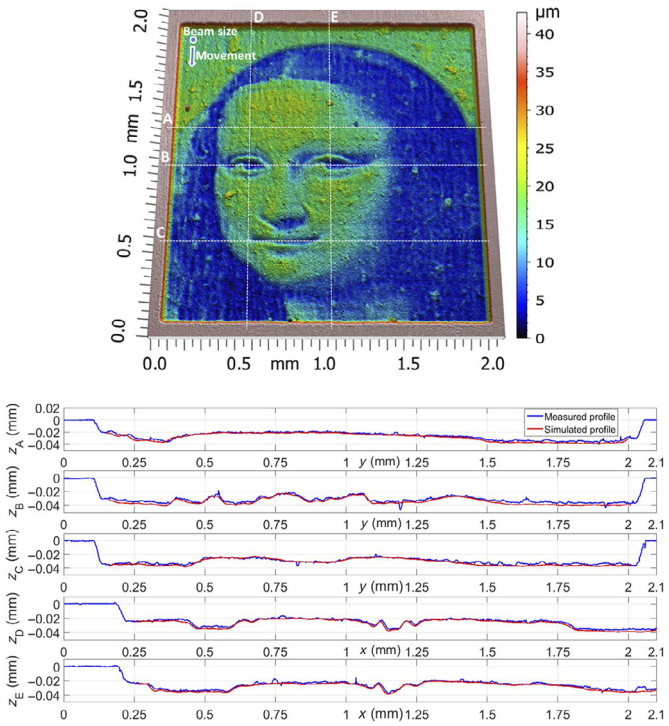

Fig. 23. Example of complex surface generated by PLA by optimized laser beam path and its feed velocity by solving the inverse problem and errors between the programmed values across different directions [15].

3.3.2. Electrical discharge machining

In electrical discharge machining (EDM) the removal action is essentially generated by a thermal input. Material is removed from the workpiece surface in discrete units by means of electrical discharges occurring between an electrically conductive tool and workpiece electrodes. The discharge cycle involves formation of arc plasma, localized heating of workpiece, tool and dielectric fluid, the formation of a local melt pool of material on tool and workpiece in correspondence of the discharge location, the formation and expansion of a gas bubble in the dielectric, ejection of molten material from the melt pools, collapse of the bubble and flushing of material debris. The gap is filled with dielectric fluid, gas bubbles, as well as tool and workpiece material debris so that the conditions in the gap vary over time and location. Thus, the complexity of the phenomena involved in material removal by electrical discharge machining makes modeling of surface generation particularly challenging. As material removal occurs also on the electrode, its change in geometry must be considered as well.

Surfaces generated by EDM consist of a distribution of small craters revealing the solidification of part of the material melted during the discharge cycle. For a given combination of tool and workpiece material and dielectric fluid, the size of individual craters is largely determined by the discharge energy. Therefore, in EDM processes, the surface topography is strictly connected to the average discharge energy and, for a stable process, is well reproducible. The main concern of surface generation modeling in EDM is then related to the accurate prediction of the part geometry and thus, to the material removal distribution in time and space. The spatial distribution of the craters is strongly affected by the conditions in the gap. As the material removal distribution depends on dimension and location of the craters, modeling of surface generation requires modeling of both aspects of the process. Hinduja and Kunieda [122] describe a generalized modeling framework for the EDM process (Fig. 24) starting from the identification of individual discharge location and sequentially followed by simulation of arc plasma, calculation of the temperature distribution, simulation of the removal by a single discharge, simulation of the flow field in the gap, including bubbles and debris, and ending with the definition of the new geometry after the discharge cycle. The sequence involves multiphysics modeling that can be implemented for the simulation of a single discharge. While this approach supports development of a deep understanding of the material removal action, the actual process involves the generation of multiple discharges at a high frequency. Due to the varying conditions in the gap, the outcome of multiple discharges cannot be obtained by simply superposing the results of single discharges [185]. With material removal per discharge that can be as low as 1 μm^3 [35], the removal of even small amounts of material requires billions of discharges. Therefore, modeling of surface generation in EDM to obtain the final geometry of a part cannot be obtained by modeling such a large sequence of discharges.

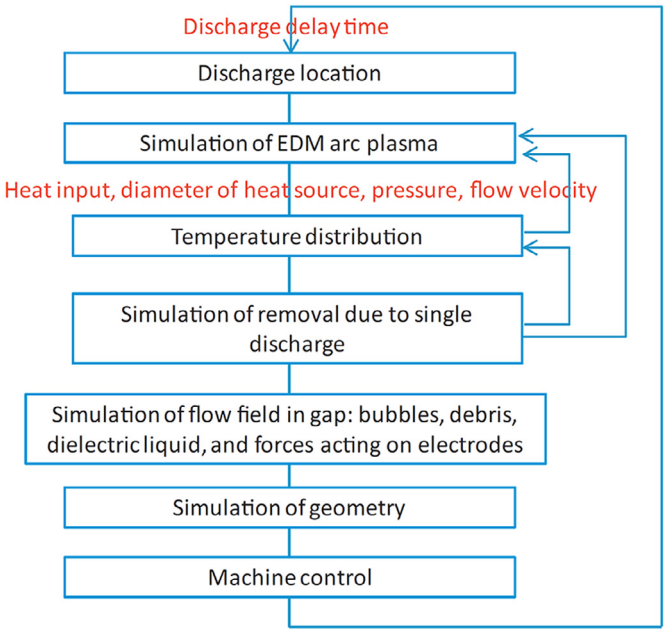

Fig. 24. Generalized model for EDM processes [122].

Simulation of material removal due to single discharge has been obtained based on temperature field calculation enabling the estimation of the material volume above melting temperature as proposed by [185]. However, actual removal occurs when the pressure in the molten pool exceeds the pressure in the gap [244] and ejection of material is hindered by the increased pressure due to bubble formation and expansion. Therefore, only a fraction of the molten pool of material is removed, estimated between 1% and 10% [122]. The largest part of the molten pool remains on the workpiece surface so that the effective material removal unit is much smaller than the size of the melt pool.

While single discharge modeling provides the means of exploration of the wavelength components of the part surface contributing to the definition of the surface topography, essentially represented by the craters shape, modeling of part geometry in EDM requires different approaches. The amount of the material removed from the two electrodes is determined by the discharge energy distributed to tool and workpiece and the diameter of the arc plasma [145]. The average discharge energy therefore determines the material removal unit, namely the resolution of the process. When the process

resolution is defined, modeling of the spatial distribution of the discharges is the key to modeling the part geometry.

In stable processing conditions, modeling of the part geometry in EDM can be obtained by assuming an average value of the material removal per discharge (MRD) or the tool wear per discharge (TWD). This approach can be convenient in process configurations where a geometrical constraint on the discharge location is provided such as EDM milling, EDM drilling and wire EDM. In [39] real time sensing of the discharge signals is used to count effective discharges in EDM milling and assigned an average TWD to each effective discharge. The calculation of the real time cumulative electrode wear thus enabled tool wear compensation by displacing the electrode axially and maintaining a constant gap. In [121] a virtual micro EDM milling simulator is developed that uses an independent Z-maps for tool and the workpiece with equal sized square elements. The material removal unit is determined through measurement of single discharge experiments in constant process settings. In the simulation, the material is removed at the locations with shortest distance between tool and workpiece and a nominal discharge frequency along the tool path is used. Considering the large number of discharges necessary for practically measurable material removal, Bissacco et al. [36] assumed that, in micro EDM milling, machining occurs by means of trains of discharges with identical distribution as that of the entire discharge population. Thus, a material removal per discharge (MRD) and a tool wear unit per discharge (TWD) of the population can be used, in combination with the nominal tool path to calculate the part geometry errors. In [37] a material removal simulation tool is developed using nominal the tool trajectory and counting the discharges for real time display of the part geometry (Fig. 25). In the simulation tool, the path interval is divided into elemental segments. The tool electrode and the workpiece are discretized in a number of dexels with square footprint equal to the average area of the discharge craters measured for the specific process settings. The simulation output consists of a areal data file suitable for analysis in image processors for measurement of part geometry.

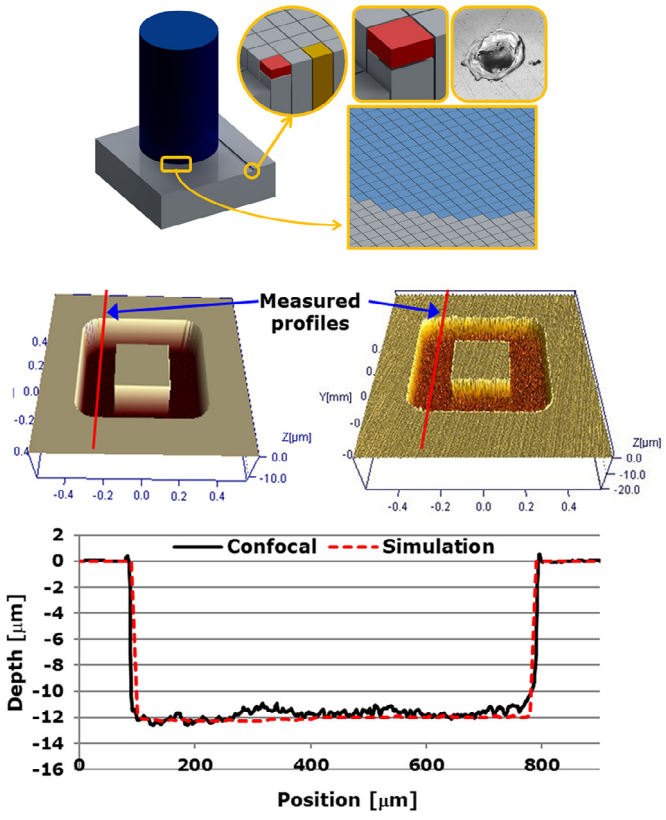

Fig. 25. Top: Schematics of the micro EDM milling simulation tool. Bottom: Comparison of measured and simulated geometry [37].

Due to electrode wear, sinking EDM requires the preparation of multiple electrodes to obtain the desired workpiece shape. Reverse simulations can be used to obtain a suitable tool electrode geometry, allowing the production of a complex part using a single electrode. Kunieda et al. [152] developed an inverse simulation method, based on the discharge location search algorithm presented in [176]. In the inverse simulation, the workpiece is treated as the electrode and fed towards the tool, and the final shape of the workpiece is regarded as its initial shape. Tool electrode, workpiece and the gap space were modeled using voxels. Experimental validation, carried out on simple conical shapes, showed that using the tool electrode obtained by reverse simulation, the workpiece shape error is reduced in comparison to the standard approach, where the tool electrode shape was obtained by offsetting the target workpiece shape with a distance equal to the gap width.

Surleraux et al. [211], proposed a machine learning based inverse model for tool shape optimization in micro EDM sinking, where the material removal unit is considered to be a spherical cap. The approach uses a predictor/corrector algorithm where the predictor step is a direct simulation of the die-sinking μEDM process, for a given iterate of the tool geometry, while the corrector step changes the shape of the tool, in an attempt to reduce the distance between the nominal target geometry of the cavity and its simulated counterpart. The ANN model was trained using resilient backpropagation algorithm with 30 different profile features. The model was applied to training sets with constant process settings, yielding an average shape error of the part produced with the optimized tool geometry within less than 4 µm and slightly more than 4 µm when the training was done with variable process settings.

3.3.3. Focus ion beam machining

Focused Ion Beam (FIB) uses accelerated ions (e.g., Ga), under vacuum conditions, that transfer their energy to the target surface from which the material is removed by momentum transfer in a process, usually called sputtering, on which ions or neutral atoms are removed. Among the secondary effects of FIB milling could be mentioned: ion implantation and redeposition of the sputtered ions which could affect the accuracy of the surface to be generated. FIB is used for micro/nano material removal which makes it an useful tool for microelectronic applications (e.g., chip repair), Fresnel microlenses, sample preparation, micro-tools, indenters and surface micropatterning [154]. However, choosing the workpiece and suitable ion combination, the material removal, as for other energy beam processes is mainly dependent, on the momentum (via acceleration energy) [25] and impact angle of the ions [243] as well as on the beam dwell-time [127] (dependent on the scan speed). The common approach by which features are FIB milled is to move the beam (with a constant dwell-time) in a succession of discrete points along a raster path and remove the material in a layer-by-layer manner. Of course, the increase of discrete points will result in added computational costs while the generation of freeforms depends on skillful selection of the etching patterns. As such, models to enable the control of FIB milling of complex surface have been developed. Borgardt et al. [41] reported on a model to determine the ion dose to enable the prediction of the FIB milled trenches/pockets in absence of sputtering effect and at small beam incidence angle.

Vasile et al. [222,223] reported on a comprehensive removal model that considers the dependence of sputter yield on the energy and the incidence angle of the beam model [243] on which a FIB of particular energy distribution (e.g., Gaussian) exposes individual pixels with varying dwell-times. To obtain smooth surfaces, the pixel dimension must be smaller than beam diameter. However, this implies that there is a need to consider the dependency of how the material removal in a certain pixel depends on the similar process happening at the neighbouring pixels.

Platzgummer at al. [190] have reported on a software (“Ionshaper”) which explicitly tracks the surface while being able to take into consideration side effects of the process such as material redeposition and secondary etching induced by the reflected ions. Kim et al. [138] presented another software (“AMADEUS 3D”, Advanced Modelling and Design Environment for Sputter Processes) and its validation, capable of simulating the areal surface topography including

angle-dependent sputtering and redeposition. On another approach, Ertl et al. [94] uses level set method for solving the time-dependent etching problem and develop a profile simulation for FIB milling topography. The validity of this has been demonstrated by etching of flat pockets.

Using the idea of a time-dependent etching rate that is the resultant of three different contributing functions (*E*, removal rate profile across the beam; *G(z)*, influence of the beam incidence angle relative to the surface; *F(z)*, effect of etching reduction caused by ion implantation, so called swelling effect, occurring at small dwell times of the beam) of etching describing different physical aspects of the removal process, Guillerna et al. [108] have solved and demonstrated the direct problem in FIB by generating real freeform surfaces. The model uses a number of coefficients that can be calibrated on the FIB machine via milling some trenches (as in the previous [15]) to determine a vector of constant parameters that characterize the model for each pair of machine set-up and material, and it is eventually able to calculate the Cartesian coordinate system (*x, y, z*) over time.

All the above models deal with the direct problem in FIB milling. However, as for other time-dependent processes, the correct approach for minimizing the errors when FIB milling of complex geometries is to address the inverse problem. As such, Axinte et al. [15], have included the approach of Guillerna et al. [108] into a generic modeling framework for solving the inverse problem in energy beam machining have generated freeform surfaces in FIB milling at very low errors (Fig. 26).

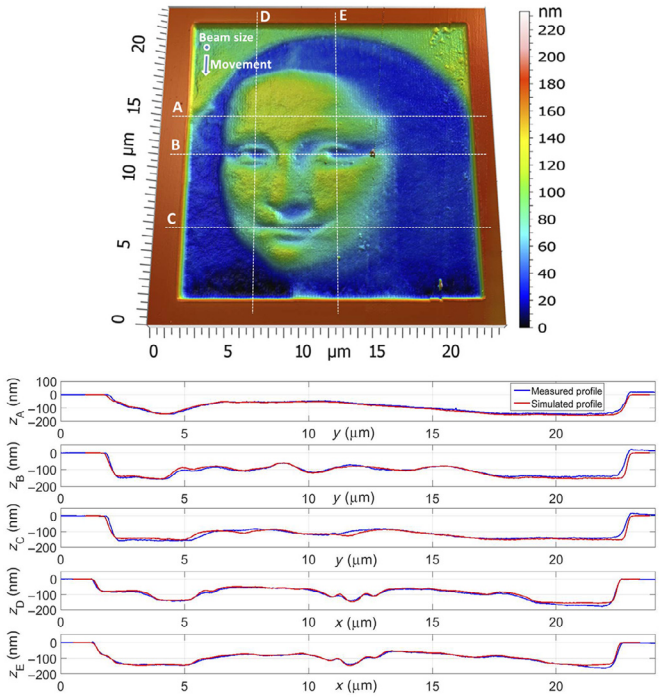

Fig. 26. Surface generated by Focus Ion Beam by solving the inverse problem and various cross sections comparison between measured and simulated surfaces [15].

3.4. Material removal by electrochemical machining

Electrochemical machining (ECM) is a non-contact controllable dissolution process [70] where a tool electrode (cathode) and a workpiece electrode (anode) are separated by a flowing electrolyte fluid. The material of the workpiece is removed by electrolytic dissolution of the anode until it is shaped. Main advantages of ECM are a relatively high material removal rate in combination with almost zero tool wear and no thermally or mechanically damaged workpiece rim zones [141]. Modeling surface generation in terms of part geometry and topography in ECM requires accurate modeling of the phenomena involved in the material removal action. Although the fundamentals of the overall process have been well known for decades [172], the phenomena affecting the spatial distribution of the material removal are still rather complex to simulate accurately.

The workpiece shape change in ECM is dependent primarily on the current density on the anode surface [122] which is affected by the spatial and temporal distribution of the ions' concentration, oxygen and hydrogen bubbles, the electrolyte flow (which can be laminar or turbulent) and the temperature distribution within the electrolyte affecting its electrical conductivity. Also, the workpiece material microstructure affects the achievable surface topography. The final geometry of the workpiece is closely related to that of the cathode tool electrode and therefore the main purpose of modeling the material removal distribution in ECM is the validation of the cathode geometry. However, the direct simulation assumes a defined geometry of the cathode and several iterations are necessary to define the optimal cathode geometry.

The earliest analytical method to calculate the workpiece geometry is the so-called cosθ method employed by Tipton et al. [215] who suggested that the gap width between cathode and anode surfaces is proportional to cosθ (where θ is the angle between the feed direction of cathode and the normal to the anode surface) [97].

Modeling of the dissolution process at the anode is based on Faraday's law of electrolysis and on this basis, potential and multi-ion models have been developed and continuously refined. In [42] a two-dimensional multi-ion transport and reaction (MITReM) model is developed. Deconinck et al. in [80] and [81] further extended the model considering concentration dependent diffusion coefficients and as well as the effects of water depletion and the temperature dependency of electrode reaction kinetics, diffusion coefficients of all ions and viscosity of the electrolyte fluid. The computed quantities are potential, temperature, fluid velocity, pressure, and ion concentrations. The equations used are the electroneutrality condition, charge conservation, the laminar Navier-Stokes equations for viscous incompressible flow, the internal energy balance and ion transport equations.

In [141] a three-dimensional multiphysics simulation model of the ECM process is developed based on conservation equations for the electric field, fluid flow and heat transfer in combination with analytical functions for the influence of temperature and gas evolution on the specific electrical conductivity. The model considers the variation of the electrical properties of the electrolyte as it flows along the working gap and includes a turbulence model to account for turbulent flow (Fig. 27

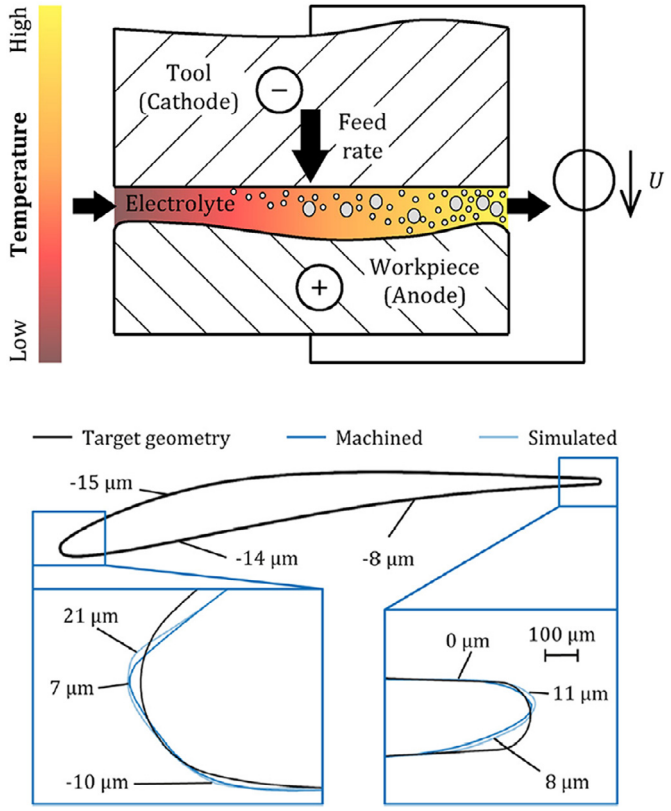

Fig. 27. Top: concept of the fluid-dependent material removal during ECM. Bottom: simulation and machined geometry comparison, with local values of difference between machined and simulated geometries [141].

top). The evolution and transport of hydrogen and its influence on the electrolyte conductivity is modelled as a two-phase bubbly-flow. The model is verified experimentally and applied to the optimization of the production of an engine blade, showing good correlation between the simulated and machined geometries, with maximum deviations in the order of 20 µm (Fig. 27 bottom). The model is further applied to the optimization of the cathode geometry.

In [97] an optimization method is developed based on an iterative solution of a multi-physical model of the gap distribution to improve the design accuracy of the cathode shape in PECM. The model used a two-phase bubbly-flow representation of the electrolyte. Van der Velden et al. [219] developed a modeling approach for the material dissolution based on the concept of effective physical properties, through the introduction of the effectively dissolved volume V_{eff} as an experimentally detected material parameter which considers anodic gas evolution as well as additional chemical reactions. The model avoids remeshing and, thus, allows for the simulation of the entire process with one mesh. The authors utilize a transient, electro-thermally coupled finite element formulation to accurately model the principal impacts in ECM and to account for the interaction between the electric and thermal field. The model was tentatively applied to the prediction of surface topography in PECM. In a following work [220], extended the model to arbitrarily shaped and moving cathodes and applied it to the simulation of blade machining. In [142] a model for anodic dissolution of multiphase alloys is presented. The model enables the simulation of surface generation of the anode at the roughness level. The model considered the existing anode material microstructure and the electrochemical behavior of each single material phase. The potential drop at the anode due to double-layer and oxide formation (for passivating electrolyte systems) is modeled by means of a thin semiconductor layer. The model is applied to steel 42CrMo4 with a ferrite-perlite grain structure, where the differing dissolution properties of ferrite and cementite, which form the perlite phase, generate characteristic surface structures. The model is constituted by domains representing the ferrite and cementite lamellae within a perlite grain (Fig. 28 top). On each lamella a semiconductor layer is implemented, and each phase is linked with a characteristic current potential curve. The electric current density at the surface of the cementite lamellae is significantly lower than in the areas of ferrite lamellae. As a result, the cementite lamellas is shown to protrude with respect to the ferrite phase (Fig. 28 bottom).

Later et al. [24] showed that the model from [142] is quantitatively compatible with the measured cementite lamellas height (in the range of 0.7–1 µm depending voltage and feed rate) and explained the formation of flow grooves on the anode surface.

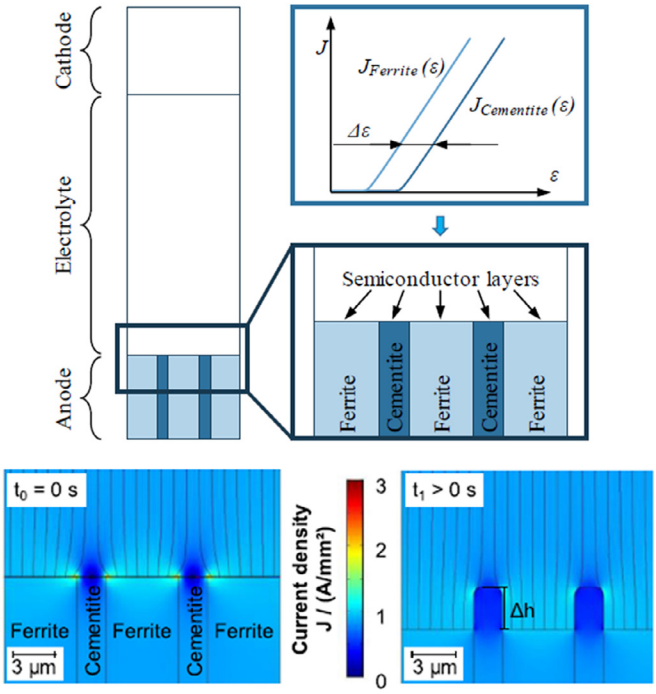

Fig. 28. Top: schematic of ECM of perlitic steel; bottom: simulation of surface generation in ECM [24,142].

4. Modeling of surface generation by material conservative processes

We classify those unit manufacturing processes that alter the part geometry without changing the overall part volume as material conservative processes, such as metal forming, injection molding, hot embossing, nanoimprinting, etc. One common theme of those processes, particularly for high volume production, is the usage of a tooling system (called die or mold), which is often fabricated and finished using the subtractive processes described in Section 3. Therefore, surface characteristics of tooling can have a direct impact on the resulting surface of workpieces in material conservative processes as discussed. In this session, we will review the formation and corresponding simulation of surface replica (i.e., surface texturing) from metal forming textured tools in Section 4.1.1, the transformation of asperity in metal forming in Section 4.1.2, injection and micro injection molding in Section 4.2, polymer micro/nano hot embossing in Section 4.3, thermal and ultraviolet nanoimprint lithography in Section 4.4.

4.1. Metal forming

4.1.1. Modeling of surface texturing

Surface texture, including micro-dimples or micro-channels, has found many engineering applications (e.g., drag reduction, friction reduction and the improvement of heat exchange efficiency) and aesthetics applications. Depending on the applications, feature sizes can vary from 10 s – 100 s µm in the planar direction and 1 s – 10 s µm in the depth direction. The transition radii can be as small as a few micrometers. Due to the large size difference between the feature size and part geometry, there exists common approaches (e.g., using continuum elements) between numerical simulations of surface texturing in bulk metal forming processes (such as forging) and sheet metal forming (such as stamping).

One most critical aspect in simulating surface texturing in metal forming is the consideration of grain size, which has three aspects: (a) grain-size dependent material constitutive model; the conventional approach is to follow the well-known Hall-Patch relation, i.e., the yield strength of the material is inversely proportional to the square root of the average grain size. However, when the average grain size is comparable with the minimum feature size in forming, the experimental results start to deviate from simulation results using the above Hall-Patch equation. Geiger et al. [102] first reviewed this phenomenon in cup extrusion and raised the need of a better model. More experimental results showed the aggregated stress-strain relationship in tensile tests or shear tests, or micro extrusion, or micro sheet forming. Consequently, a model of the overall stress-strain behavior consisting of (b) the combination of the surface layer (weak part) and the inner layer (nominal and strong part) was proposed as the engineering solution [93,188]. This approach has been extensively reviewed by Vollertsen et al. [225]. While this averaged or homogeneous approach can explain the reduced forming force seen in microforming, it cannot explain the inhomogeneous deformation or randomness of deformed shape observed in [150]. It was later explained and well-accepted in the forming community that (c) modeling polycrystalline microstructure is necessary to capture the deformation randomness as the spatial distributions and orientations of grains also affect the deformation process and hence, the predictions of final geometry and the resulting stress states. Zhang et al. [255] developed a software system (VGRAIN) that used the controlled Poisson Voronoi tessellation (CPVT) to generate the polycrystalline grain structure, which can match physical observation of grain size distribution. Fig. 29 shows the dramatic difference in surface finish of a plane strain deformation of a 100 × 30 µm specimen with the same mean grain size of 50 µm^2, but with different regularity.

The extension of the method to 3D is not trivial and has been reported in Schneider et al. [199]. Mechanical properties of each grain can be modelled using crystal plasticity and with the extension to

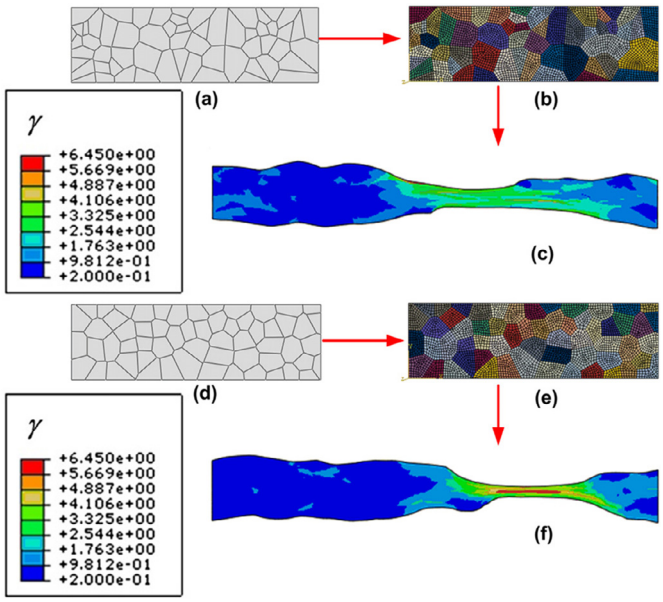

Fig. 29. Simulations of tensile deformation in the horizontal direction with irregular (a) and regular (d) grain structures [255].

strain gradient, which by itself is a very rich research topic. One example of considering crystalline microstructure in microrolling of textured surface can be found in Zhutian et al. [241], which shows a noticeable difference as shown in Fig. 30. Another example is the multi-scale simulation of incremental bulk forming to form stiffening ribs with a particular surface pattern presented by Szyndler et al. [212]. In addition to the efforts on modeling material behavior as discussed above, it has been shown numerically (Fig. 31) [195] and experimentally [150,175] that friction behavior plays an important factor in filling the die surface structures [57].

4.1.2. Modeling of asperity transformation

Metal forming can flatten asperity due to plastic deformation. One classical example is the shining surface of aluminum foil generated through the contact between the aluminum work piece and the roll in the rolling process. In recent years, hybrid additive manufacturing processes (i.e., additive manufacturing + forming) has provided additional enhancement of mechanical properties and surface finish [231].

Asperity flattening study can be extremely computationally intensive. An early study [165] developed a two-dimensional FEM model shown in Fig. 32, in which the surface roughness of the workpiece is simplified by a three-wavelength model, generated based on a power spectral density (PSD) analysis of measured data on steel sheet surfaces. The sophistication grows as computational power increases, as evident in [179], where the geometry of tool was modelled more explicitly, and in [113], where a more realistic initial surface profile was employed. Here it was found that the surface roughness of the formed part depends approximately linearly with respect to the normal contact pressure and the initial surface roughness of the workpiece (see Fig. 33), and has an exponential dependency on the surface area enlargement rate.

To reduce computational cost, elasto-perfectly plastic (EPP) modeling is often used for analyzing asperity flattening, and two methods can be adopted, i. e., to truncate the pressure peaks at a certain times of the initial yield stress σ_y, for example, $p = 2.31\sigma_y$ if the von Mises stress is calculated, or to use a plasticity model to track the stresses and strains in a contact simulation [229]. A three-dimensional elasto-plastic contact model for repeated rolling and sliding contacts of a spherical indenter over a half-space was developed in [63]. This model employed a universal integration algorithm for elastoplasticity involving isotropic and kinematic hardening and showed the surface evolution due to several cycles of repeated loading. A more sophisticated model should consider the heat generated during the contact process at the presence of the relative sliding between the tool and the workpiece. Zhang et al. [257] calculated the heat distribution between the tool and the piece using the conjugate gradient method (CGM) for searching the

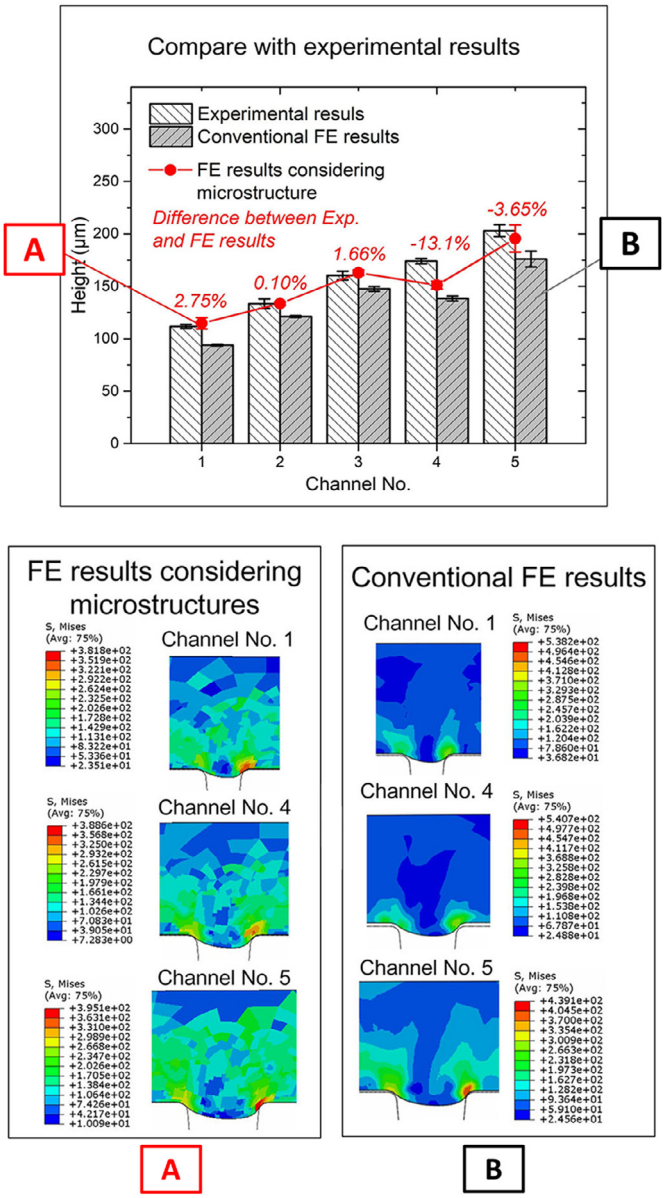

Fig. 30. Comparison between simulations and rolling experiments considering crystal orientation (A) and conventional FEM results (B) [241].

distributed tool-tip/sheet heat partition and the fast Fourier transform (FFT) for obtaining temperature solutions. The resulting temperature can be further incorporated into the material property of asperity in asperity transformation simulations.

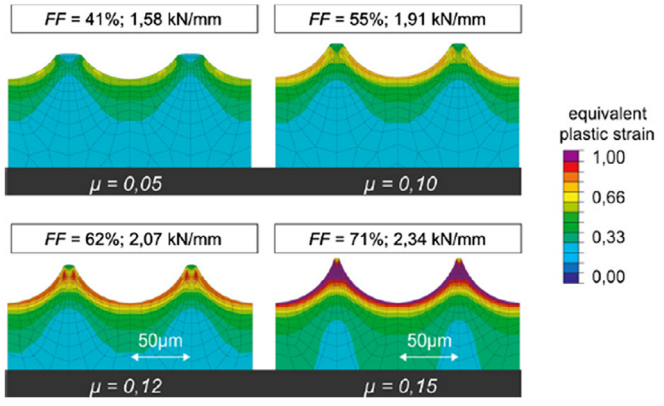

Fig. 31. Variation of riblet filling in cold rolling due to friction variation [195].

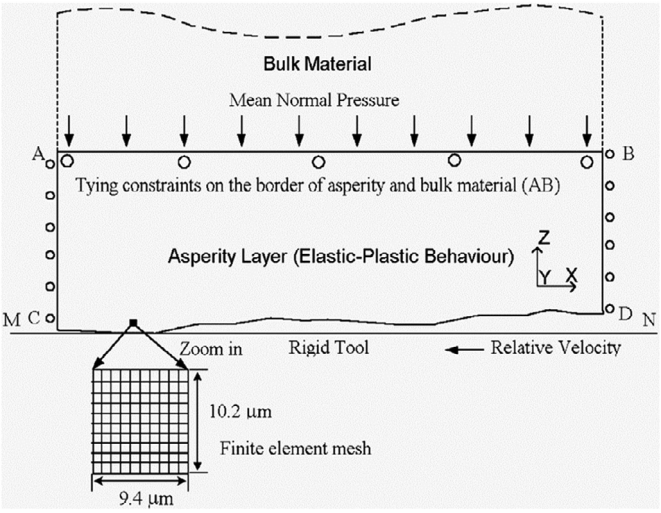

Fig. 32. Illustration of simplified asperity-flattening model setup and finite element mesh [165].

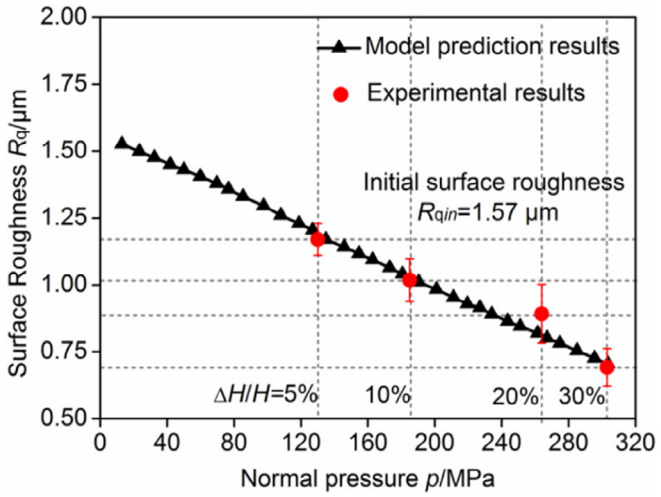

Fig. 33. Comparison of the experimental and predicted results under various normal pressures [113].

4.2. Injection molding

Process simulations have been successfully implemented in the field of injection molding (IM) for more than three decades, but it is only more recently that time and mesh resolution, along with the correspondingly required computational power, have reached such resolution levels to allow for simulation of surface generation at the micrometer scale, and in some cases at the sub-µm scale. For the case of the injection molding process, a wide range of established solutions are available and exploit different methods and software packages, along with emerging techniques for more advanced applications, particularly in the lower end of the dimensional scale.

From a modeling perspective, there are three aspects to be addressed: the physical governing equations and their associated boundary conditions; the solution domain and meshing; and the numerical method employed to solve the system of equations. The state-of-the-art in the modeling the IM process consists in the combination of two dominant physics: fluid dynamics and heat transfer. The fluid dynamics material domain utilises a Generalised Newtonian Fluid (GNF), characterised by a shear rate dependent viscosity model. With the GNF approximation, it is possible to model the polymer melt flow with a form of the Navier-Stokes equation in which the stress tensor includes shear dissipation and neglects turbulence as Reynold's numbers are expected to be close or less than 1 [162]. The heat transfer domain is described by an energy balance. Here melt compressibility and heat conduction, shear heating and the heat released during solidification are considered. The final model is eventually based on the conservation of mass, conservation of linear momentum and the energy balance, considering the temperature, density, thermal conductivity and velocity of the melt, the pressure, the viscosity, the specific heat, the isothermal volume expansion coefficient, and the heat released during melt solidification per unit time and unit volume. To consider the polymer melt properties evolution during the processes two relationships are introduced in the system: a shear- and temperature-dependent viscosity model and a pressure-specific volume-temperature property relation. The first is typically represented by the Cross-WLF model description that takes into account the temperature-dependent viscosity at zero shear rate, dependent on the glass transition temperature for amorphous polymer material, or generally on the reference temperature, that can be expressed as a function of pressure. For particularly thin cavities and highly deformed polymer flow, the Cross-WLF viscosity model is not sufficient and is corrected using an extensional viscosity model [162]. Polymer relaxation is the elastic response to the compression that stochastic polymer chain entanglements and orientations produce. A viscoelastic model can be used to describe relaxation phenomena [248]. Those phenomena occur for features smaller than 1 µm, which is often the maximum polymer chain entanglement length [162]. Due to the direct link with the dimensions and type of polymer chains, relaxation phenomena are also described as microviscosity [17,226]. Microviscosity can be introduced into the conventional Cross-WLF viscosity model using an approach presented by Rosenbaum and Hatzikiriakos [196].

At the micro and sub-micro scales, particularly relevant for simulating surface generation in injection molding, the previously mentioned governing equations might require additional physics that find more considerable significance at those dimensional scales. One of these aspects is the capillarity of the polymer melt and the effect of melt surface tension [54]. In the replication of micro and nanostructures, the wettability of the cavity surface has an effect on the flow front propagation when filling those structures. Wettability depends on the mold-polymer materials and on the geometry of the surface features [162]. A method to estimate the effect of surface tension based on temperature-dependent contact angle measurements and different material combinations was developed by Rytka et al. [197]. Once a surface tension model is found, it is possible to add the surface energy contributor as generalized stress in the model [72]. The combined effects of surface energy and air trapped counterpressure on polymer surface replication are modelled in [189].

Another aspect considered in the simulation of microstructures polymer molding is the appearance of the melt slip at wall when certain flow velocity conditions are met. Typically, in conventionally-sized injection molding, the hypothesis is that the velocity of the melt flow at wall is zero along the entire surface of the cavity. However, wall-slip may occur in case of high shear stress at walls, adhesion and polymer relaxation. A definitive wall-slip model is currently not available and extensive experimental validation has been carried out to characterize the phenomenon, which is inherently unstable and time-dependent [91,116,173]. To estimate the effect of wall-slip, a method based on inverse measurements of the effective cavity pressure drop using in-cavity-sensors was presented in [164]. This leads to the definition of the shear stress and consequently, the velocity at the wall [162], and, in turn, to a more accurate prediction of the generated surface.

Regarding energy and heat transfer, another property that has a direct effect on the surface generation modeling is the Heat Transfer Coefficient (HTC). HTC depends on process parameters selection and also on mold surface textures, which is particularly relevant in injection molding modeling at the microscale. It has been shown that HTC needs to be locally increased with respect to default values in case of microstructures replication [240,252]. HTC values optimized for micro scale simulation leads to a more accurate surface temperature prediction, that in turn can lead to better surface generation simulation. Babenko et al. [18] demonstrated that an average HTC lead to a misprediction of the surface cavity temperature up to 25 °C. With HTC values increased by a factor 5–10, simulated temperatures could be validated with thermo-camera measurements. Mold temperature also has an effect on injection pressure, so the HTC can also be

derived from in-cavity sensors using a numerical inverse-analysis as demonstrated in [164].

Several of these aspects have been implemented in injection molding simulations to predict surface generation at micro down to the nanoscale using finite element methods and molecular dynamics respectively of features such as slots, channels and pillars (see Fig. 34).

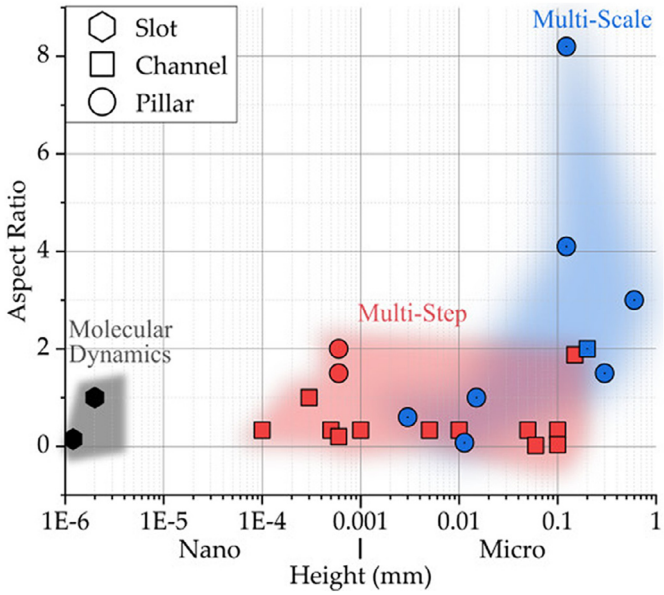

Fig. 34. Comparison of injection molding simulations methods according to micro/nano structures aspect ratio, height, and type of geometry [163].

On this regards, generally two simulation approaches can be identified: (i) multi-step simulations, where a macro scale simulation of the whole component is first performed to determined the boundary conditions at the surface, and then a subsequent simulation of only a fraction of the micro structured area is simulated using as input the pre-calculated boundary conditions (e.g., [197]); (ii) multi-scale simulations, on the contrary, integrate on the same model both the macro geometry and the micro structured surface area, so that the flow characteristics within the component and at the surface region are simultaneously determined (e.g., [171]).

4.3. Hot embossing

Hot embossing is a type of compression molding technology in which a tool is pressed against a thermoplastic foil or thin sheet near its glass transition temperature to produce micro and nano structured polymer surfaces. Typically, the challenges in hot embossing are: (i) to achieve full replication of micro down to nano structures over relatively large areas; (ii) to be able to limit the lateral shrinkage of the thermoplastic substrate upon cooling in order to preserve the structures integrity [104]; (iii) to achieve a successful demoulding of especially protruding features (such as thin walls and micro pillars) which are notoriously difficult to be released from the stamper.

Modeling and simulation of surface generation in hot embossing have been developed during the past 20 years to optimize both the process and the product design and specify the most suitable process window in terms of substrate temperature, compression speed and pressure, holding and cooling time (and therefore cooling rate), demoulding temperature, speed and force [90,232]. Typical thermoplastic materials used in hot embossing and that have been characterized for process simulations are polymethylmethacrylate (PMMA), polycarbonate (PC), polystyrene [68], polylactic-co-glycolic acid (PLGA) [227].

Shen et al. [202] presented in 2002 perhaps one of the first analytical models for the prediction of the achieved height of micro features (pillars) considering key process and material parameters such as applied pressure, surface tension force and interfacial shear force between the flowing polymer and the mold material. Micro features replication is generally improved by applying increased embossing pressure and temperatures, typically in the range of 20 °C to 40 °C higher than the glass transition temperature [204]. The effect of the micro feature geometry was investigated in [249] for features with depth ranging from 200 µm down to 6 µm. A two-dimensional simulation of hot embossing of micro walls with height of 70 µm and width of 70 µm was presented in [134]. A prismatic triangular shape (height 25 µm, width 50 µm) was simulated by Sun et al. [209] and validated by experiments demonstrating that optimal conditions for micro replication of PMMA include an embossing temperature of 105 °C and the substrate pre-heating at 110 °C.

Lin et al. [159] proposed the theoretical model for predicting the shrinkage based on the pressure-specific volume-temperature (pvT) characteristics of the material, as well as the pressure distribution over the embossing area and the demoulding load. The demoulding force depends on mold design, feature sidewall, applied pressure, material properties, demoulding temperature [181].

Integrated three-dimensional multi-scale and multi-physics simulations of hot embossing including both the component and the micro features (see Fig. 35) have been demonstrated [67,131,235]. Models are able to predict the micro cavities filling (see Fig. 36) and the demolding phase considering key characteristics such as polymer viscoelasticity (creep and relaxation), contact and friction conditions, strength of the material during demolding [256]. Using a multi-scale meshing approach, up to a quarter of 8-inch large wafer stamper was modelled and the effect of shrinkage on micro feature integrity prior demoulding was simulated [236]. The effect of a Teflon-based release coating to enhance the demoulding performance one single feature in hot embossing was numerically modelled by Guo et al. in [109] at micro scale and by Zhang et al. [257] at the 100 nm scale.

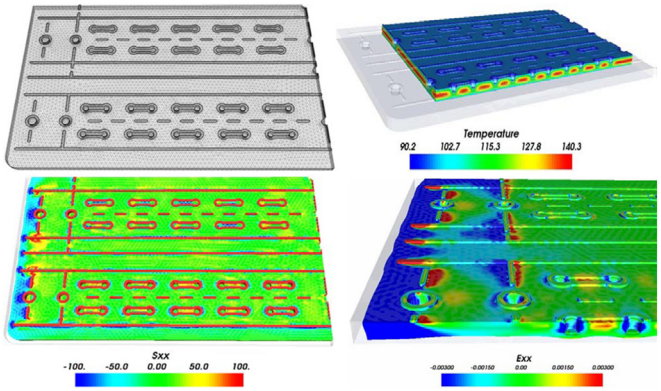

Fig. 35. Top left: full mesh of a quarter of a hot embossing tool based on a 8 inch wafer; top right: three-dimensional hot embossing cooling simulation; bottom left: stress distribution at the end of filling before demoulding; bottom right: strain distribution after cooling [236].

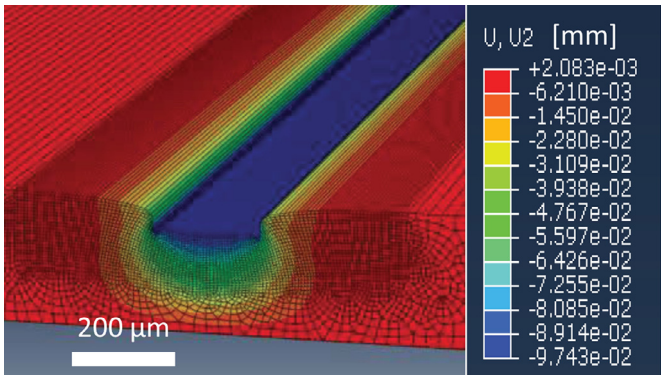

Fig. 36. Three-dimensional simulation of surface generation in micro hot embossing of a 200 µm wide channel with a compression displacement of 100 µm [68].

Hot embossing can be used also to shape metals in their viscous state such as bulk metallic glasses (BMG). Three-dimensional

modeling of micro feature generation in BMG micro forming by hot embossing was demonstrated in [183]. Hot embossing is also the process for the compression molding of glass, which is particularly suited for high-end micro-optical systems. Two-dimensional finite element simulation for the prediction micro feature filling a triangular profile (height 145 µm, pitch 500 µm) was demonstrated in [125]. Three-dimensional finite element simulation for the prediction of the replication quality of a micro pyramidal pattern (width 30 µm, height 20 µm, pitch 150 µm) was developed in [178]. The simulations demonstrated that by adding an ultrasonic assisted phase during the hot embossing of glass the replication fidelity could be improved up to 17%. In order to increase the productivity of conventional hot embossing, the compression step can be integrated into a roll-to-roll (R2R) process. Two-dimensional finite element modeling of R2R HE has been realized and presented in [210] and [250].

4.4. Nanoimprint lithography

Nanoimprint lithography (NIL) is an established process technology which is typically used for the generation of sub-µm structures with critical lateral dimensions and height/depth in the range of 10–1000 nm. The process is realized by pressing a soft stamper against a thin polymer layer in its soft state above the glass transition temperature [73].

The polymer deformation process was simulated using a two-dimensional finite element model and validated with experiments in [123] showing that the needed pressure increases for high aspect ratio patterns as well as very low aspect ratio structures. An optimum point to minimize the needed pressure was found for features having an aspect ratio (i.e., the ratio between the vertical and the lateral dimension) is around 0.8. The pressure increases when using polymer layers with an initial thickness lower than two times of groove depth in the mold. Thin walls with height and width up to 900 nm and down to 100 nm respectively could be realized and modelled.

Molecular dynamics simulations were performed, demonstrating the key role of the mold elasticity, the surface energy at the polymer melt/mold boundary, and the critical dimension of the nanocavities. The simulations revealed to be instrumental in establishing the characteristic nanofeature dimension that could be replicated for a given mold stiffness and a given polymer melt surface energy [59]. A semisphere with a radius in the range between 20 nm and 40 nm could be successfully simulated (see Fig. 37). Full three-dimensional simulation of NIL was also demonstrated by using a Lagrangian or particle finite element approach has been applied in the numerical simulations in [170] (see Fig. 38). It allowed for a time-dependent non-isothermal simulation of the NIL process, making it suitable for feature and process optimization.

In ultra-violet nanoimprint lithography (UV-NIL) the filling stage is followed by a curing stage. The UV-NIL process simulation was

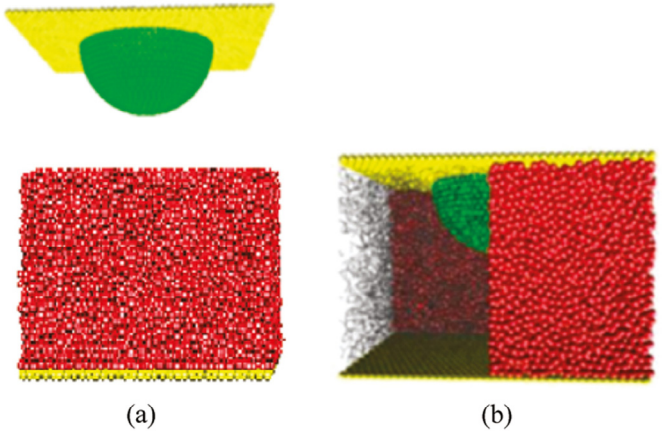

Fig. 37. Molecular dynamics simulation of the mold and replica generation in NIL: (a) mold stamper (yellow) with attached a rigid hemispherical nanoparticle (green) to be pressed at a constant force into a polymeric film consisting of polymer chains (red particles); (b) polymeric film (red) nanostructured (see green nanocavity) and subsequently annealed to relax cross-link bonds [59].

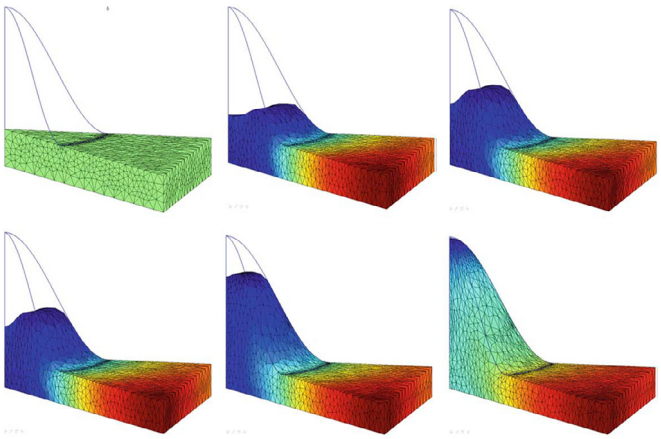

Fig. 38. Pressure development during nanostructure filling in NIL simulated by a three-dimensional particle finite element approach [170].

demonstrated in [124] and [203]. In this case the simulation is composed by four modules, each modeling the four phases of the process and their main characteristics: (1) the fluid dynamics in the resist-filling process into a pattern; (2) the optical-intensity distribution in the UV exposure process; (3) the mechanical properties during the UV curing; (4) the resist profiles induced by UV shrinkage. The simulation system allowed for the calculation of the pressure distribution and flow characteristic during filling the resist, of the formation of entrapped bubble, of the size effects, of the variation of mechanical properties of the resist by UV exposure (photo-shrinkage). Features having width down to 25–50 nm could be simulated (see Fig. 39).

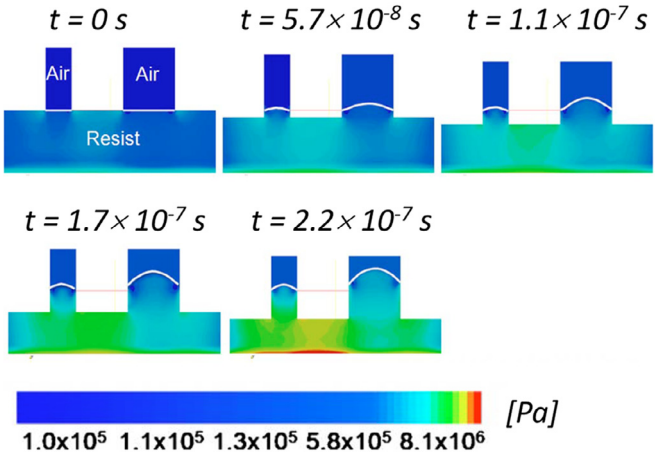

Fig. 39. Flow simulation results for the resist filling of 25 nm and 50 nm wide nanofeatures: pressure distribution at different filling times [203].

5. Modeling of surface generation by additive processes

Modeling of surface generation in additive manufacturing processes is currently an emerging field of research. Significant progress in simulating surface topography generation at the micro dimensional scale have been recently developed and demonstrated for laser powder bed fusion (Section 5.1), material extrusion (Section 5.2) and vat photopolymerization (Section 5.3) processes.

5.1. Laser powder bed fusion

Process modeling of laser powder bed fusion (LPBF) has been intensively researched for more than a decade, as reviewed in [22], and in the past five years multi-scale and multi-physics simulations have revealed the underlying process dynamics, specifically regarding surface generation, with considerably higher resolution than in the past. With high degree of discretization and the implementation of thermal, metallurgical, and mechanical models, the different

physical phenomena occurring during the LPBF processes at surface level have been simulated, particularly for metals (see Fig. 40).

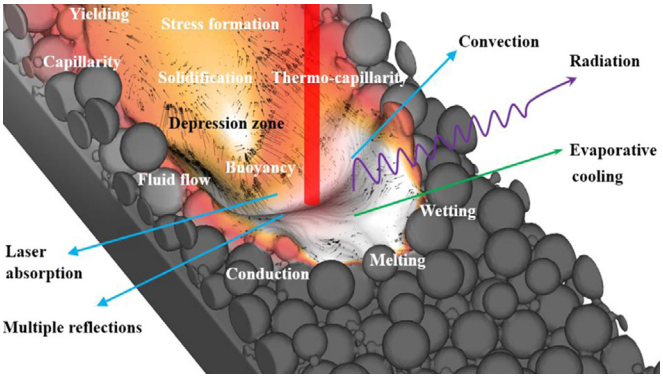

Fig. 40. The different physical phenomena occurring at surface level during the metal LPBF process [22].

Surface generation of single [156] and multiple tracks [184,239,245], single layers as well as multiple layers [20,58] have been simulated. The surface topography resulting from the process can now be predicted and compared with microscopy observations of experiments, as shown for example in [58] and [237] (see Fig. 41).

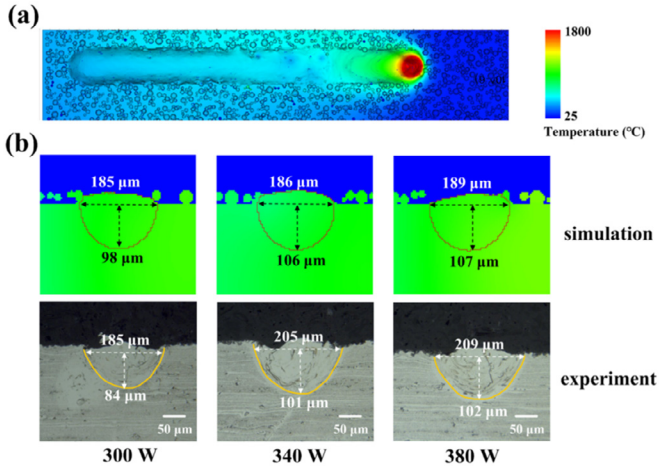

Fig. 41. (a) Temperature field at 340 W laser power and 1500 mm/s scanning speed; (b) simulated and experimental melt-pool dimensions at different laser power settings (scanning speed = 1500 mm/s) [58].

Key advancements in the understanding of the laser-powder material, and in turn of the surface generation in LPF, are related to the keyhole and subsequent porosities [21,260], inter-layer porosities [238], lack of fusion and void formation [20], thermo-capillarity (i.e., Marangoni effect) [23].

A statistical approach based on design of experiments and experimental data for modeling surface roughness in powder bed fusion is presented in [19]. The effect of key process parameters (laser power, beam speed, orientation, layer thickness, hatch spacing) on the surface roughness of both upward and downward facing surface is evaluated (ranging between 7 µm and 20 µm depending on process configuration).

An analytical model to predict the surface roughness in LPBF including (i) the staircase step effect, (ii) the effect of slope angle, (iii) the presence of particles on top surfaces is presented in [208]. The model was able to predict the measured surface roughness in the range of 14–16 µm with an accuracy of 1–2 µm for a slope angle from 10° to 90°

Time-efficient multi-physics models can be used to generate data for machine learning applications instead of experimental data. In [69], for example, LPBF simulation of track line generation are employed to train an artificial neural network for regression with the aim of establishing the statistical correlation between the AM process parameters and the final quality of the product made by additive manufacturing. Despite the convenience of this approach (that minimize the need of the experimental efforts), limitations in terms of accuracy of the prediction are observed.

5.2. Material extrusion

In material extrusion additive manufacturing, also called fused filament fabrication (FFF), the surface topography is characterized by the typical arrangement of the extruded material tracks solidified next to each other. Based on process settings, material, and machine configuration, recently it has been possible to predict the generated surface resulting from the process. Analytical modeling allows for the efficient evaluation of the correlation between key FFF process parameters (extrusion flow rate, printing head velocity and its gap from the substrate) and the characteristics of the printed material (dimensions of the deposited filament, pressure at the printing head nozzle, separating force between substrate and printing head). The typical material model adopted includes the non-Newtonian viscosity and the shear thinning behavior also used in polymer extrusion and injection molding (see Section 4.2) [1].

The geometry of the printing head-gap-deposited material-building platform can be modeled (see Fig. 42) so that the flow velocity field and the free surface of the extruded materials can be simulated (see Fig. 43) [75]. Starting from the results of the simulations in terms of size and morphology of a single track of extruded material strand validated with experiments [76,201] (Fig. 44), it is then possible to simulate the resulting generated surface when several material strands are deposited on multiple layers, both aligned in the vertical direction [174] and with perpendicular orientation [77] (Fig. 45).

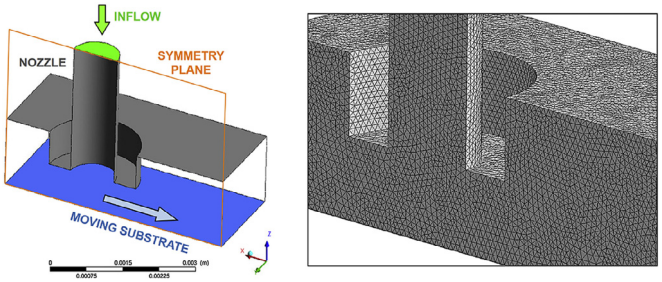

Fig. 42. Numerical geometry model (left) and tetrahedral mesh (right) of the FFF system [75].

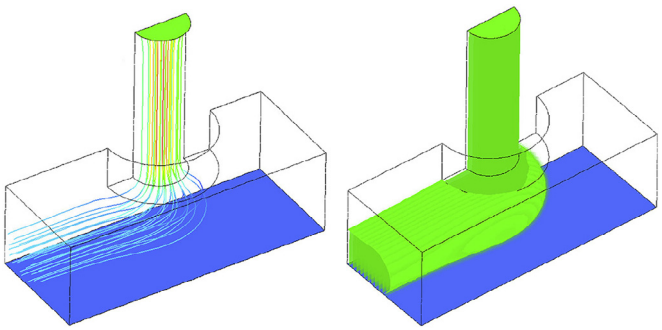

Fig. 43. Velocity field (left) and free surface of the printed strand (right) [75].

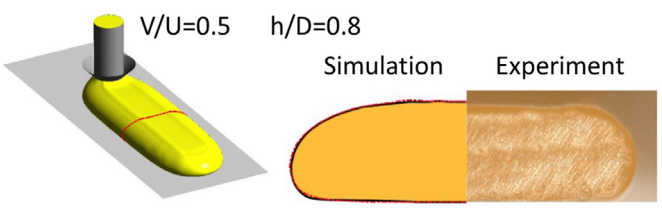

Fig. 44. Simulation and experimental validation of a single material strand (V = extrusion head cruising speed, U = extrusion speed, h = distance form build plane, D = nozzle diameter) [76].

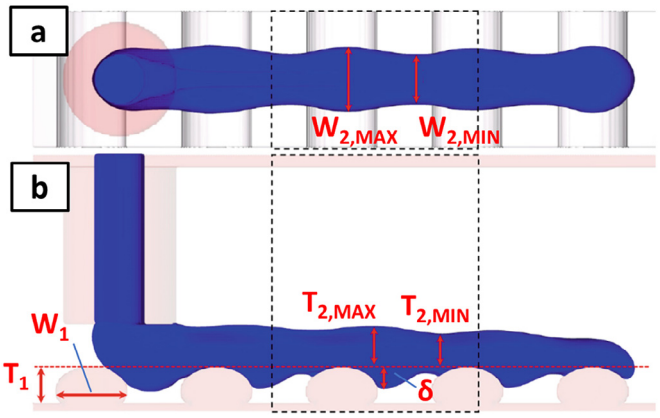

Fig. 45. Top (A) and side (B) view of a multiple layer material strand simulation FFF for the prediction of minimum and maximum track width (W_2) and thickness (T_2) based on the initial dimension of the first layer strand (W_1, T_1) [77].

Roughness parameters of surfaces generated by the FFF process can also be simulated, with relatively accuracy (80%–90%) as demonstrated in [43] by using a analytical-geometrical model of the material deposition or by using a machine learning algorithms [60] trained with experimental data. While the geometrical model can actually predict both the resulting profile (see Fig. 46) and the surface roughness parameters associated with such surface, the machine learning approach can in fact give a prediction of the parameters only.

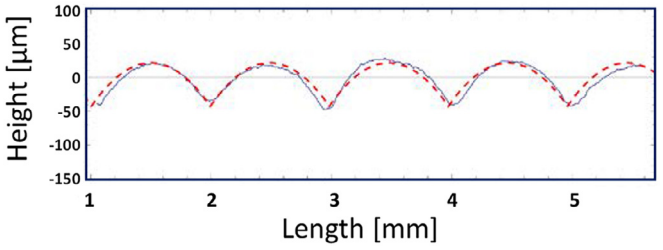

Fig. 46. FFF profile predicted by the analytical model (red dashed line) compared with the experimental surface (continuous blue line) [43].

5.3. Vat photopolymerization

In vat photopolymerization the key for process modeling is to simulate the crosslinking reaction, which mainly depends on the temperature. This can be predicted with relatively high accuracy (3% deviation) as shown in [194]. Prediction of temperature distribution, degree of conversion, internal stress and consequent three-dimensional geometry have been recently demonstrated by multi-scale process simulation of a particle-filled vat photopolymerization process [232]. These capabilities set the necessary simulation framework for the modeling of surface generation in vat photopolymerization, as shown for a profile in [228] where a comparison of predicted height as a function of time with experimental data is presented.

Ahn et al. [2] investigated the possibility of predicting the profile surface roughness as a function of the build orientation. The method is based on a polynomial regression of experimental surface roughness measurements. Deviation errors of the calculated surface roughness were for most cases in the range of 1–2 µm for *Ra* values in the range between 5 µm and 35 µm.

6. Conclusion and future developments

Modeling of surface generation for the prediction of surface topography and geometry as a result of the employed manufacturing technology has developed enormously in the past 40 years. At present time, it is indeed possible for a fairly large group of production technologies, based either on material subtractive, forming or additive processes, to predict the geometry of the surface with sufficient resolution and accuracy to enable product and process design in order to realize a certain surface with the required geometric specifications. These developments allow improved surface topography prediction and manufacturing process design prior the actual production takes place.

Depending on the simulation technique used, different simulation outcomes can be obtained. With multi-physics modeling (see left side of Fig. 2, 'Multiphysics models'), the process dynamics can be unveiled and both a profile and an areal representation of the simulated surface can be generated. Several validation studies have been examined and it was demonstrated that accuracies in terms of deviation from simulated and experimentally acquired surface geometries in the order of 5%–10% can be achieved for most processes. These results are obtained essentially due to high fidelity modeling and high-resolution geometrical modeling. By post-processing the simulated profiles or areal surface point clouds, surface roughness parameters can easily be extracted and used for surface design, tolerance verification, functionality analysis, quality control. Most of the simulation research work has focused on the so-called multi-step approach, which means that the model is capable of simulating the areal surface geometry of a relatively small portion of the component surface, acquiring the necessary boundary conditions determined by the whole component from a separated macro-scale model. This approach allows to limit the computational power and time necessary for the simulation. Future developments in terms of handling even larger sized geometrical models are required in order to achieve the full implementation of the so-called multi-scale approach, in which a single model is able to simulate the geometry of a component at both the macro-scale (i.e., component-scale) and micro-scale (i.e., surface-scale) in the same simulation. These developments are needed to enable an integrated product design based on simulation in which the actual geometry of the component at both macro-, meso-, and micro-scales are considered simultaneously.

Statistical modeling approaches (see right side of Fig. 2, 'Statistical modeling methods'), either based on design of experiments, regression techniques, or machine learning methods, on the other hand, have been demonstrated to be limited to the prediction of roughness parameters of the generated surface. Hence, their use is more suitable for quality control and tolerance verification rather than surface design and functionality analysis. An emerging trend has been observed recently, though, in which the training data set is constituted by the surface geometry represented by a profile/areal data set at the micro dimensional scale. In this way, the model is having as output both a set of desired roughness parameters, as well as a simulated surface micro geometry associated to a specific process parameters configuration [211,214]. Even though this approach is more computationally intensive (especially for the generation of a three-dimensional point cloud representing the surface) than the conventional approach, in which the model predicts the most probable value of a certain surface roughness parameter, it is still faster than the multi-physics approach in which the required computational power and time are orders of magnitude higher. It is expected that this approach will be further developed in the near future in order to fully exploit the capability of data-driven methods applied to manufacturing. One of the important bottlenecks that limits these developments is the availability of reliable large data sets that accurately describe the generated surface. These data sets are highly resource and time demanding to be produced by experimental work and physical measurements. In this perspective, a solution is made available from the use of accurate high resolution multi-physics models (as those reviewed in this paper) so that the required data is generated by models instead that by experiments. This work has demonstrated that the current

simulation technology is capable of digitally replicating the physical manufacturing processes at both the macro down and the micro dimensional scales. It is expected that the use of experimentally validated digital models to generate training large data sets for statistical model training will increase considerably in the near future.

Declaration of Competing Interest

The authors declare that they have no known competing financial interests or personal relationships that could have appeared to influence the work reported in this paper.

Acknowledgements

The authors gratefully acknowledge Prof. Hans N. Hansen, Prof. Brigid Mullany, Prof. Enrico Savio, Prof. Richard Leach for support and insightful discussions in the preparation of this paper in the early stages. Prof. Ismail Lazoglu, Dr.-Ing. Daniel Meyer, Dr.-Ing. Andreas Klink, Prof. Ping Guo, Prof. Masanori Kunieda, Prof. Chris V. Nielsen, Prof. Takahashi are thanked for their suggestions and contributions.

This research work was undertaken in the context of the DIGIMAN4.0 project ("DIGItal MANufacturing Technologies for Zero-defect Industry 4.0 Production", http://www.digiman4-0.mek.dtu.dk/). DIGIMAN4.0 is a European Training Network supported by Horizon 2020, the EU Framework Programme for Research and Innovation (Project ID: 814225).

References

[1] Agassant JF, Pigeonneau F, Sardo L, Vincent V (2019) Flow Analysis Of The Polymer Spreading During Extrusion Additive Manufacturing. *Additive Manufacturing* 29:100794.
[2] Ahn D, Kim H, Lee S (2009) Surface Roughness Prediction Using Measured Data And Interpolation In Layered Manufacturing. *Journal of Materials Processing Technology* 209:664–671.
[3] Altintas Y, Engin S (2001) Generalized Modeling of Mechanics and Dynamics of Milling Cutters. *CIRP Annals* 50/1:25–30.
[4] Altintas Y, Kilic ZM (2013) Generalized Dynamic Model Of Metal Cutting Operations. *CIRP Annals* 62/1:47–50.
[5] Altintas Y, Kersting P, Biermann D, Budak E, Denkena B, Lazoglu I (2014) Virtual Process Systems For Part Machining Operations. *CIRP Annals* 63/2:585–605.
[6] Altintas Y, Tuysuz O, Habibi M, Li ZL (2018) Virtual Compensation Of Deflection Errors In Ball End Milling Of Flexible Blades. *CIRP Annals* 67/1:365–368.
[7] Anwar S, Axinte DA, Becker AA (2013) Finite Element Modelling Of Abrasive Waterjet Milled Footprints. *Journal of Materials Processing Technology* 213(2):180–193.
[8] Anwar S, Axinte DA, Becker AA (2013) Finite Element Modelling of Overlapping Abrasive Waterjet Milled Footprints. *Wear* 303:426–436.
[9] Arcona C, Dow TA (1998) An Empirical Tool Force Model For Precision Machining. *Journal of Manufacturing Science and Engineering* 120:700–707.
[10] Arizmendi M, Fernandez J, Lopez de Lacalle LN, Lamikiz A, Gil A, Sanchez JA, Campa FJ, Veiga F (2008) Model Development For The Prediction Of Surface Topography Generated By Ball–End Mills Taking Into Account The Tool Parallel Axis Offset. Experimental Validation. *CIRP Annals* 57/1:101–104.
[11] Arizmendi M, Campa FJ, Fernandez J, Lopez de Lacalle LN, Gil A, Bilbao E, Veiga F, Lamikiz A (2009) Model for Surface Topography Prediction In Peripheral Milling Considering Tool Vibration. *CIRP Annals* 58/1:93–96.
[12] Arrazola PJ, Özel T, Umbrello D, Davies M, Jawahir IS (2013) Recent Advances In Modelling Of Metal Machining Processes. *CIRP Annals* 62/2:695–718.
[13] Aurich JC, Kirsch B (2012) Kinematic Simulation Of High–Performance Grinding For Analysis Of Chip Parameters Of Single Grains. *CIRP Journal of Manufacturing Science and Technology* 5:164–174.
[14] Axinte DA, Karpuschewski B, Kong MC, Beaucamp AT, Anwar S, Miller D, Petzel M (2014) High Energy Fluid Jet Machining (HEFJet–Mach): From Scientific And Technological Advances To Niche Industrial Applications. *CIRP Annals* 63/2:751–771.
[15] Axinte DA, Billingham J, Guillerna AB (2017) New Models For Energy Beam Machining Enable Accurate Generation Of Free Forms. *Science Advances* 3(9):e1701201.
[16] Axinte DA, Han H, Jiwang Y, Zhirong L (2022) What Micro-Mechanics Can Reveal About Machining Processes. *International Journal of Machine Tools and Manufacture* 183:103964.
[17] Azuddin M, Taha Z, Choudhury IA (2017) *Micro Plastic Part Filling Capabilities through Simulation and Experiment: A Case Study on Micro Gear Shape*, *Reference Module in Materials Science and Materials Engineering*, 1–3, Elsevier Ltd., 441–465.
[18] Babenko M, Sweeney J, Petkov P, Lacan F, Bigot S, Whiteside B (2018) Evaluation of Heat Transfer At The Cavity–Polymer Interface In Microinjection Moulding Based On Experimental And Simulation Study. *Applied Thermal Engineering* 130:865–876.
[19] Bacchewar P, Singhal S, Pandey P (2007) Statistical Modelling And Optimization Of Surface Roughness In The Selective Laser Sintering Process. *Proceedings of the Institution of Mechanical Engineers, Part B: Journal of Engineering Manufacture* 221:35–52.
[20] Bayat M, Mohanty S, Hattel JH (2019) Multiphysics Modelling Of Lack–Of–Fusion Voids Formation And Evolution in IN718 Made By Multi–Track/Multi–Layer L–PBF. *International Journal of Heat & Mass Transfer* 139:95–114.
[21] Bayat M, Thanki A, Mohanty S, Witvrouw A, Yang S, Thorborg J, Tiedje NS, Hattel JH (2019) Keyhole–induced porosities in Laser–based Powder Bed Fusion (L–PBF) of Ti6Al4V: High–Fidelity Modelling And Experimental Validation. *Additive Manufacturing* 30:100835.
[22] Bayat M, Dong W, Thorborg J, To AC, Hattel JH (2021) A Review Of Multi–Scale And Multi–Physics Simulations Of Metal Additive Manufacturing Processes With Focus On Modeling Strategies. *Additive Manufacturing* 47:102278.
[23] Bayat M, Nadimpalli VK, Pedersen DB, Hattel JH (2021) A Fundamental Investigation Of Thermo–Capillarity In Laser Powder Bed Fusion Of Metals And Alloys. *International Journal of Heat & Mass Transfer* 166:120766.
[24] Bergs T, Harst S (2020) Development of a Process Signature For Electrochemical Machining. *CIRP Annals* 69/1:153–156.
[25] Beuer S, Rommel M, Lehrer C, Platzgummer E, Kvasnic S, Bauer AJ, Ryssel H (2009) Accurate Parameter Extraction For The Simulation Of Direct Structuring By Ion Beams. *Microelectronic Engineering* 84:810–813.
[26] Bewilogua K, Bräuer G, Dietz A, Gäbler J, Goch G, Karpuschewski B, Szyszka B (2009) Surface Technology For Automotive Engineering. *CIRP Annals* 58/2:608–627.
[27] Billingham J, Miron CB, Axinte DA, Kong MC (2013) Mathematical Modelling Of Abrasive Waterjet Footprints For Arbitrarily Moving Jets: Part II — Overlapped Single And Multiple Straight Paths. *International Journal of Machine Tools and Manufacture* 68:30–39.
[28] Biondani FG, Bissacco G, Hansen HN (2017) Characterization Of Smearing Patterns In Ball Nose End Milling Process. In: *Proc. 17th Int. Conf. European Society for Precision Engineering and Nanotechnology, EUSPEN 2017*, Hannover (Germany) 257–258.
[29] Biondani FG, Bissacco G, Hansen HN (2018) Methodologies For Characterization of Smearing Micro Geometry on Ball End Milled Tool Steel Surfaces. in Valentinčič J, Byung-Guk Jun M, Dohda K, Dimov S, (Eds.) *World Congress on Micro and Nano Manufacturing WCMNM2018*, September 18-20, Portoroz, Slovenia, 4 pages.
[30] Biondani FG, Bissacco G (2019) Effect Of Cutting Edge Micro Geometry On Surface Generation In Ball End Milling. *CIRP Annals* 68/1:571–574.
[31] Biondani FG, Bissacco G (2020) Surface Topography Analysis Of Ball End Milled Tool Steel Surfaces. *Procedia CIRP* 87:153–158.
[32] Bissacco G (2004) *Surface Generation and Optimization in Micromilling* PhD thesis. Technical University of Denmark, 320.
[33] Bissacco G, Hansen HN, De Chiffre L (2006) Size Effects on Surface Generation in Micro Milling of Hardened Tool Steel. *CIRP Annals* 55/1:3–6.
[34] Bissacco G, Hansen HN, Slunsky J (2008) Modelling The Cutting Edge Radius Size Effect For Force Prediction In Micro Milling. *CIRP Annals* 57/1:113–116.
[35] Bissacco G, Valentincic J, Hansen HN, Wiwe BD (2010) Towards the Effective Tool Wear Control In Micro EDM Milling. *International Journal of Advanced Manufacturing Technology* 47:3–9.
[36] Bissacco G, Hansen HN, Tristo G, Valentincic J (2011) Feasibility Of Wear Compensation In Micro Edm Milling Based On Discharge Counting And Discharge Population Characterization. *CIRP Annals* 60/1:231–234.
[37] Bissacco G, Tristo G, Hansen HN, Valentincic J (2013) Reliability Of Electrode Wear Compensation Based On Material Removal Per Discharge In Micro EDM Milling. *CIRP Annals* 62/1:179–182.
[38] Bisterov I, Abayzeed S, Speidel A, Clare AT (2022) On-Machine Measurement With An Electrochemical Jet Machine Tool. *International Journal of Machine Tools and Manufacture* 174:103859.
[39] Bleys P, Kruth JP, Lauwers B, Zryd A, Delpretti R, Tricarico C (2002) Real–time Tool Wear Compensation in Milling EDM. *CIRP Annals* 51/1:157–160.
[40] Bogaerts A, Chen Z (2005) Effect of Laser Parameters On Laser Ablation And Laser–Induced Plasma Formation: A Numerical Modeling Investigation. *Spectrochimica Acta Part B: Atomic Spectroscopy* 60:1280–1307.
[41] Borgardt NI, Rumyantsev AV (2016) Prediction of Surface Topography Due To Finite Pixel Spacing in FIB Milling Of Rectangular Boxes And Trenches. *Journal of Vacuum Science and Technology* 34:061803.
[42] Bortels L, Deconinck B, Van Den Bossche B (1996) The Multi–dimensional Upwinding Method as a New Simulation Tool for the Analysis of Multi–ion Electrolytes Controlled by Diffusion, Convection and Migration. Part I: Steady State Analysis of a Parallel Plane Flow Channel. *Journal of Electroanalytical Chemistry* 404:15–26.
[43] Boschetto A, Giordano V, Veniali F (2013) 3D Roughness Profile Model In Fused Deposition Modelling. *Rapid Prototyping Journal* 19/4:240–252.
[44] Brinksmeier E, Preuss W, Riemer O, Rentsch R (2017) Cutting Forces, Tool Wear And Surface Finish In High Speed Diamond Turning. *Precision Engineering* 49:293–304.
[45] Brinksmeier E, Karpuschewski B, Yan J, Schönemann L (2020) Manufacturing Of Multiscale Structured Surfaces. *CIRP Annals* 69/2:717–739.
[46] Bruzzone AAG, Costa HL, Lonardo PM, Lucca DA (2008) Advances In Engineered Surfaces For Functional Performance. *CIRP Annals* 57/2:750–769.
[47] Budak E, Lazoglu I, Guzel BU (2004) Improving Cycle Time in Sculptured Surface Machining Through Force Modeling. *CIRP Annals* 53/1:103–106.
[48] Budak E, Altintas Y (1995) Modeling And Avoidance Of Static Form Errors In Peripheral Milling Of Plates. *International Journal of Machine Tools and Manufacture* 35/3:459–476.
[49] Buijs M, Korpel–van Houten K (1993) A Model For Lapping Of Glass. *Journal of Materials Science* 28:3014–3020.
[50] Butler–Smith PW, Axinte DA, Daine M (2012) Solid Diamond Micro–Grinding Tools: From Innovative Design And Fabrication To Preliminary Performance Evaluation in Ti–6Al–4V. *International Journal of Machine Tools and Manufacture* 59:55–64.

[51] Butler–Smith P, Axinte DA, Daine M, Kong MC (2014) Mechanisms Of Surface Response To Overlapped Abrasive Grits Of Controlled Shapes And Positions: An Analysis Of Ductile And Brittle Materials. *CIRP Annals* 63/1:321–324.

[52] Cadot GBJ, Axinte DA, Billingham J (2016) Continuous Trench, Pulsed Laser Ablation For Micro–Machining Applications. *International Journal of Machine Tools and Manufacture* 107:8–20.

[53] Cadot GBJ, Billingham J, Axinte DA (2017) A Study Of Surface Swelling Caused By Graphitisation During Pulsed Laser Ablation Of Carbon Allotrope With High Content Of sp3 Bounds. *Journal of Physics D: Applied Physics* 50:245301.

[54] Cao W, Kong L, Li Q, Ying J, Shen C (2011) Model and Simulation For Melt Flow In Micro–Injection Molding Based On The PTT Model. *Modelling and Simulation in Materials Science and Engineering* 19:085003.

[55] Cao ZC, Cheung CF (2014) Theoretical Modelling And Analysis Of The Material Removal Characteristics In Fluid Jet Polishing. *International Journal of Mechanical Sciences* 89:158–166.

[56] Cao ZC, Cheung CF, Ren M (2016) Modelling and Characterization Of Surface Generation In Fluid Jet Polishing. *Precision Engineering* 43:406–417.

[57] Cao J, Brinksmeier E, Fu MW, Gao RX, Liang B, Merklein M, Schmidt M, Yanagimoto J (2019) Manufacturing Of Advanced Smart Tooling For Metal Forming. *CIRP Annals* 68/2:605–628.

[58] Cao Y, Lin X, Kang N, Ma L, Wei L, Zheng M, Yu J, Peng D, Huang W (2021) A Novel High–Efficient Finite Element Analysis Method Of Powder Bed Fusion Additive Manufacturing. *Additive Manufacturing* 46:102187.

[59] Carrillo JMY, Dobrynin AV (2009) Molecular Dynamics Simulations of Nanoimprinting Lithography. *Langmuir* 25(22):13244–13249.

[60] Cerro A, Romero PE, Yiğit O, Bustillo A (2021) Use Of Machine Learning Algorithms For Surface Roughness Prediction Of Printed Parts In Polyvinyl Butyral Via Fused Deposition Modeling. *The International Journal of Advanced Manufacturing Technology* 115:2465–2475.

[61] Cha D, Axinte DA, Billingham J (2019) Geometrical Modelling Of Pulsed Laser Ablation Of High Performance Metallic Alloys. *International Journal of Machine Tools and Manufacture* 141:78–88.

[62] Chaves-Jacob J, Beaucamp A, Zhu W, Kono D, Linares J-M (2021) Towards An Understanding Of Surface Finishing With Compliant Tools Using A Fast And Accurate Simulation Method. *International Journal of Machine Tools and Manufacture* 163:103704.

[63] Chen WW, Wang Q, Wang F, Keer LM, Cao J (2008) Three–Dimensional Repeated Elasto–Plastic Point Contact, Rolling and Siding. *Journal of Applied Mechanics* 75/021021:1–12.

[64] Cheung CF, Kong LB, Ho LT, To S (2011) Modelling And Simulation Of Structure Surface Generation Using Computer Controlled Ultra–Precision Polishing. *Precision Engineering* 35/4:574–590.

[65] Chen JY, Zhao QL (2015) A model for predicting surface roughness in single–point diamond turning. *Measurement* 69:20–30.

[66] Chen G, Liu XL, Wang L, Zhou XQ (2016) The Research And Modelling About Plastic Side Flow Measurement Of Machined Surface In Precision Turning Of Hardened Steel GCr15. *International Journal of Nanomanufacturing* 12/2:154–166.

[67] Cheng G, Barriere T, Gelin J-C, Sahli M (2017) Physical Modelling Of Amorphous Thermoplastic Polymer And Numerical Simulation Of Micro Hot Embossing Process. in Oñate E, Owen DRJ, Peric D, Chiumenti M, (Eds.) *XIV International Conference on Computational Plasticity. Fundamentals and Applications COMPLAS 2017*, Barcelona (Spain) 704–711.

[68] Cheng C, Barrière T (2018) The Effects Of Polymers' Visco–Elastoplastic Properties On The Micro Cavities Filling Step Of Hot Embossing Process. In: *Proceedings of the 21st International ESAFORM Conference on Material Forming, AIP Conf. Proc.*, April 23-25, Palermo (Italy), 1960:120007–1–120007–6.

[69] Chen S (2019) *Investigation of FEM Numerical Simulation For The Process Of Metal Additive Manufacturing, In Macro Scale* PhD thesis. Mechanical Engineering, Université de Lyon. France, 235. pp.

[70] Chen Y, Jiang L, Fang M, Zhang J (2020) Multi–Time Scale Simulation Of Pulse Electrochemical Machining Process With Multi–Physical Model. *International Journal of Advanced Manufacturing Technology* 110:2203–2210.

[71] De Chiffre L, Kunzmann H, Peggs GN, Lucca DA (2003) Surfaces in Precision Engineering, Microengineering and Nanotechnology. *CIRP Annals* 52/2:561–577.

[72] Choi SJ, Kim SK (2011) Multi–scale Filling Simulation Of Micro–Injection Molding Process. *Journal of Mechanical Science and Technology* 25/1:117–124.

[73] Chou SY, Krauss PR, Renstrom PJG (1996) Nanoimprint Lithography. *Journal of Vacuum Science & Technology B: Microelectronics and Nanometer Structures Processing, Measurement, and Phenomena* 14:4129.

[74] Christensen BH, Vestentoft K, Balling P (2007) Short–Pulse Ablation Rates And The Two–Temperature Model. *Applied Surface Science* 253/15:6347–6352.

[75] Comminal R, Serdeczny MP, Pedersen DB, Spangenberg J (2018) Numerical Modeling Of The Strand Deposition Flow In Extrusion–Based Additive Manufacturing. *Additive Manufacturing* 20:68–76.

[76] Comminal R, Serdeczny MP, Pedersen DB, Spangenberg J (2019) Motion Planning And Numerical Simulation Of Material Deposition At Corners In Extrusion Additive Manufacturing. *Additive Manufacturing* 29:110753.

[77] Comminal R, Jafarzadeh S, Serdeczny MP, Spangenberg J (2021)) *Estimations of Interlayer Contacts in Extrusion Additive Manufacturing Using a CFD Model*, Industrializing Additive Manufacturing, 241–250.

[78] Correa M, Bielza C, Pamies–Teixeira J (2009) Comparison of Bayesian Networks And Artificial Neural Networks For Quality Detection In A Machining Process. *Expert Systems with Applications* 36:7270–7279.

[79] Cuba Ramos A, Autenrieth H, Strauß T, Deuchert M, Hoffmeister J, Schulze V (2012) Characterization Of The Transition From Ploughing To Cutting In Micro Machining And Evaluation Of The Minimum Thickness Of Cut. *Journal of Materials Processing Technology* 212:594–600.

[80] Deconinck D, Van Damme S, Deconinck J (2012) A Temperature Dependent Multi–Ion Model For Time Accurate Numerical Simulation Of The Electrochemical Machining Process, Part II: Numerical Simulation. *Electrochimica Acta* 69:120–127.

[81] Deconinck D, Deconinck J (2013) Multi–Ion And Temperature Dependent Numerical Simulation Of Electrochemical Machining. *Procedia CIRP* 6:475–478.

[82] De Chiffre L (1999) Industrial Survey of ISO Surface Texture Parameters. *CIRP Annals* 48/3:74–77.

[83] Demos SG, Negres RA, Raman RN, Feit MD, Manes KR, Rubenchik AM (2015) Relaxation Dynamics Of Nanosecond Laser Superheated Material In Dielectrics. *Optica* 2/8:765–772.

[84] Denkena B, Kruger M, Bachrathy D, Stepan G (2012) Model Based Reconstruction Of Milled Surface Topography From Measured Cutting Forces. *International Journal of Machine Tools and Manufacture* 54–55:25–33.

[85] Denkena B, Böß V, Nespor D, Gilge P, Hohenstein S, Seume J (2015) Prediction of the 3D Surface Topography after Ball End Milling and its Influence on Aerodynamics. *Procedia CIRP* 31:221–227.

[86] Denkena B, Krödel A, Mücke A, Ellersiek L (2021) Prediction Of Plastic Surface Defects For 5–Axis Ball End Milling of Ti–6Al–4V With Rounded Cutting Edges Using A Material Removal Simulation. *CIRP Annals* 70/1:91–94.

[87] Denkena B, Dittrich MA, Huuk J (2021) Simulation–Based Surface Roughness Modelling In End Milling. *Procedia CIRP* 99:151–156.

[88] Ding W, Dai C, Yu T, Xu J, Fu Y (2017) Grinding Performance Of Textured Monolayer CBN Wheels: Undeformed Chip Thickness Nonuniformity Modeling And Ground Surface Topography Prediction. *International Journal of Machine Tools and Manufacture* 122:66–80.

[89] Dornfeld D, Min S, Takeuchi Y (2006) Recent Advances in Mechanical Micromachining. *CIRP Annals* 55/2:745–768.

[90] Dupaix RB, Cash W (2009) Finite Element Modeling of Polymer Hot Embossing Using a Glass–Rubber Finite Strain Constitutive Model. *Polymer Engineering and Science* 49/3:531–543.

[91] Ebrahimi M, Konaganti VK, Moradi S, Doufas AK, Hatzikiriakos SG (2016) Slip of Polymer Melts Over Micro/Nano–Patterned Metallic Surfaces. *Soft Matter* 12.48:9759–9768.

[92] El–Sonbaty IA, Khashaba UA, Selmy AI, Ali AI (2008) Prediction Of Surface Roughness Profiles For Milled Surfaces Using An Artificial Neural Network And Fractal Geometry Approach. *Journal of Materials Processing Technology* 200:271–278.

[93] Engel U, Eckstein R (2002) Microforming—From Basic Research To Its Realization. *Journal of Materials Processing Technology* 125:35–44.

[94] Ertl O, Filipovic L, Selberherr S (2010) Three–Dimensional Simulation of Focused Ion Beam Processing Using the Level Set Method. IEEE–SISPAD 2010 – International Conference on Simulation of Semiconductor Processes and Devices, *September 6–8*, Bologna, Italy49–52.

[95] Evans CJ, Browy EC, Childs THC, Paul E (2015) Interferometric Measurements Of Single Crystal Diamond Tool Wear. *CIRP Annals* 64/1:125–128.

[96] Fang FZ, Zhang XD, Gao W, Guo YB, Byrne G, Hansen HN (2017) Nanomanufacturing – Perspective and Applications. *CIRP Annals* 66/2:683–705.

[97] Fang M, Chen Y, Jiang L, Su Y, Liang Y (2019) Optimal Design Of Cathode Based On Iterative Solution Of Multi–Physical Model In Pulse Electrochemical Machining (PECM). *International Journal of Advanced Manufacturing Technology* 105:3261–3270.

[98] Fang F, Lai M, Wang J, Luo X, Yan J, Yan Y (2022) Nanometric Cutting: Mechanisms, Practices And Future Perspectives. *International Journal of Machine Tools and Manufacture* 178:103905.

[99] Fan C, Liu K, Chen Y, Xue Y, Zhao J, Khudoley A (2022) A New Modelling Method Of Material Removal Profile For Electrorheological Polishing With A Mini Annular Integrated Electrode. *Journal of Materials Processing Technology* 305:117589.

[100] Galasso G, Kaltenbacher M, Tomaselli A, Scarpa D (2015) A Unified Model To Determine The Energy Partitioning Between Target And Plasma In Nanosecond Laser Ablation Of Silicon. *Journal of Applied Physics* 117:123101.

[101] García Luna G, Axinte DA, Novovic D (2022) Engineered Grinding Tools Reimplemented By Precise Sharpening: A Case Study On An Ultrahard Ceramic Matrix Composite. *CIRP Annals* 71/1:289–292.

[102] Geiger M, Kleiner M, Eckstein R, Tiesler N, Engel U (2001) Microforming. *CIRP Annals* 50/2:445–462.

[103] Gilbert D, Stoesslein M, Axinte D, Butler-Smith P, Kell J (2014) A Time Based Method For Predicting The Workpiece Surface Micro–Topography Under Pulsed Laser Ablation. *Journal of Materials Processing Technology* 214/12:3077–3088.

[104] Gomez JA, Lek D, Song I-H, You BH (2014) Study on Stress Evolution In The Cooling Process Of Micro Hot Embossing. *International Journal of Mechanical and Materials Engineering* 9:20.

[105] Grezsik W (1996) A Revised Model For Predicting Surface Roughness In Turning. *Wear* 194:143–148.

[106] Guillerna AB, Axinte DA, Billingham J (2015) The Linear Inverse Problem In Energy Beam Processing With An Application To Abrasive Waterjet Machining. *International Journal of Machine Tools and Manufacture* 99:34–42.

[107] Bilbao–Guillerna A, Axinte DA, Billingham J, Cadot GBJ (2017) Waterjet and Laser Etching: The Nonlinear Inverse Problem. *Royal Society Open Science* 4/7:161031.

[108] Bilbao–Guillerna A, Eachambadi RT, Cadot GBJ, Axinte DA, Billingham J, Stumpf F, Beuer S, Rommel M (2018) Novel Approach Based On Continuous Trench Modelling To Predict Focused Ion Beam Prepared Freeform Surfaces. *Journal of Materials Processing Technology* 252:636–642.

[109] Guo Y, Liu G, Zhu X, Tian Y (2007) Analysis of the Demolding Forces During Hot Embossing. *Microsystem Technologies* 13:411–415.

[110] Guo S, Lu S, Zhang B, Cheung CF (2022) Surface Integrity And Material Removal Mechanisms In High-Speed Grinding of Al/SiCp Metal Matrix Composites. *International Journal of Machine Tools and Manufacture* 178:103906.

[111] Habibi M, Tuysuz O, Altintas Y (2019) Modification of Tool Orientation and Position to Compensate Tool and Part Deflections in Five–Axis Ball End Milling Operations. *Journal of Manufacturing Science and Engineering, Transactions of the ASME* 141/3:031004.

[112] Hansen HN, Hocken RJ, Tosello G (2011) Replication Of Micro And Nano Surface Geometries. *CIRP Annals* 60/2:695–714.

[113] Han J, Zhu J, Zheng W, Wang G (2019) Influence Of Metal Forming Parameters On Surface Roughness And Establishment Of Surface Roughness Prediction Model. *International Journal of Mechanical Sciences* 163:105093.

[114] Han Y, Duan F, Zhu W, Zhang L, Beaucamp A (2020) Analytical And Stochastic Modeling Of Surface Topography In Time–Dependent Sub–Aperture Processing. *International Journal of Mechanical Sciences* 175/1:105575.

[115] Hashimoto F, Johnson SP, Chaudhari RG (2016) Modeling Of Material Removal Mechanism In Vibratory Finishing Process. *CIRP Annals* 65/1:325–328.

[116] Hatzikiriakos SG (2012) Wall Slip Of Molten Polymers. *Progress in Polymer Science* 37.4:624–643.

[117] He CL, Zong WJ, Sun T (2016) Origins For The Size Effect Of Surface Roughness In Diamond Turning. *International Journal of Machine Tools and Manufacture* 106 (22–42):40.

[118] He CL, Zong WJ, Zhang JJ (2017) Influencing Factors And Theoretical Modeling Methods Of Surface Roughness In Turning Process: State–Of–The–Art. *International Journal of Machine Tools and Manufacture* 129:15–26.

[119] He CL, Zong WJ, Xue CX, Sun T (2018) An Accurate 3D Surface Topography Model For Single–Point Diamond Turning. *International Journal of Machine Tools and Manufacture* 134:42–68.

[120] Hecker RL, Liang SY (2003) Predictive Modeling Of Surface Roughness In Grinding. *International Journal of Machine Tools and Manufacture* 43:755–761.

[121] Heo S, Jeong YH, Min BK, Lee SJ (2009) Virtual EDM. Simulator: Three– Dimensional Geometric Simulation of Micro–EDM Milling Processes. *International Journal of Machine Tools and Manufacture* 49:1029–1034.

[122] Hinduja S, Kunieda M (2013) Modelling of ECM and EDM Processes. *CIRP Annals* 62/2:775–797.

[123] Hirai Y, Konishi T, Yoshikawa T, Yoshida S (2004) Simulation And Experimental Study Of Polymer Deformation In Nanoimprint Lithography. *Journal of Vacuum Science & Technology B: Microelectronics and Nanometer Structures Processing, Measurement, and Phenomena* 22:3288.

[124] Hirai Y (2010) UV–Nanoimprint Lithography (NIL) Process Simulation. *Journal of Photopolymer Science and Technology* 23/1:25–32.

[125] Hu M, Xie J, Li W, Niu Y (2020) Theoretical and Experimental Study on Hot–Embossing of Glass–Microprism Array without Online Cooling Process. *Micromachines* 11:984.

[126] Huang H, Yin L, Zhou L (2003) High Speed Grinding Of Silicon Nitride With Resin Bond Diamond Wheels. *Journal of Materials Processing Technology* 141:329–336.

[127] Hung NP, Fu YQ, Ali MY (2002) Focused Ion Beam Machining Of Silicon. *Journal of Materials Processing Technology* 127/2:256–260.

[128] Ikawa N, Shimada S, Tanaka H (1992) Minimum Thickness Of Cut In Micromachining. *Nanotechnology* 3/1:6–9.

[129] Jain RK, Jain VK, Dixit PM (1999) Modeling Of Material Removal And Surface Roughness In Abrasive Flow Machining Process. *International Journal of Machine Tools and Manufacture* 39/12:1903–1923.

[130] Jain NK, Jain VK, Jha S (2007) Parametric Optimization Of Advanced Fine–Finishing Processes. *International Journal of Advanced Manufacturing Technology* 34:1191–1213.

[131] Jha JS, Joshi SS (2012) Numerical Simulation of Micro Hot Embossing of Polymer Substrate. *International Journal of Precision Engineering and Manufacturing* 13/12:2215–2224.

[132] Jiang X, Senin N, Scott PJ, Blateyron F (2021) Feature–Based Characterisation Of Surface Topography And Its Application. *CIRP Annals* 70/2:681–702.

[133] Kansal H, Singh AK, Grover V (2018) Magnetorheological Nano–Finishing Of Diamagnetic Material Using Permanent Magnets Tool. *Precision Engineering* 51:30–39.

[134] Kiew CM, Lin W-J, Teo TJ, Liang TJ, Lin W, Yang G (2009) Finite Element Analysis of PMMA Pattern Formation during Hot Embossing Process. *IEEE/ASME International Conference on Advanced Intelligent Mechatronics (AIM)*, Singapore, 314–319.

[135] Kilic ZM, Altintas Y (2016) Generalized Mechanics And Dynamics Of Metal Cutting Operations For Unified Simulations. *International Journal of Machine Tools and Manufacture* 104:1–13.

[136] Kilic ZM, Altintas Y (2016) Generalized Modelling Of Cutting Tool Geometries For Unified Process Simulation. *International Journal of Machine Tools and Manufacture* 104:14–25.

[137] Kim C-J, Mayor JR, Ni J (2004) A Static Model Of Chip Formation In Microscale Milling. *Journal of Manufacturing Science and Engineering* 126:710–718.

[138] Kim H-B, Hobler G, Steiger A, Lugstein A, Bertagnolli E (2007) Full Three–Dimensional Simulation Of Focused Ion Beam Micro/Nanofabrication. *Nanotechnology* 18:245303.

[139] Kishawy HA, Elbestawi MA (1999) Effects Of Process Parameters On Material Side Flow During Hard Turning. *International Journal of Machine Tools and Manufacture* 39(7):1017–1030.

[140] Kishawy HA, Haglund A, Balazinski M (2006) Modelling Of Material Side Flow In Hard Turning. *CIRP Annals* 55/1:85–88.

[141] Klocke F, Zeis M, Klink A (2015) Interdisciplinary Modelling Of The Electrochemical Machining Process For Engine Blades. *CIRP Annals* 64/1:217–220.

[142] Klocke F, Harst S, Karges F, Zeis M, Klink A (2017) Modeling of the Electrochemical Dissolution Process for a Two–phase Material in a Passivating Electrolyte System. *Procedia CIRP* 58:169–174.

[143] Knowles MRH, Rutterford G, Karnakis D, Ferguson A (2007) Micro–Machining Of Metals, Ceramics And Polymers Using Nanosecond Lasers. *International Journal of Advanced Manufacturing Technology* 33:95–102.

[144] Knuefermann MMW (2004) A Model for Surface Roughness in Ultraprecision Hard Turning. *CIRP Annals* 53/1:99–102.

[145] Kojima A, Natsu W, Kuneida M (2008) Spectroscopic Measurement of Arc Plasma Diameter in EDM. *CIRP Annals* 57/1:203–207.

[146] Kong MC, Miron CB, Axinte DA, Davies S, Kell J (2012) On The Relationship Between The Dynamics Of The Power Density And Workpiece Surface Texture In Pulsed Laser Ablation. *CIRP Annals* 61/1:203–206.

[147] Kong MC, Anwar S, Billingham J, Axinte DA (2012) Mathematical Modelling Of Abrasive Waterjet Footprints For Arbitrarily Moving Jets: Part I—Single Straight Paths. *International Journal of Machine Tools and Manufacture* 53/1:58–68.

[148] Koshy P, Jain VK, Lal GK (1997) Stochastic Simulation Approach To Modelling Diamond Wheel Topography. *International Journal of Machine Tools and Manufacture* 37/6:751–761.

[149] Kovac P, Rodic D, Pucovsky V, Savkovic B, Gostimirovic M (2013) Application Of Fuzzy Logic And Regression Analysis For Modeling Surface Roughness In Face Milling. *Journal of Intelligent Manufacturing* 24:755–762.

[150] Krishnan N, Cao J, Dohda K (2007) Study of the Size Effect on Friction Conditions in Micro–extrusion: Part 1 – Micro–Extrusion Experiments and Analysis. *ASME Journal of Manufacturing Science and Engineering* 129/4:669–676.

[151] Kumar M, Singh Yadav HN, Kumar A, Das M (2021) An Overview Of Magneto-rheological Polishing Fluid Applied In Nano–Finishing Of Components. *Journal of Micromanufacturing* 0(0).

[152] Kunieda M, Kanekob Y, Natsub W (2012) Reverse Simulation of Sinking EDM Applicable to Large Curvatures. *Precision Engineering* 36/2:238–243.

[153] Lai X, Li H, Li C, Lin Z, Ni J (2008) Modelling And Analysis Of Micro Scale Milling Considering Size Effect, Micro Cutter Edge Radius And Minimum Chip Thickness. *International Journal of Machine Tools and Manufacture* 48:1–14.

[154] Langford RM, Nellen PM, Gierak J, Fu Y (2007) Focused Ion Beam Micro– and Nanoengineering. *MRS Bulletin* 32:417–423.

[155] Lavernhe S, Quinsat Y, Lartigue C, Brown C (2014) Realistic Simulation Of Surface Defects In Five–Axis Milling Using The Measured Geometry Of The Tool. *International Journal of Advanced Manufacturing Technology* 74:393–401.

[156] Lee K-H, Yun GJ (2020) A Novel Heat Source Model For Analysis Of Melt Pool Evolution In Selective Laser Melting Process. *Additive Manufacturing* 36:101497.

[157] Li M, Lyu B, Yuan J, Yao W, Zhou F, Zhong M (2016) Evolution And Equivalent Control Law Of Surface Roughness In Shear–Thickening Polishing. *International Journal of Machine Tools and Manufacture* 108:113–126.

[158] Li C, Piao Y, Meng B, Hu Y, Li L, Zhang F (2022) Phase Transition And Plastic Deformation Mechanisms Induced By Self-Rotating Grinding of GaN Single Crystals. *International Journal of Machine Tools and Manufacture* 172:103827.

[159] Lin C-R, Chen R-H, Hung C (2003) Preventing Non–Uniform Shrinkage In Open–Die Hot Embossing of PMMA Microstructures. *Journal of Materials Processing Technology* 140:173–178.

[160] Liu X, DeVor RE, Kapoor SG (2006) An Analytical Model For The Prediction Of Minimum Chip Thickness In Micromachining. *Transac ASME Journal of Manufacturing Science and Engineering* 128/2:474–481.

[161] Liu K, Melkote SN (2006) Effect Of Plastic Side Flow On Surface Roughness In Micro–Turning Process. *International Journal of Machine Tools and Manufacture* 46:1778–1785.

[162] Loaldi D (2020) *Integration of Micro and Nano Structures on Injection Moulded Devices – Process Chains and Enabling Technologies* PhD thesis. Technical University of Denmark, Department of Mechanical Engineering, 1–271.

[163] Loaldi D, Regi F, Baruffi F, Calaon M, Quagliotti D, Zhang Y, Tosello G (2020) Experimental Validation of Injection Molding Simulations of 3D Microparts and Microstructured Components Using Virtual Design of Experiments and Multi–Scale Modeling. *Micromachines* 11/6:614.

[164] Lucchetta G, Masato D, Sorgato M, Crema L, Savio E (2016) Effects Of Different Mould Coatings On Polymer Filling Flow In Thin–Wall Injection Moulding. *CIRP Annals* 65/1:537–540.

[165] Ma B, Tieu AK, Lu C, Jiang Z (2003) Comparison Of Asperity Flattening Under Different Wavelength Models For Sheet Metal Forming. *Journal of Materials Processing Technology* 140:635–640.

[166] Macerol N, Franca LFP, Drazumeric R, Krajnik P (2022) The Effects Of Grit Properties And Dressing On Grinding Mechanics And Wheel Performance: Analytical Assessment Framework. *International Journal of Machine Tools and Manufacture* 180:103919.

[167] Malkin S, Changsheng G (2008) *Grinding technology: Theory and Applications of Machining With Abrasives*, Industrial Press. 372..

[168] Malekian M, Mostofa MG, Park SS, Jun MBG (2012) Modeling Of Minimum Uncut Chip Thickness In Micro Machining Of Aluminum. *Journal of Materials Processing Technology* 212:553–559.

[169] Malshe A, Rajurkar K, Samant A, Hansen HN, Bapat S, Jiang W (2013) Bio–Inspired Functional Surfaces for Advanced Applications. *CIRP Annals* 62/2:607–628.
[170] MarÍn JMR, Rasmussen HK, Hassager O (2010) 3D Simulation of Nano–Imprint Lithography. *Nanoscale Research Letters* 5:274–278.
[171] Marhöfer DM, Tosello G, Islam A, Hansen HN (2016) Gate Design in Injection Molding of Microfluidic Components Using Process Simulations. *Journal of Micro- and Nano-Manufacturing* 4/3:025001.
[172] McGeough JA (1974) *Principles of Electrochemical Machining*, Chapman & Hall-London.
[173] Mhetar V, Archer LA (1998) Slip In Entangled Polymer Melts. *Macromolecules* 31/24:8607–8616.
[174] Mollah MT, Comminal R, Serdeczny MP, Pedersen DB, Spangenberg J (2019) Stability And Deformations Of Deposited Layers In Material Extrusion Additive Manufacturing. *Additive Manufacturing* 46:102193.
[175] Mori L, Krishnan N, Cao J, Espinosa H (2007) Study of the Size Effects and Friction Conditions in Micro–extrusion: Part II—Size Effect in Dynamic Friction for Brass–steel Pairs. *ASME Journal of Manufacturing Science and Engineering* 129/4:677–689.
[176] Morimoto K, Kunieda M (2009) Sinking EDM Simulation By Determining Discharge Locations Based On Discharge Delay Time. *CIRP Annals* 58/1:221–224.
[177] Neuenschwander B, Jaeggi B, Schmid M, Rouffiange V, Martin P-E (2012) Optimization Of The Volume Ablation Rate For Metals At Different Laser Pulse–Durations From ps to fs. In: Proceedings Volume 8243, Laser Applications in Microelectronic and Optoelectronic Manufacturing (LAMOM) XVII, *SPIE LASE, 2012*, :824307.
[178] Nguyena L, Wub M-H, Hung C (2019) Finite Element Analysis Of Ultrasonic Vibration–Assisted Microstructure Hot Glass Embossing Process. *Australian Journal of Mechanical Engineering* 17/3:199–208.
[179] Nielsen CV, Zhang X, Moghadam M, Hansen N, Bay N (2021) Deformation Mechanisms in Tool–Workpiece Asperity Contact in Metal Forming. *Forming the Future* : 127–137.
[180] Oliveira FB, Rodrigues AR, Coelho RT, Souza AF (2015) Size Effect And Minimum Chip Thickness In Micromilling. *International Journal of Machine Tools and Manufacture* 89:39–54.
[181] Omar F (2013) *Hot Embossing Process Parameters*: Simulation and Experimental Studies, PhD thesis. Institute of Mechanical and Manufacturing Engineering, Cardiff School of Engineering, Cardiff University. Cardiff, Wales, United Kingdom, 207 pp.
[182] Ostaševičius V (2022) *Digital Twins in Manufacturing: Virtual and Physical Twins For Advanced Manufacturing*, Springer International Publishing, Cham, Switzerland.
[183] Pan CT, Wu TT, Chang YC, Huang JC (2008) Experiment And Simulation Of Hot Embossing Of A Bulk Metallic Glass With Low Pressure And Temperature. *Journal of Micromechanics and Microengineering* 18:025010.
[184] Panwisawas C, Qiu C, Anderson MJ, Sovani Y, Turner RP, Attallah MM, Brooks JW, Basoalto HC (2017) Mesoscale Modelling Of Selective Laser Melting: Thermal Fluid Dynamics And Microstructural Evolution. *Computational Materials Science* 126:479–490.
[185] Pandit SM, Rajurkar KP (1983) A Stochastic Approach to Thermal Modelling Applied to Electro–discharge Machining. *Journal of Heat Transfer* 105:555–562.
[186] Parandoush P, Hossain A (2014) A review of modeling and simulation of laser beam machining. *International Journal of Machine Tools and Manufacture* 85:135–145.
[187] Park S-H, Liu P, Yi K, Choi G, Jhang K-Y, Sohn H (2021) Mechanical Properties Estimation Of Additively Manufactured Metal Components Using Femtosecond Laser Ultrasonics And Laser Polishing. *International Journal of Machine Tools and Manufacture* 166:103745.
[188] Peng L, Lai X, Lee H-J, Song J-H, Ni J (2009) Analysis Of Micro/Mesoscale Sheet Forming Process With Uniform Size Dependent Material Constitutive Model. *Materials Science and Engineering: A – Structural Materials: Properties, Microstructure and Processing* 526:93–99.
[189] Piccolo L, Puleo K, Sorgato M, Lucchetta G, Masato D (2021) Modeling The Replication Of Submicron–Structured Surfaces By Micro Injection Molding. *Materials and Design* 198:109272.
[190] Platzgummer E, Biedermann A, Langfischer H, Eder–Kapl S, Kuemmel M, Cernusca S, Loeschner H, Lehrer C, Frey L, Lugstein A, Bertagnolli E (2006) Simulation Of Ion Beam Direct Structuring for 3D Nanoimprint Template Fabrication. *Microelectronic Engineering* 83/4–9:936–939.
[191] Pontes FJ, Ferreira JR, Silva MB, Paiva AP, Balestrassi PP (2010) Artificial Neural Networks For Machining Processes Surface Roughness Modeling. *International Journal of Advanced Manufacturing Technology* 49:879–902.
[192] Qian W, Cai J, Xin Z, Ye Y, Dai F, Hua Y (2022) Femtosecond Laser Polishing With High Pulse Frequency For Improving Performance Of Specialised Aerospace Material Systems: MCrAlY Coatings In Thermal Barrier Coating System. *International Journal of Machine Tools and Manufacture* 182:103954.
[193] Ramsden JJ, Allen DM, Stephenson DJ, Alcock JR, Peggs GN, Fuller G, Goch G (2007) The Design and Manufacture of Biomedical Surfaces. *CIRP Annals* 56/2:687–711.
[194] Rehbein T, Lion A, Johlitz M, Constantinescu M (2020) Experimental Investigation And Modelling Of The Curing Behaviour Of Photopolymers. *Polymer Testing* 83:106356.
[195] Romans T, Hirt G (2010) Rolling of Drag Reducing Riblet Surfaces. *51st AIAA/ASME/ASCE/AHS/ASC Structures, Structural Dynamics, and Materials Conference*, Orlando, FL (USA) 2010–3062.
[196] Rosenbaum EE, Hatzikiriakos SG (1997) Wall Slip in the Capillary Flow of Molten Polymers Subject to Viscous Heating. *AIChE Journal* 43/3:598–608.
[197] Rytka C, Lungershausen J, Kristiansen PM, Neyer A (2016) 3D Filling Simulation Of Micro– And Nanostructures In Comparison To Iso– And Variothermal Injection Moulding Trials. *Journal of Micromechanics and Microengineering* 26/6:065018.
[198] Schwarz–Selinger T, Cahill DG, Chen S-C, Moon S-J, Grigoropoulos CP (2001) Micron–Scale Modifications Of Si Surface Morphology By Pulsed–Laser Texturing. *Physical Review B* 64:155323.
[199] Schneider Y, Weber U, Wasserbäch W, Zielke R, Schmauder A, Tillmann W (2020) A Numerical Method For The Generation Of Hierarchical Poisson Voronoi Microstructures Applied In Micromechanical Finite Element Simulations—Part I: Method. *Computational Mechanics* 66:651–667.
[200] Sencer B, Altintas Y, Croft E (2008) Feed Optimization For Five–Axis CNC Machine Tools With Drive Constraints. *International Journal of Machine Tools and Manufacture* 48:733–745.
[201] Serdeczny MP, Comminal R, Pedersen DB, Spangenberg J (2018) Experimental Validation Of A Numerical Model For The Strand Shape In Material Extrusion Additive Manufacturing. *Additive Manufacturing* 24:145–153.
[202] Shen X-J, Pan L–W, Lin L (2002) Microplastic Embossing Process: Experimental And Theoretical Characterizations. *Sensors and Actuators A* 97–98:428–433.
[203] Shibata M, Horiba A, Nagaoka Y, Kawata H, Yasuda M, Hirai Y (2010) Process–Simulation System for UV Nanoimprint Lithography. *Journal of Vacuum Science & Technology B* 28:C6M108.
[204] Shu SG (2014) *Physical Modeling, Numerical Simulation And Experimental Investigation Of Hot Embossing Process With The Amorphous Thermoplastic Polymers* PhD thesis. Mechanics, Université de Franche–Comté, France183.
[205] Son SM, Lim HS, Ahn JH (2005) Effects Of The Friction Coefficient On The Minimum Cutting Thickness In Micro Cutting. *International Journal of Machine Tools and Manufacture* 45/4:529–535.
[206] Speidel A, Bisterov I, Saxena KK, Zubayr M, Reynaerts D, Natsu W, Clare AT (2022) Electrochemical Jet Manufacturing Technology: From Fundamentals To Application. *International Journal of Machine Tools and Manufacture* 180:103931.
[207] Stafe M (2012) Theoretical Photo–Thermo–Hydrodynamic Approach To The Laser Ablation Of Metals. *Journal of Applied Physics* 112:123112.
[208] Strano G, Hao L, Everson RM, Evans KE (2013) Surface Roughness Analysis, Modelling And Prediction In Selective Laser Melting. *Journal of Materials Processing Technology* 213:589–597.
[209] Sun J, Wu D, Liu Y, Dai L, Jiang C (2016) Numerical Simulation And Experimental Study Of Filling Process Of Micro Prism By Isothermal Hot Embossing In Solid–-Like State. *Advances in Polymer Technology* 37:1581–1591.
[210] Sun L (2020) *Polymethyl Methacrylate in Roll–to–Roll Hot Embossing of Microfluidic Channels* PhD thesis. Loughborough University, Loughborough, England, United Kingdom1–176.
[211] Surleraux A, Lepert R, Pernot JP, Kerfriden P, Bigot S (2020) Machine Learning–Based Reverse Modeling Approach for Rapid Tool Shape Optimization in Die–Sinking Micro Electro Discharge Machining. *Journal of Computing and Information Science in Engineering* 20. 031002–1.
[212] Szyndler J, Grosman F, Tkocz M, Delannay L, Wang J, Muszka K, Madej L (2021) Through Scale Material Flow Investigation In Novel Incremental Bulk Forming Process. *Journal of Materials Processing Technology* 287:116487.
[213] Tani G, Orazi L, Fortunato A, Cuccolini G (2008) Laser Ablation of Metals: A 3D Process Simulation for Industrial Applications. *Journal of Manufacturing Science and Engineering* 130/3:031111.
[214] Tani S, Kobayashi Y (2022) Ultrafast Laser Ablation Simulator Using Deep Neural Networks. *Scientific Reports* 12:5837.
[215] Tipton H (1970) Calculation Of Tool Shapes For Electrochemical Machining. *Journal of The Electrochemical Society* 117:8.
[216] Todhunter LD, Leach RK, Lawes SDA, Blateyron F (2017) Industrial survey of ISO surface texture parameters. *CIRP Journal of Manufacturing Science and Technology* 19:84–92.
[217] Torrubia PL, Axinte DA, Billingham J (2015) Stochastic modelling of abrasive waterjet footprints using finite element analysis. *International Journal of Machine Tools and Manufacture* 95:39–51.
[218] Uhlmann E, Ardelt T, Spur G (1999) Influence of Kinematics on the Face Grinding Process on Lapping Machines. *CIRP Annals* 48/1:281–284.
[219] van der Velden T, Rommes B, Klink A, Reese S, Waimann J (2021) A Novel Approach For The Efficient Modeling Of Material Dissolution In Electrochemical Machining. *International Journal of Solids and Structures* 229:111106.
[220] van der Velden T, Ritzert S, Reese S, Waimann J (2022) Modeling The Moving Boundary Value Problem In Electrochemical Machining. *PAMM – Proceedings in Applied Mathematics and Mechanics* 22(1):e202200147.
[221] van Luttervelt CA, Childs THC, Jawahir IS, Klocke F, Venuvinod PK (1998) Present Situation and Future Trends in Modelling of Machining Operations Progress Report of the ClRP Working Group 'Modelling of Machining Operations. *CIRP Annals* 47/2:587–626.
[222] Vasile MJ, Nassar R, Xie J, Guo H (1999) Microfabrication Techniques Using Focused Ion Beams And Emergent Applications. *Micron* 30:235–244.
[223] Vasile MJ, Xie J, Nassar R (1999) Depth Control Of Focused Ion–Beam Milling From A Numerical Model Of The Sputter Process. *Journal of Vacuum Science & Technology B* 17:3085.
[224] Vogler MP, DeVor RE, Kapoor SG (2004) On the Modeling and Analysis of Machining Performance in Micro–End milling, Part I: Surface Generation. *Journal of Manufacturing Science and Engineering* 126:685–694.
[225] Vollertsen F, Biermann D, Hansen HN, Jawahir IS, Kuzman K (2009) Size Effects In Manufacturing Of Metallic Components. *CIRP Annals* 58/2:566–587.
[226] Wang L, Li Q, Zhu W, Shen C (2012) Scale Effect On Filling Stage In Micro–Injection Molding For Thin Slit Cavities. *Microsystem Technologies* 18/12:2085–2091.
[227] Wang X, Li W, Chen T (2015) Simulation and Experimental Validation of the Hot Embossing Process of Poly(Lactic–Co–Glycolic Acid) Microstructures. *International Journal of Polymer Science* 520512.

[228] Wang J, Zhao C, Zhang Y, Jariwala A, Rosen D (2017) Process modeling and In–Situ Monitoring Of Photopolymerization For Exposure Controlled Projection Lithography (ECPL). *Solid Freeform Fabrication 2017: Proceedings of the 28th Annual International Solid Freeform Fabrication Symposium – An Additive Manufacturing Conference*, Austin, TX (USA) 1718–1734.
[229] Wang Q, Zhu D (2019) *Interfacial Mechanics, Theories and Methods for Contact and Lubrication*, CRC Press. Boca Raton, London, New York ISBN: 978–1–4398–1510–6, 978–1–1387–4890–3.
[230] Wang Z, Li HN, Yu TB, Wang ZX, Zhao J (2019) Analytical Model Of Dynamic And Overlapped Footprints In Abrasive Air Jet Polishing Of Optical Glass. *International Journal of Machine Tools and Manufacture* 141:59–77.
[231] Webster S, Lin H, Carter F, Ehmann K, Cao J (2021) Physical Mechanisms in Hybrid Additive Manufacturing: A Process Design Framework. *Journal of Materials Processing Technology* 291:117048.
[232] Westbeek S, Remmers JJC, van Dommelen JAW, Geers MGD (2020) Multi–Scale Process Simulation For Additive Manufacturing Through Particle Filled Vat Photopolymerization. *Computation Materials Science* 180:109647.
[233] Whitehouse DJ, Bowen DK, Venkatesh VC, Lonardo P, Brown CA (1994) Gloss and Surface Topography. *CIRP Annals* 43/2:541–549.
[234] Woon KS, Rahman M, Fang FZ, Neo KS, Liu K (2008) Investigations Of Tool Edge Radius Effect In Micro Machining: A FEM Simulation Approach. *Journal of Materials Processing Technology* 195:204–211.
[235] Worgull M, Heckele M, Hétu JF, Kabanemi KK (2006) Modeling And Optimization Of The Hot Embossing Process For Micro– And Nanocomponent Fabrication. *Journal-ofJournal of Microlithography Microfabrication and Microsystems* 5/1:011005–011013.
[236] Worgull M, Kabanemi KK, Marcotte J-P, Hetú J-F, Heckele M (2008) Modeling Of Large Area Hot Embossing. *Microsystem Technologies* 14:1061–1066.
[237] Wu Y-A, San C-H, Chang C-H, h–j Lin, Marwand R, Babad S, Hwang W-S (2018) Numerical Modeling Of Melt–Pool Behavior In Selective Laser Melting With Random Powder Distribution And Experimental Validation. *Journal of Materials Processing Technology* 254:72–78.
[238] Xia M, Gua D, Yua G, Dai D, Chen H, Shia Q (2017) Porosity Evolution And Its Thermodynamic Mechanism Of Randomly Packed Powder–Bed During Selective Laser Melting Of Inconel 718 Alloy. *International Journal of Machine Tools and Manufacture* 116:96–106.
[239] Xia H, Lu J, Tryggvason G (2019) A numerical Study Of The Effect Of Viscoelastic Stresses In Fused Filament Fabrication. *Computer Methods in Applied Mechanics and Engineering* 346:242–259.
[240] Xu G, Yu L, Lee LJ, Koelling KW (2005) Experimental And Numerical Studies Of Injection Molding With Microfeatures. *Polymer Engineering & Science* 45/6:866–875.
[241] Zhutian X, Peng L, Lai X (2020) Investigation On The Roll–To–Plate Microforming Of Riblet Features With The Consideration Of Grain Size Effect. *International Journal of Advanced Manufacturing Technology* 109:2055–2064.
[242] Xu L, Huang C, Li C, Wang J, Liu H, Wang X (2021) An Improved Case Based Reasoning Method And Its Application In Estimation Of Surface Quality Toward Intelligent Machining. *Journal of Intelligent Manufacturing* 32:313–327.
[243] Yamamura Y, Itakawa Y, Itoh N (1983) Angular Dependence Of Sputtering Yields Of Monoatomic Solids. *Physics of Plasmas* . IPPJ–AM–26.
[244] Yang XD, Han X, Zhou F, Kunieda M (2013) Molecular Dynamics Simulation of Residual Stress Generated in EDM. In: *Proc. of the 17th CIRP Conf. on Electro Physical and Chemical Machining (ISEM)*, Leuven (Belgium) 433–438.
[245] Yan W, Ge W, Qian Y, Lin S, Zhou B, Liu WK, Lin F, Wagner GJ (2017) Multi–Physics Modeling Of Single/Multiple–Track Defect Mechanisms In Electron Beam Selective Melting. *Acta Materialia* 134:324–333.
[246] Yang Y, Li H, Liao Z, Dragos DA (2019) A Curious Observation Of Phenomena Occurring During Lapping/Polishing Processes. *Proceedings: Mathematical, Physical and Engineering Sciences* 475/2230:20190304.
[247] Yang Y, Li H, Lia Z, Axinte DA, Zhu W, Beaucamp A (2020) Controlling Of Compliant Grinding For Low–Rigidity Components. *International Journal of Machine Tools and Manufacture* 152:103543.
[248] Yao D, Kim B (2002) Simulation Of The Filling Process In Micro Channels For Polymeric Materials. *Journal of Micromechanics and Microengineering* 12/5:604–610.
[249] Yao D, Virupaksha VL (2005) Study on Squeezing Flow During Nonisothermal Embossing of Polymer Microstructures. *Polymer Engineering and Science* 45:652–660.
[250] Ye H, Yu Y, Zhang T (2019) Simulation And Optimization Of Roll To Roll Hot Embossing Based On Viscoelastic Material PMMA. *IOP Conf Series: Materials Science and Engineering* 768:042024.
[251] Yousef BF, Knopf GK, Bordatchev EV, Nikumb SK (2003) Neural Network Modeling And Analysis Of The Material Removal Process During Laser Machining. *International Journal of Advanced Manufacturing Technology* 22:41–53.
[252] Yu L, Lee LJ, Koelling KW (2004) Flow And Heat Transfer Simulation Of Injection Molding With Microstructures. *Polymer Engineering & Science* 44/10:1866–1876.
[253] Yuan ZJ, Zhou M, Dong S (1996) Effect Of Diamond Tool Sharpness On Minimum Cutting Thickness And Cutting Surface Integrity In Ultraprecision Machining. *Journal of Materials Processing Technology* 62/4:327–330.
[254] Zhang L, Kuriyagawa T, Kaku T, Zhao J (2005) Investigation Into Electrorheological Fluid–Assisted Polishing. *International Journal of Machine Tools and Manufacture* 45/12–13:1461–1467.
[255] Zhang P, Balint D, Lin J (2011) An Integrated Scheme For Crystal Plasticity Analysis: Virtual Grain Structure Generation. *Computation Materials Science* 50/10:2854–2864.
[256] Zhang R, Wang Q, Zheng X, Ma L, Zhang J (2016) Effects Of Friction Coefficient And Cohesion Between A Mold And A Polymer Resist During Demolding Process In Hot Embossing. *Journal of Photopolymer Science and Technology* 29/1:39–44.
[257] Zhang X, He T, Miwa H, Nanbu T, Murakami R, Liu S, Cao J, Wang QI (2019) A New Approach For Analyzing The Temperature Rise And Heat Partition At The Interface Of Coated Tool Tip–Sheet Incremental Forming Systems. *International Journal of Heat & Mass Transfer* 129:1172–1183.
[258] Zhang X, Yu T, Zhao J (2020) Surface Generation Modeling Of Micro Milling Process With Stochastic Tool Wear. *Precision Engineering* 61:170–181.
[259] Zhang Y, Zhu S, Zhao Y, Yin Y (2022) A Material Point Method Based Investigation On Crack Classification And Transformation Induced By Grit Geometry During Scratching Silicon Carbide. *International Journal of Machine Tools and Manufacture* 177:103884.
[260] Zheng M, Wei L, Chen J, Zhang Q, Zhong C, Lin X, Huang W (2019) A Novel Method For The Molten Pool And Porosity Formation Modelling In Selective Laser Melting. *International Journal of Heat & Mass Transfer* 140:1091–1105.
[261] Zhu W-L, Yang Y, Li HN, Axinte DA, Beaucamp A (2019) Theoretical and Experimental Investigation Of Material Removal Mechanism In Compliant Shape Adaptive Grinding Process. *International Journal of Machine Tools and Manufacture* 142:76–97.
[262] Zhu W-L, Beaucamp A (2020) Compliant Grinding And Polishing: A Review. *International Journal of Machine Tools and Manufacture* 158:103634.
[263] Zhu W-L, Jain C, Han Y, Beaucamp A (2021) Predictive Topography Model For Shape Adaptive Grinding Of Metal Matrix Composites. *CIRP Annals* 70/1:269–272.
[264] Zhu W-L, Beaucamp A (2022) Generic Three–Dimensional Model Of Freeform Surface Polishing With Non–Newtonian fluids. *International Journal of Machine Tools and Manufacture* 172:103837.